PREDICTION OF PV/T PERFORMANCE USING DIFFERENT COOLING SYSTEM STRUCTURES

2022
MASTER THESIS
MECHANICAL ENGINEERING

Mohammed GUMAR AJEL

Thesis Advisors
Assoc. Prof. Dr. Engin GEDİK
Assist. Prof. Dr. Hasanain A. Abdul WAHHAB

PREDICTION OF PV/T PERFORMANCE USING DIFFERENT COOLING SYSTEM STRUCTURES

Mohammed Gumar AJEL

Thesis Advisors

Assoc.Prof.Dr. Engin GEDİK

Assist. Prof. Dr. Hasanain A. Abdul WAHHAB

T.C.

Karabuk University

Institute of Graduate Programs

Department of Mechanical Engineering

Prepared as

Master Thesis

KARABÜK

December 2022

I certify that in my opinion the thesis submitted by Mohammed Gumar AJEL titled "PREDICTION OF SOLAR COLLECTOR PERFORMANCE FOR PV PANEL THERMAL CONTROL APPLICATION " is fully adequate in scope and quality as a thesis for the degree of Master of Science.

Assoc. Prof. Dr. Engin GEDİK .....
Thesis Advisor, Department of Mechanical Engineering

Assist. Prof. Dr. Hasanain A. Abdul WAHHAB .....
Thesis Advisor, Department of Mechanical Engineering

This thesis is accepted by the examining committee with a unanimous vote in the Department of Mechanical Engineering as a Master of Science thesis. 22/12/2022

Examining Committee Members (Institutions)	Signature
Chairman : Prof. Dr. Kamil ARSLAN (KBU)	.....
Member : Assoc. Prof .Dr .Mustafa YILMAZ (MU)	.....
Member : Assoc. Prof.Dr. Engin GEDİK (KBU)	.....
Member : Assist. Prof. Dr. H. A. Abdul WAHHAB (UOTECH)	.....
Member : Assist. Prof. Dr .Mutlu TEKİR (KBU)	.....

The degree of Master of Science by the thesis submitted is approved by the Administrative Board of the Institute of Graduate Programs, Karabuk University.

Prof. Dr. Muslum KUZU .....
Director of the Institute of Graduate Programs

"I declare that all the information within this thesis has been gathered and presented in accordance with academic regulations and ethical principles and I have according to the requirements of these regulations and principles cited all those which do not originate in this work as well."

Mohammed Gumar AJEL

ABSTRACT

M. Sc. Thesis

PREDICTION OF PV/T PERFORMANCE USING DIFFERENT COOLING SYSTEM STRUCTURES

Mohammed Gumar AJEL

Karabük University
Institute of Graduate Programs
The Department of Mechanical Engineering

Thesis Advisors:
Assoc. Prof. Dr. Engin GEDİK
Assist. Prof. Dr. Hasanain A. Abdul WAHHAB
December 2022, 113 pages

This thesis presents an experimental and theoretical study to improve the performance of the PV/T system. This work was carried out in Baghdad at the University of Technology. Using two electric cells side by side, one connected to the collector and water cooled and using two new collector designs. The first type contains 120 cubes (8 * 15) each cube has dimensions (15 * 15 * 15 mm), the second type contains spherical shapes with a diameter of (25 mm). Using different flow rates 1.5, 2, 2.5 and 3.5 l/min. The design effect on the performance of the PV/T system was studied. The cell surface temperature was reduced by (8.4%) (9.8%) for CC and SS respectively compared to the uncooled cell. . An increase in the electrical efficiency by (6.6%) and (8.08%) for the CC and SS models, respectively, compared to the uncooled cell The thermal efficiency of the SS model was higher by (6.06%)

than the thermal efficiency of CC. The percentage of the total difference (error) between the numerical and the experimental was 9.8% for 3.5 l/min.

Key Words : Photovoltaic, Solar, Thermal, Water Collector, Investigation.
Science Code : 91408

ÖZET

Yüksek Lisans Tezi

PREDICTION OF PV/T PERFORMANCE USING DIFFERENT COOLING SYSTEM STRUCTURES

Mohammed Gumar AJEL

Karabük Üniversitesi
Lisansüstü Eğitim Enstitüsü
Makina Mühendisliği Anabilim Dalı

Tez Danışmanları:
Doç. Dr. Engin GEDİK
Dr. Öğr. Üyesi Hasanain A. Abdul WAHHAB
Eylül 2022, 113 sayfa

Bu tez, PV/T sisteminin performansını iyileştirmek için deneysel ve teorik bir çalışma sunmaktadır. Bu çalışma Bağdat'ta Teknoloji Üniversitesi'nde gerçekleştirildi. Biri kollektöre bağlı ve su soğutmalı iki elektrik hücresini yan yana kullanmak ve iki yeni kollektör tasarımı kullanmak. Birinci tip 120 küp (8 * 15) içerir, her küpün boyutları (15 * 15 * 15 mm), ikinci tip (25 mm) çapında küresel şekiller içerir. 1,5, 2, 2,5 ve 3,5 l/dk farklı akış oranları kullanılarak. PV/T sisteminin performansı üzerindeki tasarım etkisi incelenmiştir. Hücre yüzey sıcaklığı, soğutulmamış hücreye kıyasla sırasıyla CC ve SS için (%8,4) (%9,8) azaltıldı. . Soğutmasız hücreye kıyasla CC ve SS modellerinde elektrik verimliliğinde sırasıyla (%6,6) ve (%8,08) artış SS modelinin ısıl verimi CC'nin ısıl veriminden (%6,06) daha yüksekti . Sayısal ve deneysel arasındaki toplam farkın (hata) yüzdesi 3,5 l/dk için %9,8 idi.

Anahtar Kelimeler : Your abstract ıs chaotıc correct abstract then ı can wrıte turkısh abstract or gıve help someone then ı wıll correct.

Bilim Kodu : 91408

ACKNOWLEDGMENT

Praise be to God Al-Mannan, without whom there is no pen or tongue, and may prayers and peace be upon the most eloquent tongue of the people.

I extend my sincere thanks and gratitude to Assoc. Prof. Dr. Engin GEDIK and Co-Supervisor Dr. Hasanain Adnan Abdul Wahhab for this letter for the assistance they provided and for providing us with the necessary information to complete this research. We give them all our respect and appreciation.

I extend my thanks and gratitude to my father, my mother, my wife, my brothers and all my family. A fragrant greeting with the scent of roses. I dedicate it to all my friends.

Finally, words of thanks are incapable of achieving self-esteem of gratitude and appreciation to everyone who helped me complete my letter.

CONTENTS

Page

Page

Page

Page

LIST OF FIGURES

Page

Page

Page

LIST OF TABLES

Page

SYMBOLS AND ABBREVIATIONS

SYMBOLS

A*c*	:	Area collector channel surface
A	:	Area of the PV module m2
Ac	:	Area of collector m2
AL	:	Altitude of location above mean sea level km
AM	:	Air mass kg
Bv	:	Viscous friction coefficient Nms/rad
Cp	:	Specific heat capacity J/kg.oC
Cpf	:	Heat capacity of the base fluid J/kg.oC
Cpnf	:	Heat capacity of the nanofluid J/kg.oC
Cpp	:	Heat capacity of the nanoparticles J/kg.oC
D	:	Tube diameter m
De-s	:	Distance between the earth and the sun m
Dm	:	The mean sun earth distance m
dn	:	Number of days
Ece	:	Electrical energy produced by photovoltaic cell J
Ect	:	Thermal energy released by photovoltaic cell J
Eloss	:	Energy losses J
ET	:	Equation of time minutes
ET	:	RATE of solar energy absorbed by Tedlar (Back sheet) J
F	:	Friction factor
G (t)	:	Solar irradiation incident on the glass cover W/m2
hc	:	Convection coefficient of fluid flow in the pipe W/(m2.K)
hg	:	Convective heat transfer coefficient of the glass W/(m2.K)
hs	:	Hour angle degree
Ia	:	Current in phase (*a*) A
Ib	:	Beam radiation W/m2

Ib	:	Current in phase (*b*) A
Id	:	Diffuse radiation W/m2
Imp	:	PV current at maximum power point under standard condition
Impp	:	Maximum power point current A
Io	:	Extraterrestrial solar radiation W/m2
Isc	:	Solar constant
J	:	Moment of inertia kg-m2
Kf	:	The base fluid thermal conductivity W/m.oC
Km	:	Motor constant Vs/rad
Knf	:	Thermal conductivity of the nanofluid W/m.oC
$K\rho$	:	Thermal conductivity of the nanoparticle W/m.oC
L	:	Latitude angle degree
La	:	Self-inductance in phase (a) mH
Lb	:	Self-inductance in phase (b) mH
LST	:	Local standard time hr
Lst	:	Standard meridian for local time zone degree
Nr	:	Number of the teeth on the rotor
P	:	Cell packing factor
Pmax	:	Maximum power W
qc	:	Heat flux which transferred to the fluid flow in the cooling pipes
R	:	Resistance in each phase ohm
ST	:	Solar time hours
Ta	:	Ambient temperature oC
Tc	:	Cell temperature oC
Te	:	Electromagnetic torque Nm
Tg	:	Glass temperature oC
Tin	:	Inlet temperature of the cooling fluid oC
Tl	:	Load torque Nm
To	:	The temperature of standard condition oC
Tout	:	Outlet temperature of cooling fluid oC
V	:	Wind speed m/s
Vmp	:	PV voltage at maximum power point under standard condition
Vmpp	:	Maximum power point voltage V

VNP	:	Volume of the nanoparticles m3
VT	:	Total volume m3
αs	:	Solar altitude angle deg
γz	:	Solar azimuth angle deg
ϕ	:	Volume concentration ratio of the nanoparticles
v	:	Kinematic viscosity m2/s
va	:	Voltage in phase (a) V
vb	:	Voltage in phase (b) V
λ	:	Wavelengths μm
αc	:	Cell absorptivity to sunlight
αg	:	Absorptivity of glass
αnf	:	Thermal diffusivity of nanofluid m2/s
αT	:	Absorptivity of the Tedlar
β	:	Temperature coefficient of silicon cell
δs	:	Sun's declination angle deg
εg	:	Emittance of the glass
ηel	:	Electrical efficiency
ηo	:	Nominal electrical efficiency under standard condition
ηth	:	Thermal efficiency
$\eta total$	:	Total efficiency
θ	:	Module inclination to the horizontal deg
θi	:	Incident angle deg
θz	:	Zenith angle deg
μnf	:	Nanofluid dynamic viscosity kg/m.s
μw	:	Water dynamic viscosity kg/m.s
ρf	:	Density of the base fluid kg/m3
ρnf	:	Density of the nanofluid kg/m3
ρp	:	Density of the nanoparticles kg/m3
τg	:	Transmitted through the front glass
Re	:	Reynolds number
Nu	:	Nusselt number

Pr	:	Prandtl number
Pe	:	Peclet number
el/insul	:	Electrical/insulator
f	:	Fluid
nf	:	Nanofluid
p	:	Particle
e-s	:	Earth to sun
el	:	Elictrical
th	:	Thermal
loss	:	Losses
T	:	Tedlar
C	:	Cell
g	:	Glass
b	:	Beam
np	:	Nanoparticles
d	:	Diffuse
a	:	Ambient
in	:	Inlet
out	:	Outlet

ABBREVIATIONS

AC	:	Alternating current
Al_2O_3	:	Alumina oxide
CdS	:	Cadmium sulfide
CNT	:	Carbon nanotubes
COP	:	Coefficient of performance
CPC	:	Compound parabolic concentrator
Cu2S	:	Copper sulfide
DC	:	Direct current
ETR	:	Extraterrestrial solar radiation
EVA	:	Ethylene vinyl acetate
FPPV	:	Flat plate photovoltaic

PV/T	:	Flat plate solar collector
HSM	:	Hybrid stepping motor
IPVTS	:	Integrated photovoltaic and thermal solar system
IR	:	Infrared
LDR	:	Light Dependent Resistors
LFR	:	Linear Fresnel Reflector
MPPT	:	Maximum power point tracking
Mtoe	:	Million tonne of oil equivalent
MWCNT	:	Multi-Walled Carbon Nanotube
PLC	:	Programmable Logic Controller
PV	:	photovoltaic
PV/T	:	photovoltaic/thermal hybrid system
SW H	:	Solar water heater
TiO_2	:	Titanium oxide
TPT	:	Tedlar/Polyester/Tedlar
TW	:	Trillion watt

PART 1

INTRODUCTION

1.1. BACKGROUND

There are two types of energy depending on their sources: Renewable and nonrenewable energy sources. Non-renewable resources are natural resources that cannot be replenished readily replenished with our demand, and for that reason, these resources are steadily depleting. Additionally, to being limited, non-renewable energy sources have negative health effects on humans, and they are not environmentally friendly. These reasons led to the search for alternative energy. Renewable energy refers to energy derived from naturally replenished resources. These sources are usually considered sustainable, readily available, and clean energy sources which include rain, tides, sunlight, wind, waves, and geothermal. Because of sunlight's vast availability, the world has been turning more and more to it as a source of energy in past years. Sun radiation can be used to produce not only electricity but also thermal energy at the same time by using hybrid solar collectors (Photovoltaic Thermal collectors) [1]. Figure 1. solar energy system is given [1].

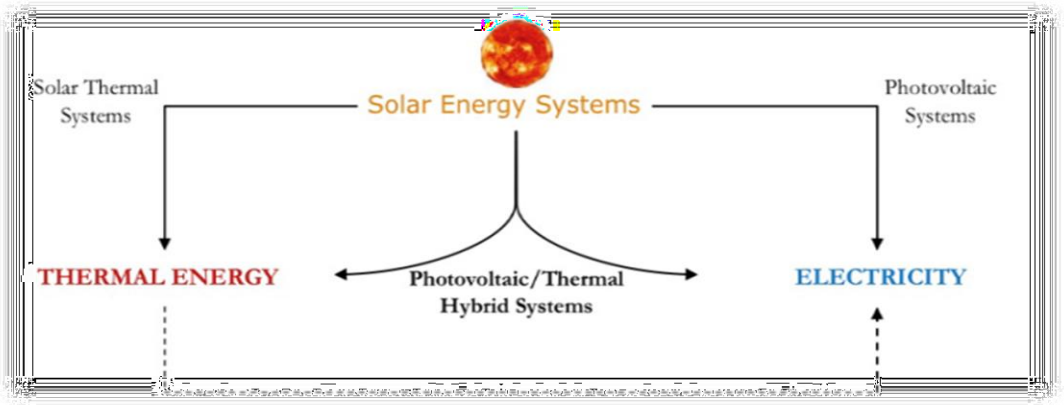

Figure 1.1. Solar energy system [1].

1.2. SOLAR ENERGY

Solar energy makes a great source for renewable energy for a multitude of reasons. Firstly, it replaces depleted sources with a renewable source that is easily accessible and available to most of the planet directly. Secondly, solar energy does not produce waste and is generally harmless regarding humans' health, as opposed to traditional energy sources. Lastly, it requires simple maintenance which makes it less costly. For these reasons, solar energy has become an important source of energy globally due to its economic and environmental advantages its easy accessibility. Solar energy has various uses of ways. The most important of which are steam production which can be used for industrial purposes and to generate electricity, heating water, drying crops, desalination of water, etc.

Solar panels consist of six layers as shown Figure 1.2. Collection of individual solar cells make up solar panels. Electricity is generated when the sunlight falls on these cells. Photovoltaic cells are usually made up of two layers of semiconductor material. One of which the first is positively charged (P type), and the second is negative charge (N type). The two layers meet and create the PN junction in figure (1.3) where electric currents pass when sunlight falls on these [2].

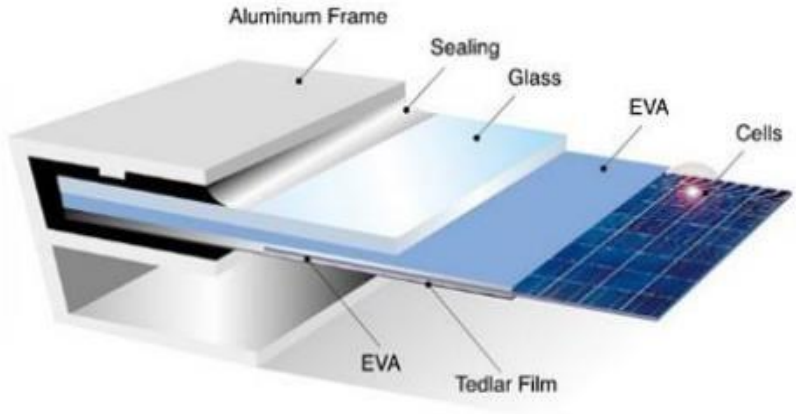

Figure 1.2. Schematic of a module PV [2].

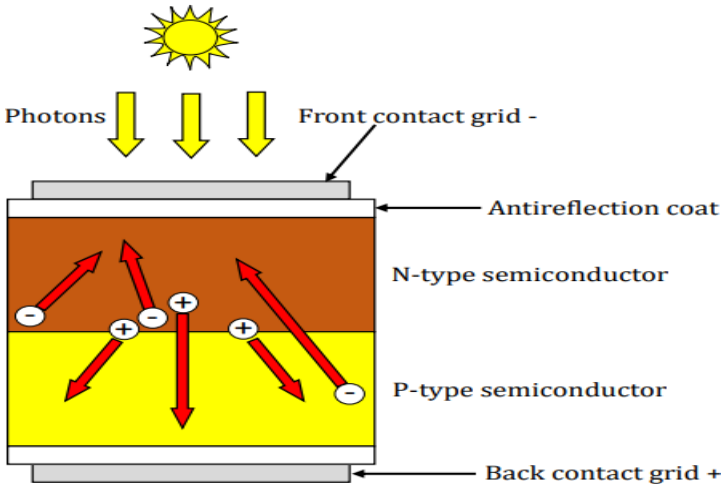

Figure 1.3. Diagram of a PV cell principle [2].

1.2.1. Types of Photovoltaic Technology

Photovoltaic panels can be classified the four following types:

1. Monocrystalline silicon photovoltaic panels: they have a complex process of manufacturing which makes them one of the most expensive types. They are silicon panels cut into slices. This type's efficiency is the highest, it reaches up to 15% [3].
2. Polycrystalline silicon photovoltaic panels: they are made of silicon that has been melted and recrystallized. They cost less than the first type. They have an efficiency of up to 12% [3] .
3. Thick film silicon photovoltaic panels: they are made by depositing silicon onto base material.
4. Amorphous silicon photovoltaic panels: they are shaped in thin layers on the surface of base material form and are made from the depositing silicon. It is cheap and streamlined shaped. The efficiency reaches up to 6% [3].

1.3. WATER SOLAR COLLECTORS

It is a solar collector which contains metal tubes in which water passes. These tubes are in direct contact with a flat metal plate. The heat is absorbed because of the water having to pass through the tubes and then leaves the system at a higher temperature

than it enters it. This heat can be used right away or converted to other types of energy.

1.3.1. Solar Water Heaters

Solar water heaters have the following advantages:

1. Solar thermal panels convert approximately 80% of the solar radiation they receive into energy, indicating a high efficiency.
2. Solar thermal panels usually take up less space in area than PV panels.
3. A couple of panels are generally cheaper than large home installations, therefore it is less costly to use solar thermal panels than fuel for gas heating systems.
4. Solar panels have a lifespan of approximately 20 years. and they do not require a lot of maintenance after initial installation in homes.
5. Solar thermal panels make homes greener and more environmentally friendly.

Despite of the many advantages of solar thermal panels, they have a few disadvantages:

1. Solar thermal collectors require sufficient space to accommodate them.
2. Solar thermal collectors require direct sunlight to work.
3. The system does not function on foggy, rainy, or cloudy days.

1.4. HYBRID SOLAR COLLECTOR (PV/T)

Hybrid solar collectors are collectors which generate heat in addition to electricity by combining thermal collectors and photovoltaic systems as shown in Figure 1.4. To prevent solar cells from overheating and having low efficiency, Heat is removed using fluids such as air or water from the solar panels [4].

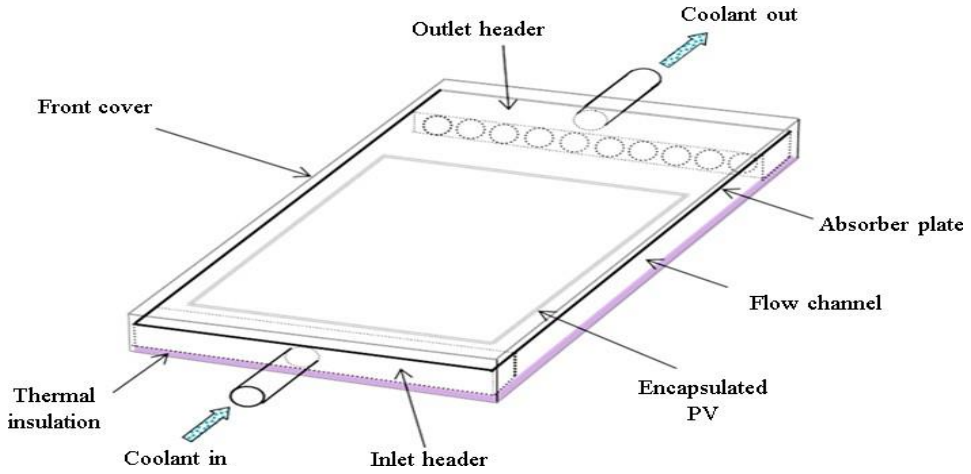

Figure 1.4. Simple parts of a hybrid solar collector (PV/T) [4].

1.4.1. Types of Hybrid Solar Collectors (PV/T)

There are four types of Hybrid collectors:

1. PV/T Water Collectors: In water collect so that the heat from the panels can be extracted tors, water is the fluid used is the coolant medium so that the heat from the panels can be extracted. The water can then be stored or used later. To prevent the water from freezing in bad weather, it is sometimes mixed with ethane or glycol as shown in Figure 1.5 [5].

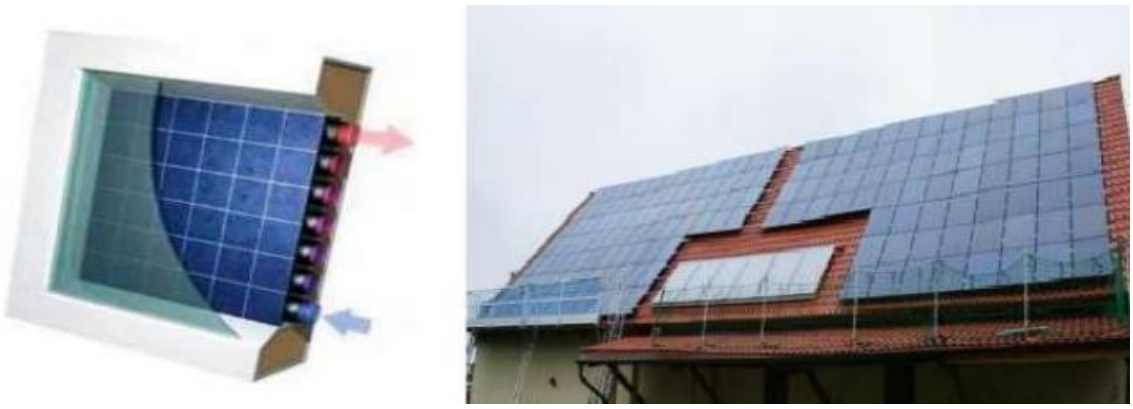

Figure 1.5. Hybrid water solar collector [5].

2. PV/T Air Collectors: In air collectors, air is the coolant medium used, which can be later used for heating. This type is less expensive than the previous one. There is no risk of freezing and no risk of damage to the system in the case of leaking air when compared to water collectors. However, compared to water collectors, it has a lower thermal performance and lower specific heat capacity compared to water the solar air is depicted in Figure 1.6 [5].

Figure 1.6. Hybrid air solar collector [5].

3. Solar Cell Ventilation with Heat Recovery: These systems are usually attached to roofs or sides of buildings as shown in Figure 1.7. They are installed on rooftops in rows. They recover the heat from the air in nature. Additionally, they protect buildings they are used on by forming a shield which reduces cooling loads during hot weather. Also, because it is used as a cladding material, it reduces the cost of construction. One downside of these systems is that they require large tubes because they need space for air circulation, and they have high heat loss compared to other types [5].

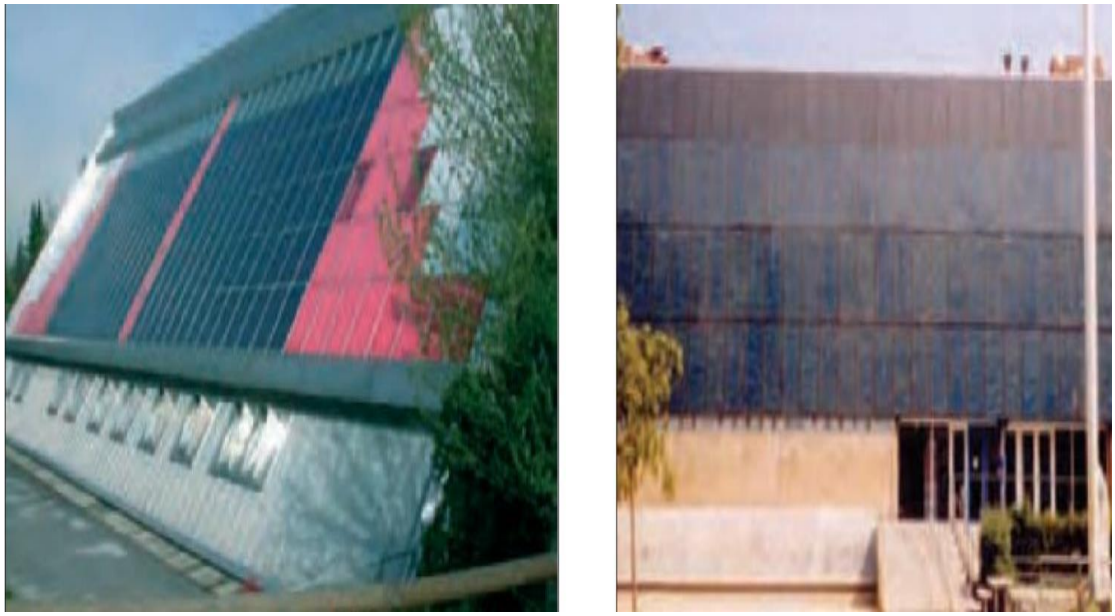

Figure 1.7. Solar cell ventilation collector with heat recovery on the facade of buildings [5].

4. Concentrated PV/T Collectors: Concentrated PV/T collectors are curved collectors which collect and reflect sun rays at a central point. This collector is less expensive than other types because it uses reflective material instead of photovoltaic units. Because of the reflection however, this type of collector increases in temperature easily which makes it require constant cooling as shown in Figure 1.8 [5].

Figure 1.8. Concentrated PV/T collector [5].

1.4.2. The Advantages of Hybrid Solar Collector

The hybrid solar collector has many advantages which include its lightweight when compared to other types of collectors like electrical and thermal units, low cost, aesthetically better than other systems, it repurposes high heat which usually would decrease the efficiency of a system, subsequently, it is more efficiency, it takes less space, it does not emit harmful gases, and lastly, it does not make any noise and thus can be used in urban areas.

1.5. PROBLEM STATEMENT

Photovoltaic (PV) solar cells convert the light energy produced by the sun into electricity. Semiconducting materials are used to make photovoltaic cells, which convert energy into electricity by absorbing heat from solar radiation. This heat reduces the efficiency of electricity generation. Many Several studies have been done on PV/T, to reduce the temperature of the PV panels to increase the power in them. Cost reduction is the most important concern in industry, followed by reduced power consumption. The temperature reduction for PV panels achieved using a new PV/T design increases power generation and improves the cooling process for PV panels. Therefore, in this current study, the new models of PV/T were applied to cooling the PV panel after enhancing the flat collector by adding different bulge shapes to the collector cover to increase heat transfer area. The investigation of PV/T has been performed and analyzed using experimental and numerical methods.

1.6. RESEARCH OBJECTIVES

The primary objectives of this research are to design, characterize, and evaluate the performance of an integrated PV/T system. The following are the specific goals of this work:

1. To undertake simulation and evaluate the performance enhancement of the PV/T collector by integration of open-loop and operational modes.

2. To investigate the influence of the new models of PV/T on PV/T system characteristics by additives of cubic and sphere bulge shapes.
3. To computationally simulate the transient thermal behavior of the PV/T collector system using ANSYS and compare it with experimental data.

1.7. THE SCOPE OF THE PRESENT RESEARCH

All previous research studies have demonstrated that researchers are eager to find a way to harness solar energy. It's a good alternative. Solar energy does not leave polluting residues such as fossil fuels or others. A hybrid solar collector is a collector that generates electricity and heat at the same time. This collection consists of solar cells with and without glass, an aluminum or copper plate, and an insulating frame. Solar cells suffer from overheating and low efficiency has been studied in several designs to find the best solar panel cooling efficiency. It was found through the previous research study that researchers had. They did not study the effect of a change in water velocity on the square cubes and spheres installed inside the hybrid solar collector. An experimental study of hybrid solar energy was conducted in this study. The complex was made using a multi-speed flow with a study of its effect on the properties of the heat transfer system.

1.8. THESIS OF LAYOUT

The following chapters make up this thesis Introduction, review of the literature, research methodology and theoretical work, experimental work, results and discussions, conclusions, and recommendations The chapters' summary is described below:

The first chapter provides the study's context, focusing on the f-Flat Solar Collector PV/T application in the PV/T system. The problem statements, study objectives, and the study's scope are also included. The second chapter provides a review of PV/T systems, experimental and theoretical background on PV/T models, an explanation and discussion of collector design characteristics in various types, and a review of temperature measurement techniques.

The third chapter discusses research methodology and theoretical simulation, as well as the numerical simulation for the PV/T system. The model is built by combining the model configuration, assumptions, and governing equations that describe the behavior of the PV/T model. These equations' numerical solutions were used. The numerical simulation technique was carried out using the commercial software ANSYS FLUENT 17.

The fourth chapter describes the experimental set - up of the PV/T system and measurement techniques because of the new collector design. This study will be subjected to an experimental investigation. Temperature measurement techniques were used to identify PV/T performance. Experiment measurements were used to validate the results of the CFD simulation.

The fifth chapter discusses the findings and presents the analysis, which is broken down into the sections below. a) The findings of the PV/T system experimental models; b) The results of the PV/T system performance sensitivity analysis numerical simulation; and c) Validation and comparison of simulation and experimental results are revealed.

The sixth chapter presents the work's conclusions as well as recommendations for future work.

PART 2

LITERATURE REVIEW

2.1. INTRODUCTION

In 1973, the scientist Boer proposed the first hybrid antenna to collect solar energy [6] and the idea was originally created to assemble photovoltaic cells as well as thermal systems. These systems themselves depend to a great extent on solar energy. For this reason, experiments and studies were accomplished in the past, and till now the process has been continued. These theoretical and experimental systems were the subject of recent research and studies for the sake of improving them. This chapter highlights the main points related to the literature review concerning the subject under study and all items related will be viewed. Electrical and thermal efficiency will be improved in this chapter as well. The chapter also reviews the past related studies.

2.2. REVIEW OF PREVIOUS RESEARCH

Past studies will show how the subject under investigation was tackled differently and will show also how the idea within the current research benefited from earlier ideas to construct the current research. This section is divided into three subsections which are: Research related to Air PV/T Solar Collectors, Research related to PV/T Water Collectors and Research related to water and air complexes PV/T.

2.2.1. Research Related to Air PV/T Solar Collectors

Othman et al [7]: To quantify the thermal and electrical efficiency, theoretical and practical investigations of the influence of the fins on the solar hybrid air collector were conducted, as shown in Figure 2.1.

Use air as for heat transfer. for solar cells and to boost electrical efficiency Lowering the operating temperature will help you get a decent level. It was determined that cooling medium such as fins are required. The fins are a crucial aspect of the development of absorbent elements to accomplish the PV/T hybrid's high-power thermal and electrical efficiency.

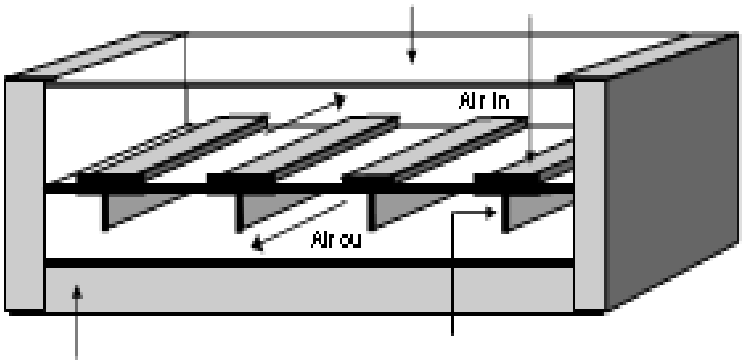

Figure 2.1. Hybrid solar collector (PV/T) with fins [7].

Joshi et al [8]: The study contrasted two types of PV modules. The following findings apply to photovoltaic. The modules shown are glass to glass and glass to tedlar in Figure 2.2. The rear surface temperature of the PV module is observed to be greater in air to PV/T glass than those in collector to tedlar glass. In both circumstances, the total thermal efficiency falls with channel length, while the thermal efficiency rises with increasing air mass velocity. Glass air on PV/T glass has a higher overall thermal efficiency superior to glass-to-tedlar air collector

Figure 2.2. Hybrid solar collector with single pass (PV/T) [8].

Adnan Ibrahim [9]: This research will help to enhance electricity efficiency by cooling solar cells and generating thermal energy in the form of hot air. The tunnel absorber was created by fabricating a long tunnel absorber that was installed on the rear side of a typical PV panel. As seen in figure 2.3 , they are connected in parallel. When a solar cell becomes cooled by air movement, its efficiency rises. When compared to a standard solar collector, the rectangular tunnel absorber gives greater electrical and thermal efficiency. With a solar irradiation of 817.4W per square meter as well as a mass flow rate of 1.2 l/min , the combined photovoltaic, thermal, and thermal efficiencies are 10.02, 54.70, and 64.72 percent.

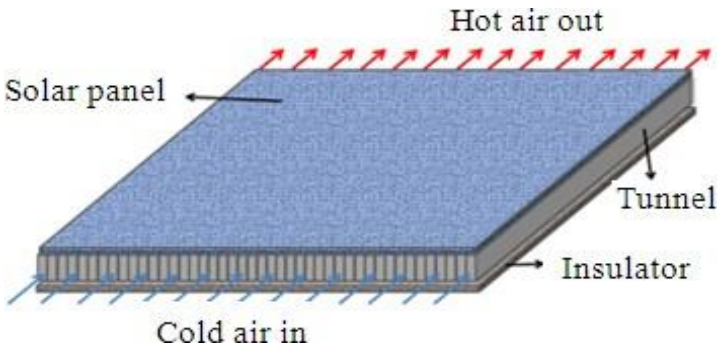

Figure 2.3. Solar Photovoltaic thermal air collector [9].

Sarhaddi et al. [10]: This study looked at the electrical and thermal performance of a PV/T hybrid solar thermal collector. The open circuit voltage and current were measured. for the electrical model, while the thermodynamic model calculated all collector temperatures and discovered that the electrical and thermal efficiency, as well as the overall collector efficiency, were 10.01 percent, 17.01 percent, and 45 percent, respectively.

Teo et al. [11]: The solar-powered cooling system was built and tested by building parallel channels with consistently flowing air on the back of the panel. An experiment with and without cooling was carried out, and a linear connection between efficiency as well as temperature was discovered. Only without cooling can efficiency be found. After the system was hot, the efficiency of the solar cells ranged from 8 to 9 percent, but when it was cooled, the temperature dropped and the effectiveness of the percentage of solar cells increased to between 12 and 14 percent.

The simulation of heat transfer system is designed to compare with actual heat to ensure that the simulation and testing results accord.

Yeh et al [12]: The researcher theoretically examined a solar air heater designed with an absorption plate and fins attached to it and achieved an increase in collector efficiency because the fins provide great heat transfer; the collectors were double pass with fins > double pass without fins > single pass and without fins.

Amori and Taqi al-Najjar [13]: Models were utilized in this study to handle electrical and thermal concerns. When the numerical as well as empirical findings of earlier studies are compared, these models were considerably wiser in terms of error rates. Another simulation was run based on the climatic conditions of Fallujah in the summer and Baghdad in the winter, with the thermoelectric efficiency in the winter being 12.3 percent and 19.4 percent, respectively. Summertime electrical and thermal efficiency were 9 and 22.8 percent, respectively.

Bakari et al [14]: One of the researchers conducted an experimental investigation into the effect of glass thickness on performance of four solar collectors and was aware of the effect of glazing thickness on surface solar collectors. He produced assemblies with a 10-degree angle and several varieties of 3mm, 4mm, 5mm, as well as 6mm glass. When the four models were analyzed and compared, it was discovered that collectors with a thickness of 4 mm had the highest effectiveness of 35.4 percent, compared to 27.8 percent for glass with a thickness of 6 mm.

Amori and Abd-AlRaheem [15]: The performance of wind-hybrid solar PV collectors was compared to three other collectors in this study. It is divided into four sections. The temperature of the PV's upper and bottom surfaces is one of the metrics monitored. Matlab was created to solve mathematical problems. The experimental findings reveal that the third model complex (double duct, single lane) has a high overall efficiency greater than the second (single channel duplex) and fourth models (single channel single channel). The fourth model performed better. The fourth figure was discovered to be 3.22 percent and 18.04 percent, respectively. The linear correlation coefficients (r) computed are 0.977 and 0.965, respectively.

Leow et al. [16]: The researcher investigated the simulation of the three-dimensional panel model under the effect of varied wind speeds in this work. They were 0 m/s, 0.43 m/s, 2.5 m/s, and 6.95 m/s, respectively. They investigated the performance of solar panels and calculated theoretical values with ANSYS. Theoretical findings revealed that higher wind speeds and lower temperatures can provide additional cooling while maintaining good performance

Boulfaf et al. [17]: The researcher theoretically investigated two figures to evaluate performance of the hybrid solar collector PV/T that warms the air while also producing energy. As well as the influence of mass flow rate, radiation intensity, and collector length on collector performance. To comprehend and solve thermal equilibrium equations, they have used the finite element approach. According to the findings of the study, a rise in ambient temperature and radiation intensity can cause an increase in the temperature of solar panels and a loss in electrical efficiency. The enhanced mass flow rate also boosted the electrical efficiency of the solar panels. In addition, they demonstrated an increase in collector length, which enhances thermal efficiency.

Ahmed and Mohammed [18]: They discovered experimentally that dust affects both the electric cell's efficiency and the thermal efficiency of the hybrid collector, as seen in Figure 2.4In practice, they discovered that dust had an influence on solar energy performance when it was outside the solar panels. In the case of dust, the data suggest that the collector lowered thermal efficiency by 13.4 percent. The maximum electrical efficiency was obtained in the absence of dust on the collector at 10.24 percent, while in the presence of dust, the electrical efficiency was recorded at 5.67 percent. Whereas the overall efficiency of the hybrid collector decreased by 17.5% in the case of dust compared to the clean collector.

Figure 2.4. Collector (PV/T) in case of dust [18].

Slimani et al. [19]: A numerical comparison study was conducted to compare four PV module configurations (PV-I), standard hybrid PV solar system (PV/T-II), single-pass glass solar collector (PV/T-III), and double-pass glass solar collector (PV/T-IV). The model was created and confirmed using numerical data, which shows that the four-module solar collector does have a total daily efficiency of 29.63 percent, 51.02 percent, 69.47 percent, and 74 percent, with an air flow rate of 0.023 kg/s.

Ahmed and Mohammed [20]: The experiment was carried out on a dual-path solar air collector (PV/T) using porous material. According to the study, porous material enhances heat transmission, which increases thermal efficiency as well as the temperature exiting the collector for the air. They have discovered a 3% improvement in composite efficiency whenever the porous material was utilized in the channels, as illustrated in Figure 2.5. The daily heat and electricity efficiency achieved for the collector with a cover glass and a porous medium were 80.23 percent and 8.7 percent, respectively. They were distinguished by outstanding thermal efficiency and everyday electrical efficiency. The results of the verification without the porous medium as well as glass cover revealed that the compound's efficiency is 51.25 percent and 10.91 percent, respectively. The study also found that increasing the flow rate improves thermal efficiency.

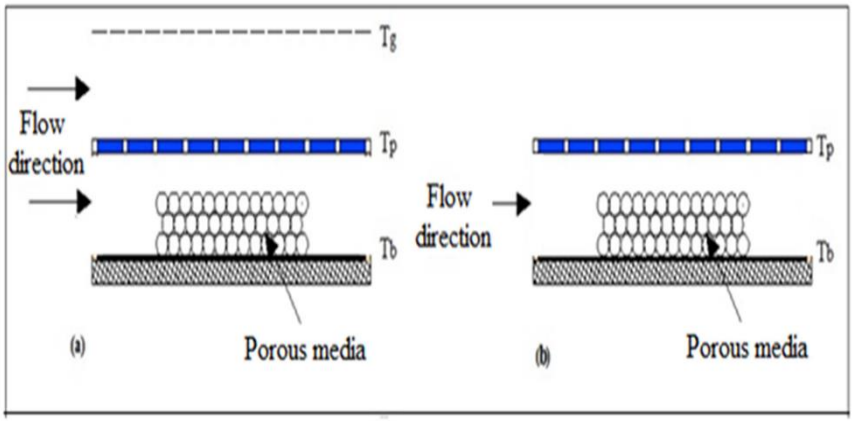

Figure 2.5. Diagram of a hybrid solar collector (PV/T) in the case of porous media [20].

Kasaeian et al. [21]: The effect of imposed load on the effectiveness of a single-pass PV/T antenna system was investigated by the researcher. As indicated in Figure 2.6, select four fans to produce a forced load. The study discovered that decreasing the channel depth boosts thermal efficiency while ignoring the influence on electrical efficiency. When the air mass flow rate is increased, the thermal efficiency increases, as does the electrical efficiency slightly. The thermal efficiency was measured at 0.05 m depth and flow rates ranging from 10.08 l/min to 3.6 l/min. 15 percent - 31 percent, while electrical efficiency was 12 percent - 12.46 percent.

Figure 2.6. Hybrid solar collector (PV/T) [21].

Omer and Zala [22]: An experimental setup and a simulation investigation were created for this aim to anticipate electrical and thermal performance. The actual and theoretical findings for the air temperature departing the PV/T hybrid composite as well as the cell temperature agreed well. When the liquid mass rate rises from 0.024 to 0.057 m^3/S , the electrical efficiency (20%) as well as thermal efficiency (44%), respectively, rise. Energy is affected by changes in solar radiation and reaches its peak around midday before declining. According to the findings, the air temperature leaving the vitrified collector is approximately 7% greater than that of the unglazed collector. In terms of everyday efficiency, it has the greatest value.

Lenin et al. [23]: In southern India, there are two types of hybrid PV/T thermal collectors. for enforced and natural air flow through wooden ducts attached to the collector from the back were examined. When forced load electricity is employed, this is what happens. Thermal efficiency was 23.71 percent and electrical efficiency was 13.56 percent, respectively. Thermal and electrical efficiency were 7.33 percent and 11.41 percent, respectively, under normal use.

Sang-Myung Kim [24]: The thermoelectric collector was designed in this research, as well as the thermal and electrical performance, as well as the specifications of the air-dependent photovoltaic collector, were measured. The collector includes curved circular heat sink plates that optimize the air flow pattern, and it has been designed to increase thermal performance. The electrothermal performance of the air-operated PVT collector was investigated experimentally under the same conditions. Increased air flow to the PVT collector has a substantial impact in terms of thermal efficiency. Thermal effectiveness rose from 29 to 42 by increasing the flow rate from 60 to 200 m^3/h and assuming an average radiation of 950 W/m^2. Electricity efficiency was also studied because it increased under the same operating circumstances as the PV/T complex. This study is shown in the following Figure 2.7:

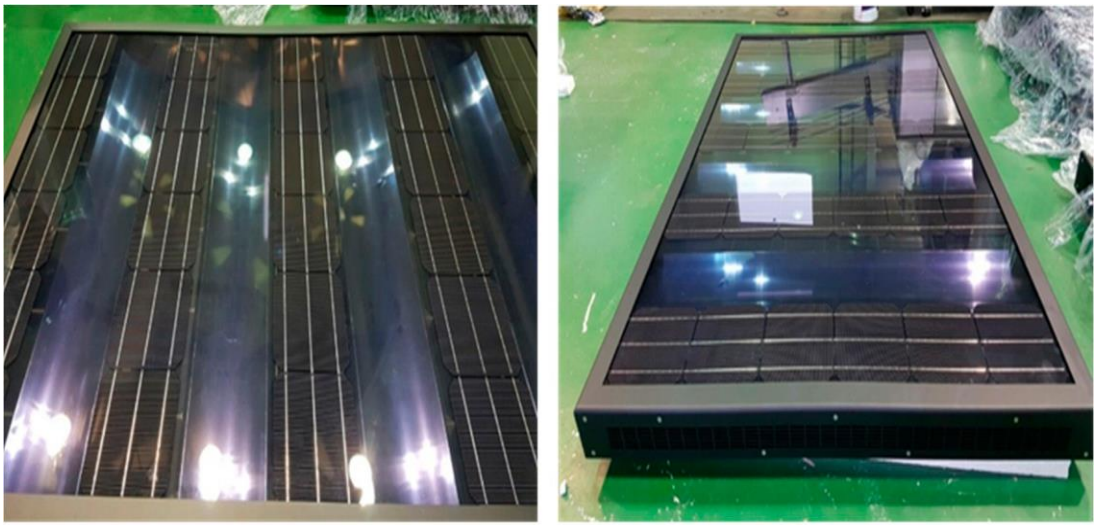

Figure 2.7. Designed PVT collector [24].

Choi and Choi [25]: A hybrid solar air collector's thermal and electrical properties (PV/T) are studied using an experimental design. This system has a twin channel and a single pass. To boost heat transfer rates, an uneven cross rib is inserted on the rear surface of the solar cells. The studies were carried out in a realistic environment with various air mass fluxes ranging from 1.188 l/min to 4.618 l/min . They concluded that average thermal efficiency improved by 32.2 percent -56.72 percent and average electrical efficiency increased by 14.81 percent _14.23 percent. This study is shown in the following Figure 2.8:

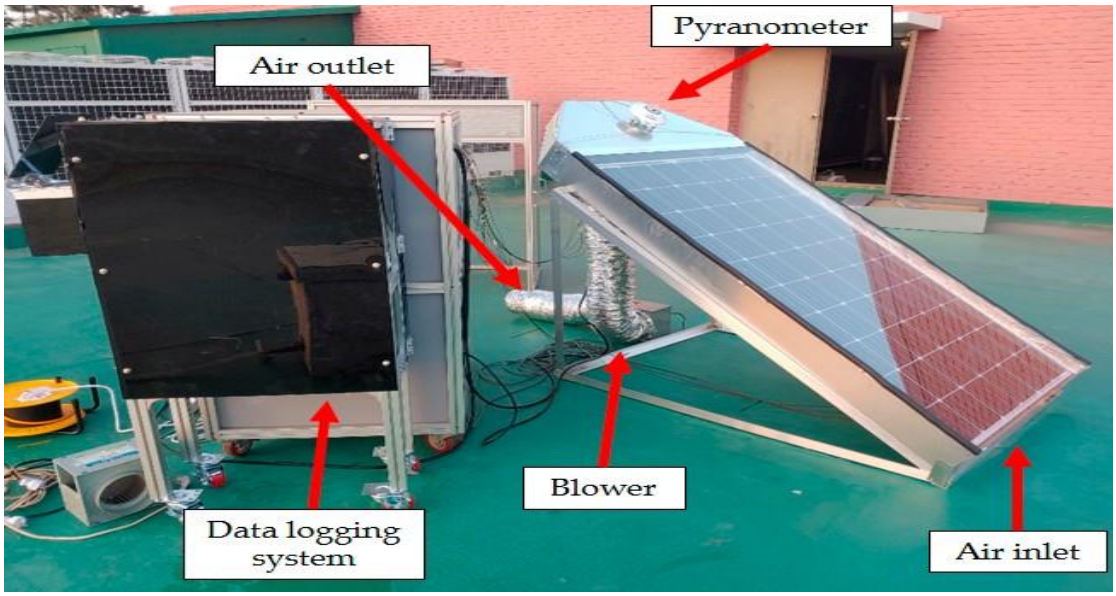

Figure 2.8. Schematics of the experimental setup [25].

Jong-Jun-Tae Kim [26]: In this work, the researchers created a PV/T antenna array with curved baffles to test the thermal and electrical efficiency from the outside. Using the TRNSYS simulation system to predict annual review based on the design characteristics of the PV/T complex as well as experimental evidence, it was discovered that the thermal and electrical mal efficiencies of the newly developed PVT complex were 37.1 percent and 6.4 percent (by unit area), respectively, and that comparing the experimental and simulation results revealed a 4 percent and 0.24 percent error between thermal and electrical efficiency. The yearly solar radiation gain was 644 kWh/year, while the output energy was 118 kWh/year.

2.2.2. Research related to PV/T Water Collectors

Chow [27]: It has been found to be suitable for warm temperature applications by Applied Energy. The PV/T system helps decrease collector heat loss. When solar cells operate as a heat absorber, as well as when a windshield is added, heat loss is reduced even further, but reflecting losses rise. A new design is being researched and developed. Water collector in the form of a flat box for polycrystalline PV modules. Aluminum alloy is used to make and test the heat sink. The findings concerned strength performance. He discovered a thermal efficiency of around 40%, which is roughly 0.8 for a traditional solar heat collection device. The new energy system has better efficiency than the previous system.

Othman [28]: Simulation revealed that numerous design elements and operational circumstances influence the effectiveness of hybrid PV/T. As a result, seven of the combinations are tailored to sorption complexes. A well-absorbed design with great efficiency was also evaluated, contrasted, and simulated (total efficiency). The mathematical system examined a variety of characteristics, including solar radiation, flow rate, and air temperature, and decided that the collector should be a heat collector with a flat plate and a glass plate. Through mathematical research, it was discovered the helical flow design was found to be the most efficient, with a maximum thermal efficiency of 50.12 percent and an electrical cell efficiency of 11.98 percent.

Andrew [29]: Two types of thermal photovoltaic (PV/T) cells (type A and type B) were constructed and tested in the Singapore climate (NUS). Type A PV modules feature monocrystalline Si cells and employ a paper tube type thermal collector, whereas type B PV modules do not. The photovoltaic module is made up of polycrystalline solar cells as well as a parallel thermal collector. Experiments were carried out under everyday settings at mass flow rates ranging from 1.8 l/min to 3.6 l/min. According to the results, the average thermal as well as photoelectric effectiveness of type A is 40.7 percent and 11.8 percent, respectively, while type B is 39.4 percent and 11.5 percent. The average photovoltaic effectiveness of PV/T modules is found to be around 0.4 percent higher than that of a standard PV module.

Rahou et al. [30]: The design and testing of solar roofing systems to enhance electricity efficiency and supply on-site hot water applications are covered in this study. These systems are made up of an ordered succession of amorphous solar cells with an oscillating flux linked by glass wool from the bottom of the photovoltaic panel. With a combined efficiency of 70.53 percent to 81.5 percent, the PV/T collector is fitted for a portable solar tracker that can be de for example, mass flow rate and signed to expose to the greatest amount of radiation with changing variables such as mass flow rate and solar radiation.

Jee Joe Michael [31]: This study describes research on an aqueous PV/T compound created by laminating solar cells over a copper heat absorber. This adjustment lowered thermal resistance by 9.93%, improving heat transmission from solar cells to liquid. The water was sent through a canal that was linked to an open tank. Experiments were carried out with and without glass, at various mass flow rates and steady circumstances, as well as with convection, absence, as well as thermal stress tests. With verification and a mass flow rate of 6 l/min for the PV/T collector, the overall efficiency was 87.52 percent.

Al-Shamani et al. [32]: The job was completed outside under Malaysia's climatic conditions. The key constraints that drove the creation of heat transfer fluids were the low conductivity of the working fluids, that saves energy, and the greater collector performance. The PV/T complex's intentions include a pipe absorber in the shape of

a rectangle attached to the bottom of the photovoltaic unit, made of (stainless steel material, 15 mm height, 25 mm width, and 1 mm thickness) to promote heat transfer with high heat conductivity. This new generation of heat exchangers is known as nano fluids, and it improves heat transfer capabilities in PV/T complexes by employing materials such as (SiO2-TiO2-SiC). The results were for the PV/T complex. The nanofluidic-containing (SiC) compound has a flow rate of 10.2 l/min. The overall efficiency was 81.73 percent, with an electrical efficiency of 13.52 percent. with a radiation intensity of 1000 W/m^2.

Hussein et al. [33]: The researcher investigated the photovoltaic cell's performance in Iraq, where the temperature is scorching. Figure 2.9 shows an example of active cooling technology, which is a tiny heat exchanger with tubes that circulate water Variances in radiation mostly affect power generation, whereas temperature differences affect the electric motor. When cooling is employed, the temperature drops from 76 to 70. With a mass flow rate of 2 l/min, electrical efficiency has grown by 6.5 percent, and thermal efficiency has increased by 60 percent. When he employed nanoparticles (Zn-H2O) at a concentration of 0.3 percent and a flow rate of 2 l/min, the temperature dropped by 58 degrees Fahrenheit, and the electrical efficiency increased by 7.8 percent. The increased power was due to the greater temperature.

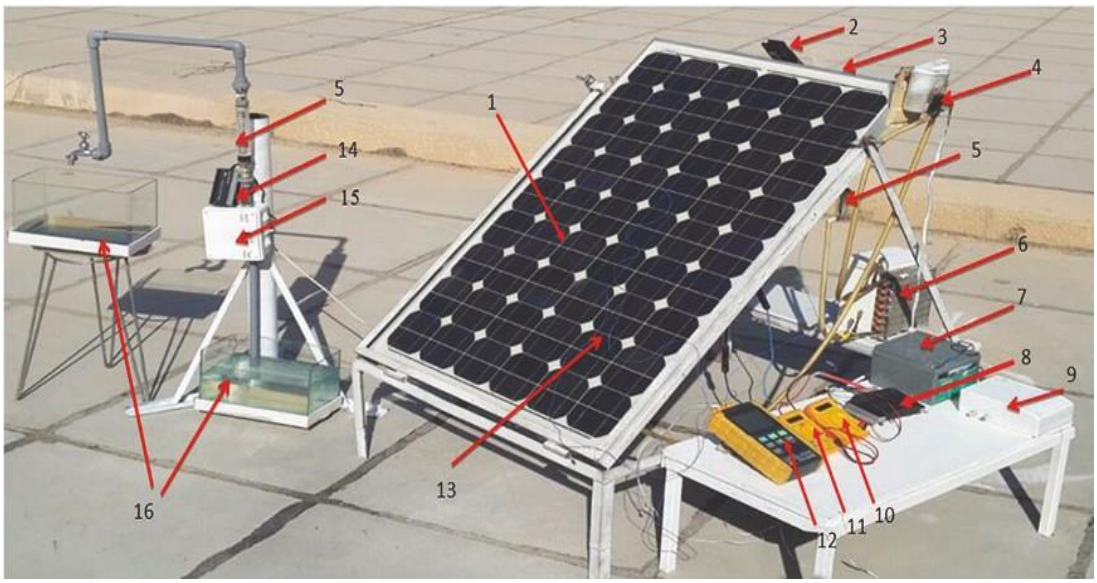

Figure 2.9. Hybrid solar collector (PV/T) using a heat exchanger [33].

Sachit et al. [34]: Because traditional flat-panel solar collectors are a crucial component of PV/T systems, our research focuses on their development. When employing liquid as a heat transfer medium to extract amounts of usable heat from the rear surfaces of solar cells, new design concepts developed in Figure 2.10. Traditional PV/T complex design and PV/T system total performance, particularly electrical and thermal efficiency assessment. The findings revealed that the novel hybrid solar collector designs PV/T system total performance, particularly electrical and thermal efficiency, may be increased.

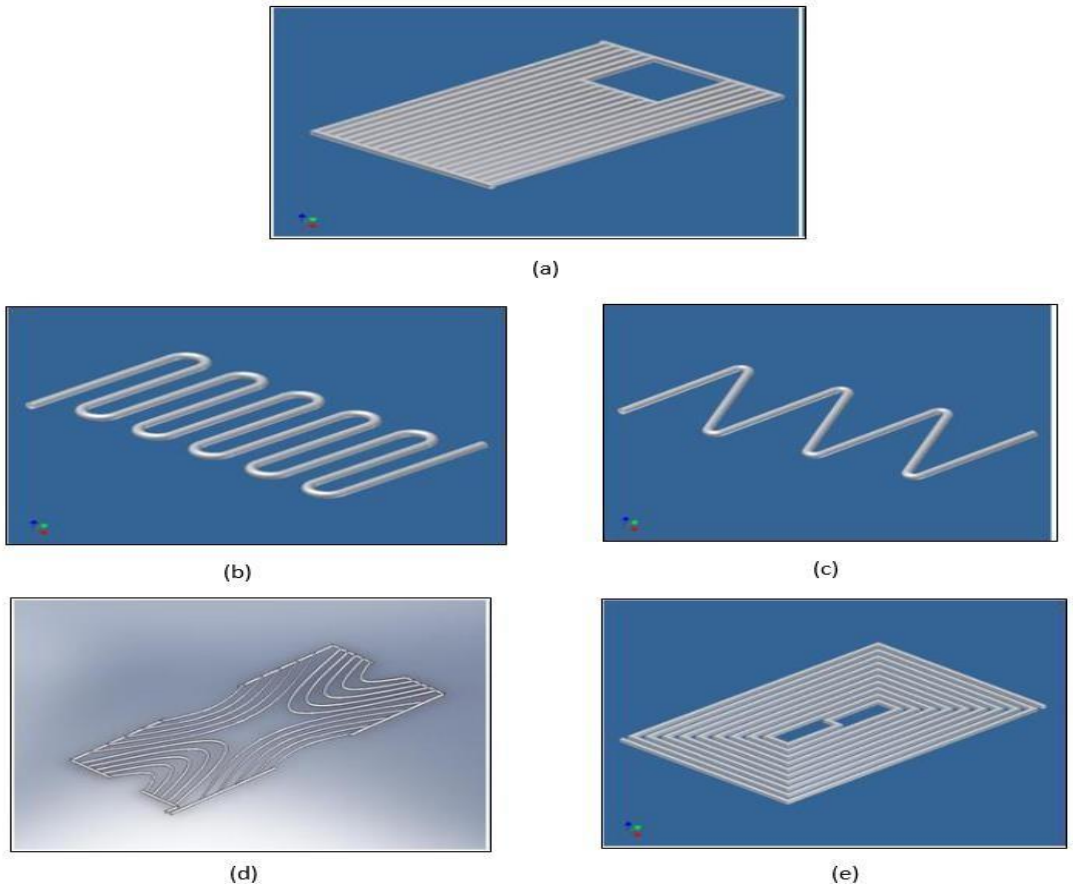

Figure 2.10. a) Direct flow design (b) Oscillatory Flow Design (c) Serpentine Flow Design (d) Web flow design (e) Spiral Flow Design [34].

Abdulrasool [35]: This study employs an indoor solar system simulation test to evaluate the performance of a water jet-powered solar photovoltaic thermal PV/T collector. At previous levels of solar radiation, the mass rate changes from 0.033 to 9.6 l/min as the radiation level increases from 500 to 1000 W/m^2. The coefficient of heat transfers between the solar panel and the cooling medium was calculated.

discovered using water jets at their maximum temperature. At 1000 W/m2 of solar energy, the PV/T efficiencies with jet impingement were 72 percent, 11.35 percent, and 81 percent. There was mathematical agreement with the experimental model in the creation of colliding jet aircraft. This resulted in photovoltaic as well as thermal efficiencies of 95.8 and 99.6 percent, respectively.

Weiqi, et al. (2018) [36]: The researchers carried out experiments in this study to determine and evaluate the performance of PV/T based on certain water pipes with PV/T based on micro-channel heating tubes (MHPA) and standard PV modules with high outside temperatures PV/T cell temperature on average based on hydroponic tubes, micro channel PV/T cells, and standard PV modules was discovered to rise in the morning and fall in the afternoon. It almost got to 70° C. The electrical efficiency dropped with rising photovoltaic temperature for the three systems at 70, 90, as well as 100 °C, respectively, falling from 11.2 percent to 10%, 9.6 percent to 7.7 percent, and 8.6 percent to 7.0 percent. PV/T stands for power from the mains. Using MHPA, it can increase photovoltaic and photovoltaic/T cell performance PV/T-based water-based pipe performed better than PV/T-based MHPA-based pipe.

Ahmad et al [37]: It is named photovoltaic thermal because it is built on the foundation of merging solar energy technology with photovoltaic cells (PV/T). Because the effectiveness of photovoltaic cells declines with rising temperature, the solar collector cools the cells while also enhancing the overall efficiency of the system. PV/T tests were carried out to evaluate the performance of the PV/T system. The outcom the system's overall efficiency PV/T tests were performed to assess the performance of the PV/T system.es were as follows: The PV/T water collector's efficiency ranged from 28.5 percent to 85 percent and from 6.8 percent to 14 percent, respectively.

Mohd, et al [38]: In this experiment, solar radiation was converted into electrical and thermal energy using photovoltaic panels and a photovoltaic/thermoelectric collector. The test was carried out on a PV/T complex with mass flow rates ranging from 0.72 l/min to 1.53 l/min. Water flows into the PV/T collector via convection by absorbing stainless steel aids in heat transmission. With rising radiation, production rises. The

effectiveness of PV/T changes with radiation intensity. An energy plus stress study was performed. The overall power output was compared to the power output of the PV panel without absorption. For 700 W/m^2, the electrical power grew by 22.48 percent, whereas for 900 W/m2, it climbed by 20.87 percent.

Hussein [39]: This study describes the design of a water-based PV/T, as well as the performance assessment and hot water generation as well as performance evaluation under Oman's weather circumstances. This report concentrated on the electrical as well as system performance over the course of three days of examination. The findings were that changes in ambient conditions and solar radiation influence both PV panels and PV/T collectors that are standard. The PV/T combination demonstrated better electrical performance during screening, but traditional PV efficiency remains unchanged. The electrical power and voltage of the system peaked at around 67 WP and 18.9V, respectively. Furthermore, the PV/T panel's average power was 6% higher than that of a traditional PV panel.

Abdullah and Sachit [40]: This project involves the creation of PV/T designs. Water performance depends on PV/T Collector identification based on the comparison of different forms of sorption complexes. The fluids used in PV/T systems can be used to classify them. The absorption design features were created by the researcher. There were two forms of suction used: 1.water flow tube and channel, and 2. exposed or covered glass design components. However, the spiral suction design provides the best performance. The thermal efficiency of the exposed collectors was reduced in a prior study. The uncovered PV/T collectors have a high electrical efficiency because of heat loss from the top surface

Qiongwan et al [41]: A highly detailed explanation of the dynamic phases of the PV/T flat-panel collector was used in this investigation, so that the uneven distribution of radiation had a substantial influence on photovoltaic efficiency but only a little impact on photo thermic efficiency. The shadow shifted from 0% to 80%, and the solar efficiency declined by 42.26 percent while the thermal efficiency improved by 9.81 percent, indicating that the mass flow rate impacts the thermal performance more and more strongly than the photovoltaic efficiency. When the

mass flow rose from 0.3 l/min to 1.8 l/min (and the speed for the copper tube increased from 0.0112 m/s to 0.0674 m/s), the photovoltaic efficiency climbed from 9.46 percent to 9.54 percent, and the optical efficiency increased from 32.62 percent to 35.83 percent.

Ganiyu et al. [42]: The experiment was conducted in Ghana in a dynamic environment to analyze the water flow rate of a PV/T system while considering the effect of flow rate and radiation on the PV/T performance. As the mass flow rate increases, so does the temperature and the electrical efficiency, and vice versa. Radiation, on the other hand, reduces electrical efficiency by raising the temperature of the cell.

When a high mass flow rate is combined with constant radiation, heat gain increases while water temperature decreases. Increased radiation at a constant flow rate thus improves thermal efficiency and output temperature. The maximum flow rate that does not exceed what is expected to determine the cooling improvement is (3.78 l/min). The electrical efficiency of the PV/T system was approximately 12.75% with a flow rate of 1.98 l/min and variable irradiance. PV/T Efficiency.

It is less efficient than conventional PV for radiation below 790 W/m^2. Was electrical efficiency (13.0-12.75% for radiation ranging from 710-790 W/m^2), but heat gain can be used for higher radiation (>790 W/m^2). • The thermal efficiency represents an average value for other experimental PV/T systems because commercial energy efficiency is typically greater than 50%, indicating that it can compete with discrete solar heating system installations.

Hazim et al. [43]: In this numerical analysis, a cooling mechanism was added to the solar panel in addition to modeling to tackle the problem. As a result, the advantage of solar cell cooling is that it improves electrical efficiency while also allowing heat gain in the form of liquid heating. At ambient temperature, the modeling results reveal that the heat collection channel pipette has a maximum electrical effectiveness of 14.6674 percent and a maximum thermal efficiency of 82.532 percent (27The flow rate (1-5) L/min increased (1 l/min). When solar radiation increased by 100

(W/m2) between 300 and 1000 (W/m^2), and the contact area between photovoltaic cells were very efficient.

Yingbo Chao & Yang [44]: This research proposes a new cooling system that will boost solar radiation and mass flow rate. As demonstrated in Figure 2.11 a-b, the coolant is guided towards an aperture with an optimal diameter of 0.005 m. When solar radiation increases from 300 W/m^2 to 1200 W/m^2, thermal and electrical efficiency decrease by 0.11 and 0.25 percent, respectively, for every 100 W/m^2. Furthermore, every 0.06 l/min increase in intake mass flow rate increased thermal and electrical efficiency by 0.086 and 0.92 percent, respectively., respectively (inlet mass flow rate varied from 0.12 to 1.2 l/min). The total efficiency of the new cooling duct is approximately 4% greater than that of the conventional duct for solar radiation and inflow mass flow rate.

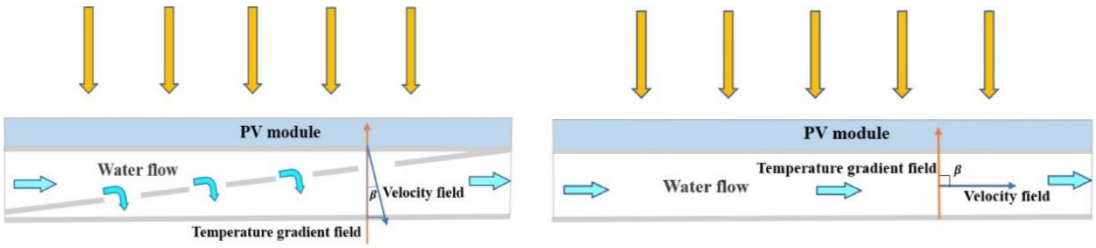

(a) PV module with new cooling channel (b) PV module with conventional channel

Figure 2.11. Analysis and comparison of two kinds of cooling channels [44].

Rachid [45]: An integrative thermal model of the PV/T complex is dependent on water, a tedlar layer, and parallel water in tubes in this experiment. The simulation emphasized the suggested model's coherence: First, when the solar radiation changes, the product of the water temperature increases quicker than the temperature falls; the design of the insulator is an essential parameter that has an influence. The higher the water outlet temperature, the thicker the insulator, although a thickness larger than 0.14m is not necessary since the power loss remains constant. The thermal efficiency increases as the wind speed decreases. Increasing the finite mass flow rate improves thermal efficiency. As wind speeds escalate from 1 m/s to 5 m/s, thermal efficiency falls from 70% to less than 40%.

2.2.3. Research Related to Water and Air Complexes PV /T

Jie Ji [46]: The experimental results in this article were consistent. The relative errors for thermal and electrical efficiency for photovoltaic/air heating are less than 2.6 percent and 8.2 percent, respectively. The standard deviations for electrical and in the PV/water heating mode, thermal efficiency is less than 3.1 percent and 6.7 percent, respectively: At zero degrees, the thermal efficiency of photovoltaic/air heating decreases, and then when:

- The temperature drops from 42.9 percent to 37.7 percent, and the total heat increases with an increase in the collector's loss factor from 4.96 to 5.93 Kelvin sq m/s, but with an increase in airspeed from 1 to 4 m/s.
- For thermal and electrical efficiency, the recommended air flow rate is 0.02 kg/m 2 (this establishes a balance between both the thermal system and temperature rise) .
- The daily thermal efficiency of photovoltaic/water heating falls as wind speed increases. However, it has little impact when the speed is high 5 m/s. Thermal performance at the lower temperature is zero, or 35.0 percent.

Mojumder et al. [47]: It is proposed to use a single-pass PV/T complex single-pass antenna system for performance analysis. The heat dissipation assembly consists of several thin rectangular fins connected by a flat metal plate. Using the energy balance equations, an analytical expression is obtained for each component of the design. The temperatures of the top and bottom surfaces of solar panels, as well as the temperatures of the rear surfaces and the entrance and exit of the collector, were measured experimentally using different fins (0-4 fins), air mass flow rate (1.2 - 8.4 l/min), as well as solar radiation (200 - 700 W/m^2). The maximum electrical and thermal efficiency were 13.75 and 56.19 percent, respectively.

Su et al [48]: The temperature of the water exiting the dual-channel PV/T collector varies with the ambient temperature. As solar radiation increases, thermal power and efficiency increase, while overall efficiency remains roughly constant at 80-83 percent. Figure 2.12 a b c d shows that in the water-to-water case, power reached a

maximum of 978 Watts at 12:00, and thermal efficiency reached a maximum of 64.4 percent at 14:00. Water-cooled PV/T complexes the best electrical and thermal performance was demonstrated. When the mass flow rate of water is 9 l/min, increasing the rate of water flow and the aspect ratio between the upper and lower tubes increases electrical efficiency and overall efficiency to 7.8 and 84.2 percent, respectively. When the ratio was 3:1, the electrical and total efficiency were 7.8 and 83.4 percent, respectively.

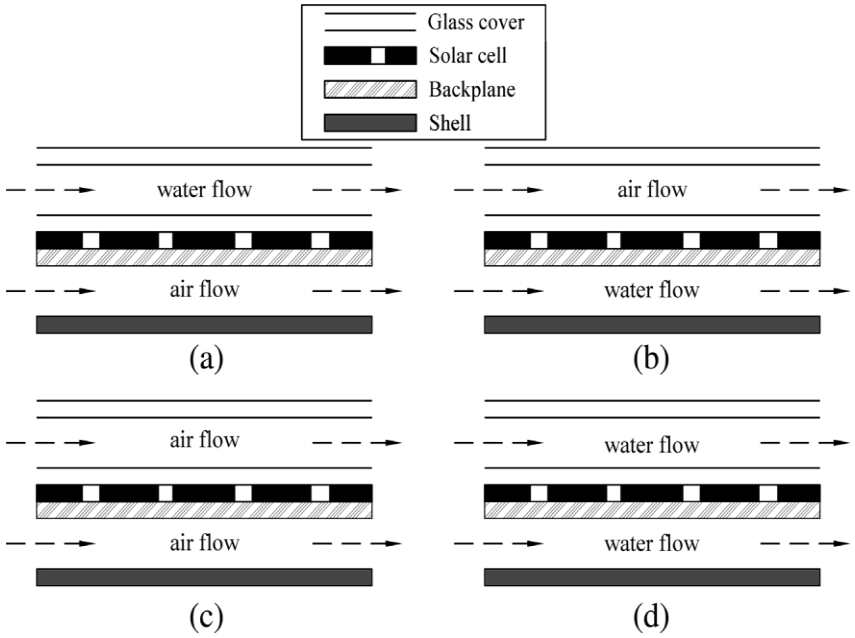

Figure 2.12. The PV/T collector with dual channels for different fluids [48].

Husain and Kim [49]: It comprises a performance assessment analysis of two PV/T system modulations, Glass to Glass and PV to Glass, which use a dual-liquid heat exchanger to cool the solar cell using water and air. As well as performing energy balance calculations utilizing MATLAB software using PV/T system These two arrangements work concurrently and produce more electrical output than heat output. Overall efficiency for thermal and electrical installations from glass to glass were 14.31 percent and 52.22 percent, respectively, throughout the year, while for glass to PV they were 13.92 percent and 48.25 percent, respectively.

PART 3

RESEARCH METHODOLOGY AND THEORETICAL WORK

3.1. CHAPTER OVERVIEW

This chapter describes the methodology and the theoretical analysis, the numerical method and new models utilized to achieve the research objectives. The whole of the numerical investigation is included into two models of PV/T collector. The simulation analysis was carried out using the ANSYS FLUENT 17.0 software and various PV/T collector modules. The CFD simulation is used to forecast collector performance for cooling PV panel under the effect of changing the geometrical collector dimensions on the shape of the bulges and the water flow rate conditions The final section discusses collector thermal performance, which is typically expressed as useful heat output in relation to its surroundings as a function of input radiation and collector operating temperature.

3.2. RESEARCH METHODOLOGY

The flow chart in Figure 3.1 depicts the research topology sequence used in this study. A more detailed explanation of the experimental work will be provided later in Chapter 4. The numerical implementation combined the two methods used in this study. The two approaches contain; the first part included firstly, to draw of the collector geometry for different shapes of bulges. Secondly, to simulate these models of different. The theoretical approach was adopted to simulate the designs of thermal collectors to investigate the effect of heat on photovoltaic panels before and after they are cooled with water by means of a PV/T collector installed on the back of the cell.

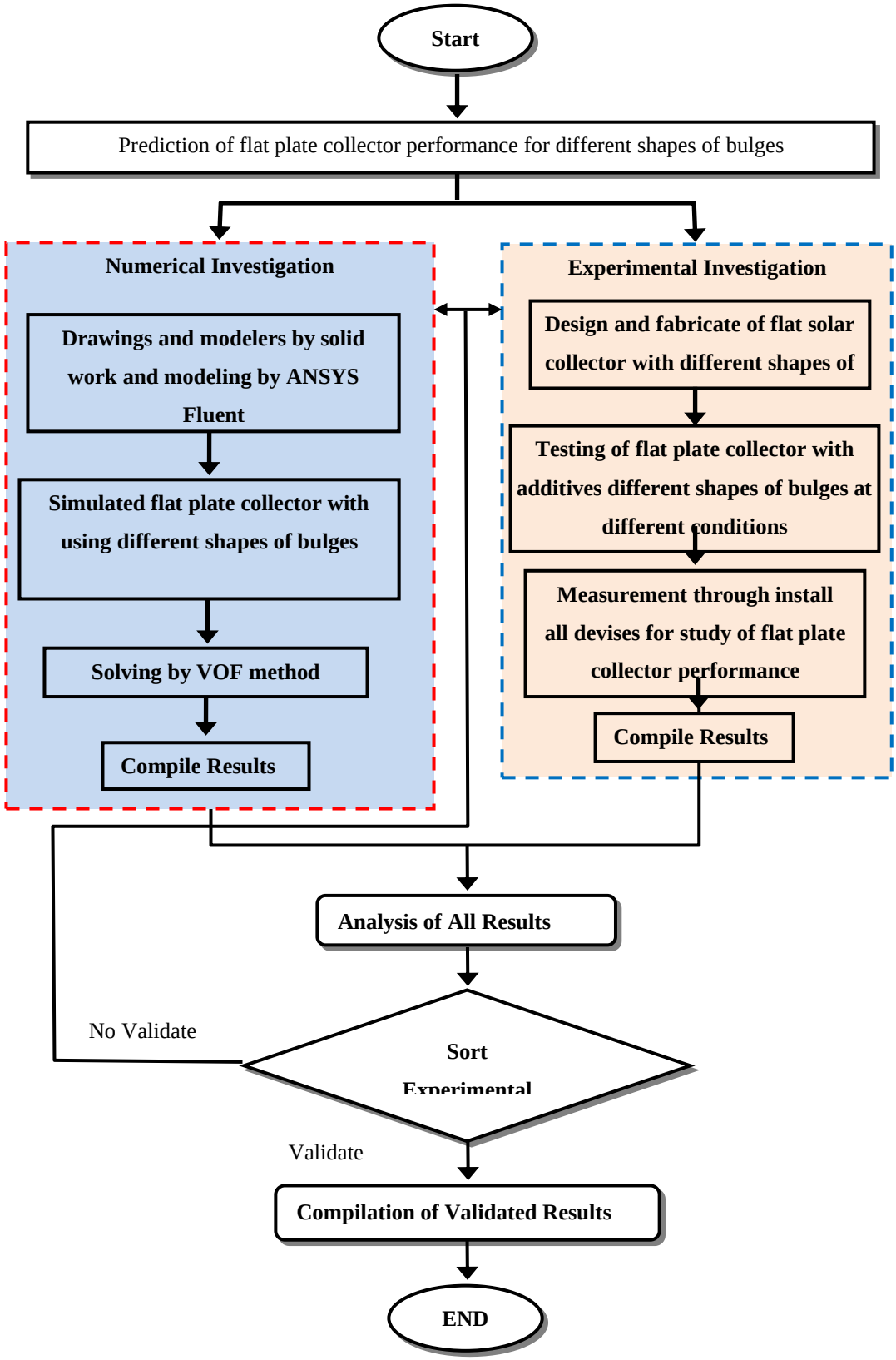

Figure 3.1. Sequence of research methodology flow chart.

3.3. CFD SIMULATION OF FLAT SOLAR COLLECTOR

For engineering applications, CFD simulation techniques are a powerful tool for modeling mechanical problems and analyzing their physical phenomena. The radiation model pre-processing tool in the commercial CFD software ANSYS 17.0 FLUENT was used in the current simulation (provides a solar load model for calculating radiation effects from sun rays entering a computational domain) sold work ver. 2019, was used to model, the two types of solar flat collector. To run the simulations, several steps must be completed; these steps are depicted in Figure 3.2.
In sold work, the modeling is completed, and the resulting mesh is imported into the FLUENT Radiation Module for solution and post-processing as a solar collector problem. Based on the research objectives, this simulation is divided into two flat plate collector PV/T models. A benchmark comprehensive numerical model to simulate the PV/T was developed to predict the thermal-hydrodynamic behavior of the system. The model's solution procedure was accomplished through computational coding in the ANSYS environment. The models' results were validated by comparing them to experimental measurements.

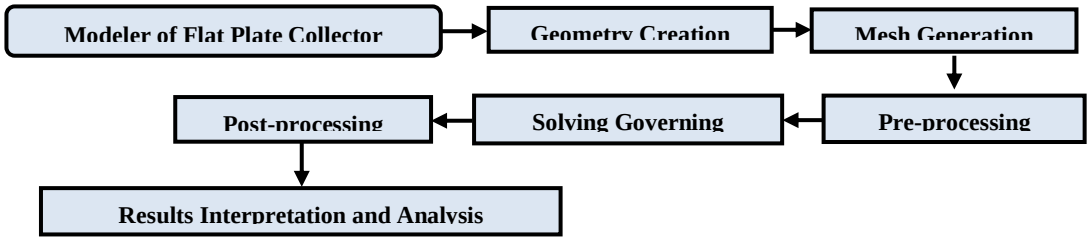

Figure 3.2. Simulation steps in ANSYS 17.0

3.3.1. Pre-Processing of Flat Solar Collector

CFD program is used to show the thermal loads distribution for various shapes and parameters, such as inlet and outlet water temperatures and temperature distribution on the collector surface. Preparing a computational domain is the first step in CFD simulation. Model-CC and model-SS are 3D-dimensional flat plate collector models created in Solid work software. The dimensions of collector’s geometry are taken from experimental setup and is shown in Table 3.1. The geometrical models of PV/T

are shown in Figure 3.3. These collectors are designed with a different bulge, cubic and sphere. The dimension of the collector is (600×1100×30 mm). The water inner and outer pipe diameters of the collector are 13 mm. Two shapes of aluminum bulges with 120 pieces are used. The first shape is cubic at dimensions 15×15×15 mm, while the second shape is a sphere at diameter 25 mm.

Table 3.1. Dimensions of PV/T models.

Model	Parameters
Model -SS	Collector dimension (600*1100*30mm)
	Bulge shape (sphere)
	Bulge No.(120PCS)
	Bulge dia.(25mm)
Model -CC	Collector dimension (600*1100*30mm)
	Bulge shape (cubic)
	Bulge No.(120PCS)
	Cubic length (15mm)

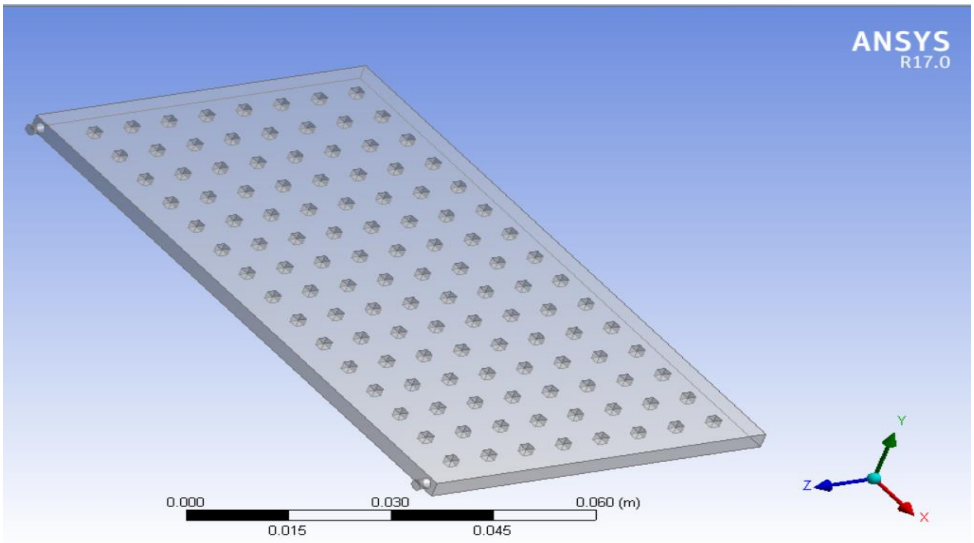

(a) Model-CC

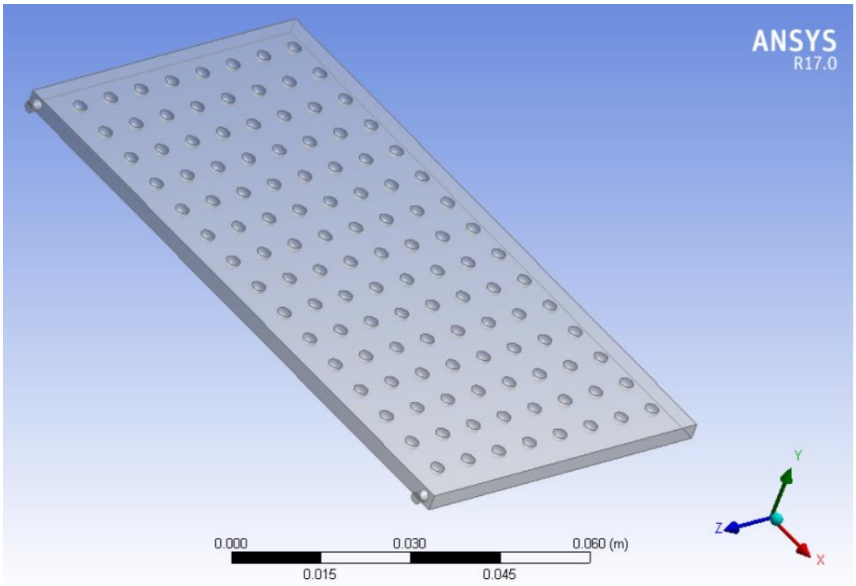

(b) Model-SS

Figure 3.3. Computational domain prepared of Flat collector; (a) model-CC, and (b) model-SS.

3.3.2. Computational Grid

One of the most important steps in CFD is the creation of the mesh structure which is made up of computational cells. In computational cells, the governing equations are solved. Unstructured meshing is used to mesh the collector domain with tetrahedral elements. Because of the complex geometry, an unstructured tetrahedral meshing was chosen. A mesh independent solution is recommended for removing the influence of mesh size. When the mesh size has no effect on the solution, the optimal mesh size is chosen.

The 3D meshed geometrical flat solar collector model is shown in Figure 3.4 It depicts the collector with (a) coarse, (b) medium, and (c) fine mesh. Figure 3.4 shows a closer look at the meshed bulges in the collector (d). The fine meshing scheme produced the most accurate and comparable results for heat transfer inside the collector, velocity, and temperature distribution behavior under influence of a bulge shape. As a result, the fine mesh was chosen for the simulations and result interpretation. Model-CC had 96914 nodes and 564314 fine mesh elements, respectively. While fine mesh nodes and elements for Model-SS were 94844 and 523711, respectively.

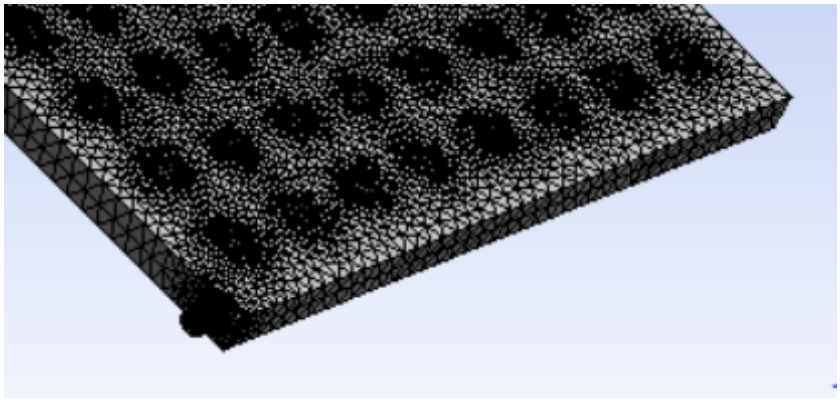

(a) Coarse mesh

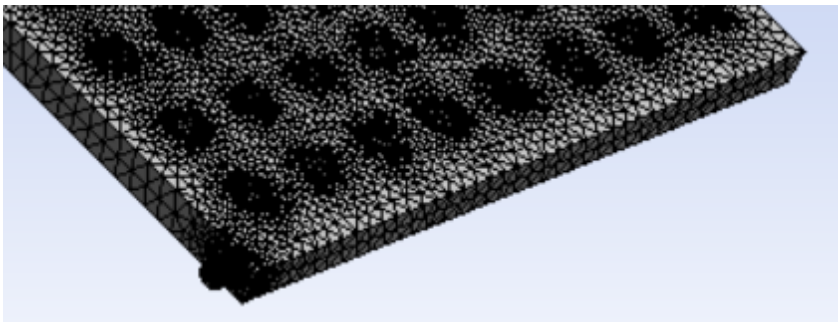

(b) Medium mesh

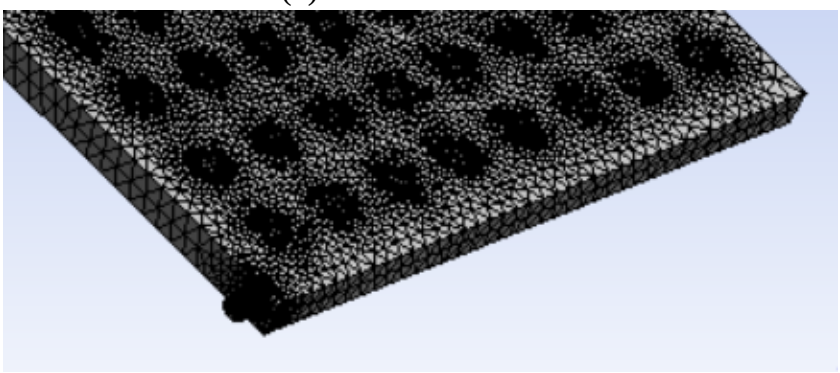

(c) Fine mesh

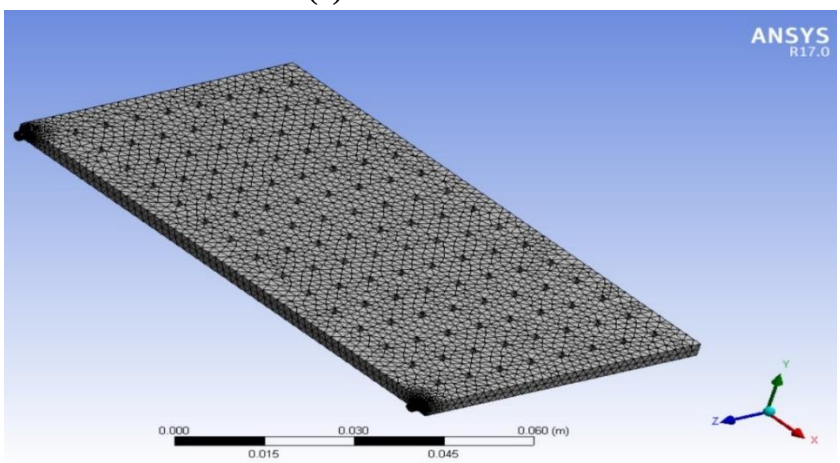

(d) Close view of bulge shape

Figure 3.4. Flat plate collector geometrical mesh model. (a) Coarse mesh, (b) Medium mesh, (c) Fine mesh, and (d) a close-up of the bulge shape.

3.3.3. Solving Governing Equations

- Under turbulent and steady conditions, the PV/T model and domain were simulated in three dimensions. In 3D Cartesian coordinates, the governing equations of continuity, Navies-Stocks, and thermal energy are as stated in equations [50].
- The continuity equation is obtained by expressing each term in terms of velocity components.

$$\frac{\partial \rho}{\partial t} + \frac{\partial}{\partial x}(\rho u) + \frac{\partial}{\partial y}(\rho v) + \frac{\partial}{\partial z}(\rho w) = 0 \tag{3.1}$$

- Momentum equation.

$$\rho \frac{D\vec{V}}{Dt} = \rho \vec{g} - \nabla \vec{P} + \frac{1}{3}\mu \nabla\left(\nabla . \vec{V}\right) + \mu \nabla^2 V \tag{3.2}$$

- Energy equation.

$$\rho c_p \frac{DT}{Dt} = \nabla . k \nabla T + \beta T \frac{DP}{Dt} + \mu \emptyset \tag{3.3}$$

β is the thermal expansion coefficient, which is defined as

$$\beta \quad = \frac{1}{\rho}\left[\frac{\partial \rho}{\partial T}\right]_P \tag{3.4}$$

And the dissipation function ϕ is associated with frictional energy dissipation. It is critical in high-speed flow and for extremely viscous fluids [51]. ϕ is given in Cartesian coordinates by:

$$\emptyset = 2\left[\left(\frac{\partial u}{\partial x}\right)^2 + \left(\frac{\partial v}{\partial y}\right)^2 + \left(\frac{\partial w}{\partial z}\right)^2\right] + \left[\left(\frac{\partial u}{\partial y} + \frac{\partial v}{\partial x}\right)^2 + \left(\frac{\partial v}{\partial z} + \frac{\partial w}{\partial y}\right)^2 + \left(\frac{\partial w}{\partial x} + \frac{\partial u}{\partial z}\right)^2\right] - \frac{2}{3}\left(\frac{\partial u}{\partial x} + \frac{\partial v}{\partial y} + \frac{\partial w}{\partial z}\right)^2 \tag{3.5}$$

3.3.4. Parameters Used in Simulation Analysis

The values of the input parameters, which are the temperature and the water mass rate, to the PV/T system are obtained from the flat solar collector measured data from the experimental model. Table 3.2 shows the experimental parameters measured at the PV/T's inlet and outlet, as well as on the collector surface. The numerical simulation was then performed for the same experimental conditions. The PV/T numerical simulation was successfully completed, and the results were compared to experimental measurements.

Using significant values of the same parameters, the effects of increasing temperature, water flow rate, and bugles shape on PV panel cooling were investigated further. The simulation variables are configured in Table 3.2. These parameters and variables were fed into the CFD simulation as inputs, and the output parameters were related to temperature distribution, pressure distribution, velocity gradation of tangential and vertical components and so on.

Table 3.2. Simulation parameters.

Model-CC		
	Description	**Initial-reference values**
Temperature (K)	**Water Flow Rate (l/min.)**	Density=1000 kg/m^3 Tamb =303 K
Tco = 303 to 357	1.5 l	Viscosity=1.0016 kg/m.s
Twin= 303 to 314	2.0	Solar intensity 24 to 1112 Watt/m^2
Two = 325 to 345	2.5	Gravitational acceleration
	3.5	for (z-axis) = -9.81 m/s^2
Model-SS		
Temperature (K)	**Water flow rate (l/min.)**	**Initial-reference values**
Tco = 303 to 357	1.5	Viscosity=1.0016 kg/m s
Twin= 303 to 314	2.0	Solar intensity 29 to 1112 W/m^2
Two = 325 to 345	2.5	Gravitational acceleration
	3.5	for (z-axis) = -9.81 m/s^2

3.3.5. Numerical Solution Setup

The high degree of coupling between momentum equations causes difficulties in solving swirling and rotating flows. that occurs when rotational terms have a large

influence. A large radial pressure gradient is created by a high degree of rotation, which promotes flow in both axial and radial directions [52]. The following setup is one solution technique that may be useful in swirling flow calculations:

1. "Pressure-Based" scheme and absolute velocity formulation were used as the solver type.
2. Selecting a k - epsilon model with RNG technique for turbulent flow; The near-wall treatment employs standard wall functions.
3. Fluid water for the PV/T interior and computational domain; upper collector cover made of solid aluminum; and cubic and sphere bulges beneath the collector cover are among the zone materials.
4. Table 3.2 describes the boundary conditions.
5. The solution method makes use of "Pressure - Velocity Coupling" with:
    - SIMPLEC scheme for skewness correction zero.
    - To solve the nonlinear momentum, energy, turbulent kinetic energy, and turbulent dissipation rate equations, spatial discretization employs a "Green - Gauss Cell Based" gradient for linearization, PRESTO pressure gradient scheme, and second order upwind
6. Solution controls:
    - For pressure, under - relaxation factors = 0.2, and
    - 0.5 for the remaining variables (density, body forces, momentum, turbulent kinetic energy, turbulent dissipation rate, and turbulent viscosity are all variables to consider. and energy are all variables to consider).
7. The solution begins with the Pressure, X, Y, and Z velocities, as well as k, epsilon, and temperature are all initialized, and the iteration process is repeated until convergence is reached. Finally, the results were represented graphically as contours, vectors, path lines, and XY plots.
8. When for each control volume, the maximum mass imbalance ratio is less than 0.01, the velocities and k-viscous are less than 0.001, and the energy is less than 10-6, the convergence criterion is met.

3.4. MESH INDEPENDENT

A suggested method for eliminating the effect of size of mesh was required then, and a mesh independent solution has been pursued. The optimum size of grid is chosen, where the solution isn't influenced via the size of grid. The highly precise and analogous out comes for the water velocities in the flow region, difference of temperature as well as surface of collector temperature beneath the effect of different values of water flow rates were determined via the fine mesh. Therefore, this fine mesh was chosen for performing the simulations in addition to the interpretation of result. For all domain, 2.0× 10^6 number of cells selected in all simulations according to grid dependency as shown in Figure 3.5

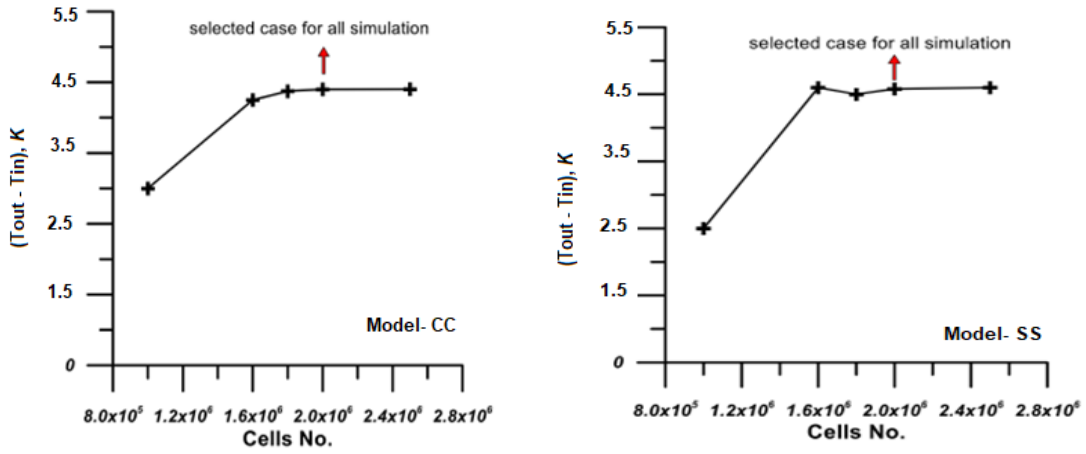

Figure 3.5 Cells selected for all simulation models.

3.5. PERFORMANCE OF PV/T COLLECTOR

3.5.1. Principle of Flat Plate Collector

The steady-state thermal efficiency (ήth) of a flat plate solar collector is calculated as [50]:

$$\eta_{th} = \frac{Q_u}{G} \tag{3.6}$$

Furthermore, the collected useful heat (Qu) is given by:

$$Q_u = \dot{m}Cp(T_o - T_i) \tag{3.7}$$

Q_u, It is simply the ratio of absorbed solar radiation to heat. losses:

$$Q_u = A_c F_r\left[S - U_L(T_{p,m} - T_a)\right] \tag{3.8}$$

Where,

$$F_r = \frac{\dot{m}cp}{A_c U_L}\left[1 - e^{\frac{A_c U_L F'}{\dot{m}Cp}}\right] \tag{3.9}$$

In Equation (3.9) *F* ‘is the collector efficiency factor calculated as follows:

$$F' = \frac{\frac{1}{U_L}}{W\left[\frac{1}{U_L[d_o + (W - d_o)F']} + \frac{1}{C_b} + \frac{1}{\pi d_i h_{fi}}\right]} \tag{3.10}$$

The collector's total heat loss coefficient is the sum of the top, edge, and bottom loss coefficients:

$$U_L = U_t + U_b + U_E \tag{3.11}$$

Edge losses are almost for a well-designed collector with a very low perimeter-to-area ratio, this is negligible [55]. The bottom loss coefficient, Ub, is calculated using the bottom insulator's thermal conductivity, ks, and thickness, Ls:

$$U_b = \frac{k_s}{L_s} \tag{3.12}$$

Thus,

$$U_L = U_t + U_b \tag{3.13}$$

The top loss coefficient equation, U_t as (Yeh et al., 2003):

$$U_T = \left[\frac{N}{\frac{C}{T_{p,m}}\left[\frac{T_{p,m}-T_a}{N+f}\right]^e} - \frac{1}{h_w}\right]^{-1} + \frac{\sigma\left(T_{p,m}+T_a\right)\left(T_{p,m}^2+T_a^2\right)}{\left[\left(\varepsilon_p + 0.00591Nh_w\right)^{-1} + \frac{\left[2N+f-1+0.133\varepsilon_p\right]}{\varepsilon_g} - N\right]} \quad (3.14)$$

$$f = (1 + 0.089hw - 0.1166hw\ \varepsilon_p)(1\ +\ 0.07866N) \quad (3.15)$$

$$C_{air}\ =\ 520\ (1 - 0.00005\beta^2) \quad (3.16)$$

$$e\ =\ 0.43\ (1 - \frac{100}{T_p}) \quad (3.17)$$

β, the collector tilt is and σ the Stephan Boltzmann constant is. The wind velocity determines the convective heat-transfer coefficient hw for air flowing over the outside surface of the glass cover V. [56]:

$$h_w = 5.7\ +\ 3.8\,V \quad (318)$$

3.5.2. Theory of Photovoltaic Modules (η_{el})

A PV module's electrical efficiency (η_{el}) is given by:

$$\eta_{el} = \frac{I_m V_m}{G A_c} \quad (3.19)$$

As previously stated, a photovoltaic module's performance degrades with increasing temperature, and this dependence of PV module electrical efficiency on PV module temperature is typically given. by Zondag et alEquation .'s (3.20) [53]:

$$\eta_{el} = \eta_o(1 - \beta[T - 25^oC]) \quad (3.20)$$

Table 3.3 contains the constants and calculated variables needed for the expressions above.

Table 3.3. Variables and constants for use in efficiency expressions.

G	**1112 W/m^2**
η_0	0.177
$\boldsymbol{U_L}$	14.8
$\eta_{el.ref}$	16%
β_{eref}	0.005
T	313 K

3.5.3. Energy into the Collector

The useful heat output of a collector as a function of input radiation and collector operating temperature in relation to its surroundings. is commonly used to describe collector thermal performance. When the equation for a specific solar collector's performance curve is known, the system designer has the information needed to use any of several recognized computational techniques to predict the collector's daily, seasonal, or annual energy output under the system's anticipated use conditions. The analytical derivation of this efficiency is briefly reviewed in the section expression below [53, 57].

The net rate of solar radiation absorbed by a collector, q solar, is determined by the radiation on the cover plate as well as the optical and radiative properties of the absorber and cover plate materials. Because no true glazing material is completely transparent, one part of the radiation that strikes the cover is absorbed and the other part is reflected; only a small fraction passes through the cover. Part of the reflected radiation is transmitted, part of it is absorbed, and part of it is reflected to the absorber. Due to multiple absorption, reflection, and transmission, only a fraction of the radiation is eventually absorbed by the collector [57].

The effective transmittance-absorptance product, $(\tau\alpha)$e, is the parameter that quantifies the collector's ability to absorb solar radiation. is called the effective transmittance of the glazing (s) and the absorptance of the absorber plate surface determine the energy absorbed primarily, the complex interactions discussed above alter the product $(\tau\alpha)$e in complex ways. Collectors with two or more glazing layers.

$(\tau\alpha)$e can be used to express the net rate of incoming solar energy absorbed by a collector [57]:

$$q_{solar} = GA_a[(\tau\alpha)_e] \quad (3.21)$$

Where G denotes total incident radiation per unit area measured in the collector's aperture plane, and Aa denotes collector absorber area. Because these material properties influence radiative heat losses from the absorber plate, the relationship between collector performance and cover and absorber physical properties is more complicated than the preceding discussion suggests.

3.5.4. Heat Losses from the Collector

Solar collector thermal losses occur in three ways: conduction, convection, and radiation. Conduction heat losses are typically insignificant unless the collector case or mounting structure comes into direct thermal contact with the absorber or inlet and outlet piping due to poor collector design or construction. The temperature difference between the collector glazing and the surrounding air determines convective losses. Wind damage to the outer glazing can result in significant losses. Convection also transfers heat from the absorber to the collector's glazing(s). Radiative losses are minimal at standard domestic water or space heating temperatures. However, because these losses are proportional to the difference in absorber absolute temperature and sky absolute temperature, which is usually several degrees lower than the ambient air temperature, they are not a perfect match. They are not a good investment. At higher operating temperatures, radiative losses may become significant. Even though convective and radiative losses occur from all exposed collector surfaces, the total heat loss is commonly expressed as a function of absorber area, Aa. This is because most radiative and convective losses in a well-insulated collector are accounted for by the glazing.

It is common practice to combine the convection and radiation heat transfer terms to yield a single heat loss coefficient based on the temperature difference between the average collector absorber plate temperature and the ambient temperature for both

experimental and analytical purposes. The radiation heat transfer term must then be linearized. Thus.

$$U_L = F'(U_{conv.} + U_{rad.}) \tag{3.22}$$

And

$$Q_{loss} = U_L A_a (T_p - T_a) \tag{3.23}$$

Where $U_{conv.}$ and $U_{rad.}$ are, respectively, the linearized overall radiation heat transfer coefficient and the linearized overall convection heat transfer coefficient. Tp is the average temperature of the absorber.

3.5.5. Useful Energy from the Collector

The equation describing the quasi-steady performance of a solar collector is obtained by substituting the previously developed expressions for qsolar and qloss [58]:

$$q_{useful} = A_n F'[(\tau\alpha)_e G - U_L(T_n - T_a)] - q_{el} \tag{3.24}$$

A linear relationship between irradiance and temperature difference can be used to approximate the electrical energy extracted from the collector $T_n - T_a$

$$q_{el} = A_n E_0[(\tau\alpha)_e G - E_t(T_n - T_a)] \tag{3.25}$$

Where E_0 the PV efficiency is represented by cells, their temperature coefficient is E t. As a result, we can write:

$$q_{useful} = A_n[(F'(\tau\alpha)_e - E_0)G - (F'U_L - E_t)(T_n - T_a)] \tag{3.26}$$

Let $B_L = F'U_L - E_t$ and $\eta_{o,e} = F'(\tau\alpha)_e - E_0$, then the above equation can be written as:

$$q_{useful} = A_n[\eta_{o,e}G - E_L(T_n - T_a)] \quad (3.27)$$

The new parameters B_L and $\eta_{o,e}$ represents the effective optical efficiency and the effective heat loss coefficient, respectively. These are the fundamental equations for constructing models for describing collector performance The useful energy delivered to storage or load by a collector can also be measured experimentally by measuring the inlet and outlet collector temperatures, heat transfer fluid properties, and mass flow rate of that fluid through the collector; thus,

$$Q_{useful} = \dot{m}C_p(T_o - T_i) \quad (3.28)$$

Where m is the fluid flow rate through the absorber, C p is the fluid's specific heat capacity, and denotes the temperature of the outlet fluid, and Ti denotes the temperature of the inlet fluid.

3.5.6. Collector Efficiency

The PV/T collector's thermal and electrical efficiency should be measured separately. The ISO 9806-1 standard is used to measure thermal efficiency, and I-U curves with a capacitive load are used to determine electrical efficiency [50]. A flat-plate solar collector's thermal efficiency is defined as the ratio of useful heat delivered by the collector to total solar radiation intercepted by the collector. Substitution boosts collector efficiency by doing the following:

$$\eta = (\tau\alpha)_e - U_L(T_p - T_a)/G \quad (3.29)$$

The problem with using this equation is that the average temperature of the absorber plate, Tp, is frequently unknown. However, because the fluid temperature is similar to that of the storage or supply water main, the system designer knows or can reasonably estimate Ti denotes the temperature of the fluid entering the collector. Whillier rewrote this equation to provide a more useful expression for collector efficiency, substituting Ti for Tp and including the collector heat removal factor, Fr, to account for the lower heat losses. [58, 59]. Hence,

$$\eta = F_r[(\tau\alpha)_e - U_L(T_i - T_a)/G] \quad (3.30)$$

Fr denotes the proportion The ratio of maximum possible useful energy gains to actual useful energy gain. When the entire collector is at the inlet fluid temperature Ti, the maximum possible useful energy gain occurs. Heat losses to the surroundings are kept to a minimum in such an ideal case. Water collectors typically have Fr values ranging from 0.7 to 0.9. So, Fr cannot be greater than one.

Similarly, if we use the mean collector fluid temperature, the efficiency increases [56]:

$$\eta = F'[(\tau\alpha)_e - U_L(T_m - T_a)/G] \quad (3.31)$$

Where

$$T_{m=} - T_i + \frac{T_o - T_i}{2} \quad (3.32)$$

If F', Fr, UL, and e T* is a linear function of reduced temperature difference if $(\tau\alpha)$e were constant.

$$\eta = \eta_0 - F'U_L T^* \quad (3.33)$$

Where,

$$T^* = \frac{T_m - T_a}{G} \quad (3.34)$$

This is not exactly true in practice because UL varies with fluid and air temperature, $(\tau\alpha)$e is affected by the relative proportion of beam, diffuse, and ground-reflected radiation, and Fr is affected by UL on a weekly basis. As a result, it appears that a higher order correlation between ήo and T* is more likely [60].

$$\eta = \eta_0 - a_1 T^* - a_2 G T^{*^2} \quad (3.35)$$

In which a1 and a2 are the fitting constants. The ordinate intercept, ήo, measures the ability of the collector to absorb solar energy and transfer it to the collector fluid. According to the first law of thermodynamics, if electrical energy is extracted from the collector, this ability is reduced to ήo,e. [54]. The slope of the equation denotes the collector's ability to prevent heat losses to the environment. This ability is enhanced when electrical energy is extracted from the collector BL.

PART 4

EXPERIMENTAL WORK

4.1. CHAPTER OVERVIEW

This chapter describes the main research strategy as well as the techniques used in the study, namely CFD simulation and experimental investigation. Two experimental PV/T models were designed and built to confirm prediction and CFD simulation results. The models were subjected in relation to a measurement program, which will be described further in the chapter. The entire experimental facility is divided into sections. These parts discuss the changing the design of PV/T and how does it affect the cooling of the photovoltaic panel (PV), describe of PV/T analysis utilized, measurement system concerning the characterization of collector performance, data collection. While the last section illustrates the uncertainty analysis [61].

4.2. LAYOUT OF THE PV/T SYSTEM

- The PV/T's performance is influenced by the working environment. The PV/T models developed and built in this study have been installed at the University of Technology in Iraq's solar research site. The latitude is N33.3123o, the longitude is 44.446 E, and the elevation is 21.23m. Meteorological data measured within the university for sunrise (7 a.m. - 7 p.m.) as a working period of the flat plate collector are as follows:
    - The average wind speed is 1.7 m/s.
    - The intensity range of solar radiation is 24 -1112 W/m^2.
    - The average ambient air temperature (and range) is 34 degrees Celsius (2643 degrees Celsius).
    - The average (and range) of ambient air pressure is 100200 Pa (99891100540 Pa).

- The PV/T models are divided into two categories: Model-CC and Model-SS.
- The PV/T's conceptual design outlines are explained in the following sections.

4.3. DESIGN OF FLAT PLATE COLLECTOR (PV/T)

The temperature drops from the amount of solar radiation that reaches the PV panel's back surface determines the flat plate collector surface. the area of the collector, and the absorber materials. Because the future goal is to increase the amount of electricity generated by the PV panel by using PV/T, it is suggested that it be installed in an open environment and use water as a solar radiation absorbing medium.

As a result, the flowing water would be the absorber material, while a collector cover with high conductivity could be used; preferably for investigation objectives, aluminum plates would be used. Depending on the area, the collector area could be calculated. of PV panel and heat flux which reaches this cover in the model location. The collector has a slope angle of 30^{o} to enhance the projection model of solar radiation within its daily range.

4.3.1. Specification of New Design of Flat Plate Collector

The function of the PV/T is to subtract the heat from the back surface of the photovoltaic panel to the water flowing into it. The parameters involved in the collector are the tangential and vertical parts of internal geometry, and the increasing of contact area between the heat transfer material and hot surfaces, furthermore, temperature difference between water entering PV/T and ambient air. New design utilizes aluminum uniform bulges connected with collector cover from bottom to provide powerful heat transfer and water movement in a smooth, slow motion This is possible because the velocity components of water flow are more value when the collector cover was without bulges. In the new design of the present work, two

models of bulges utilized: cubic shape (Model-CC), and sphere shape (Model-SS). The PV/T geometry for these models could be described as below:

- Design and fabricate Model-CC: this model has a number 120 cubic bulges, dimensions 15×15×15 mm, and is made of aluminum to allow powerful heat transfer. These bulges were evenly distributed on the collector cover's bottom surface so that they were 8 cubes within one row, while the number of rows was 12, as shown in Figure 4.1.

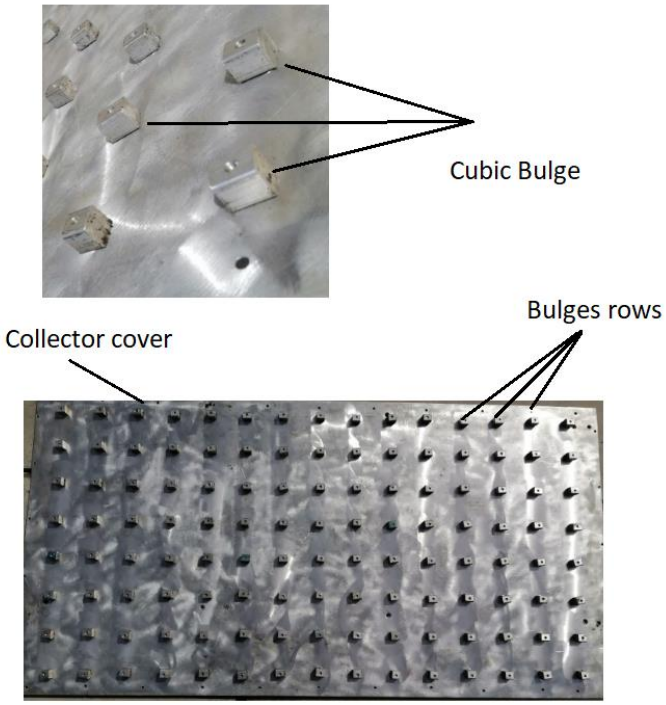

Figure 4.1. Structural pictures of a Model-CC.

- Design and fabricate Model-SS: this model has a number 120 sphere bulges, a 25 mm diameter, and is made of aluminum to allow powerful heat transfer. These bulges were evenly distributed on the collector cover's bottom surface so that they were 8 spheres within one row, while the number of rows was 12, as shown in Figure 4.2.

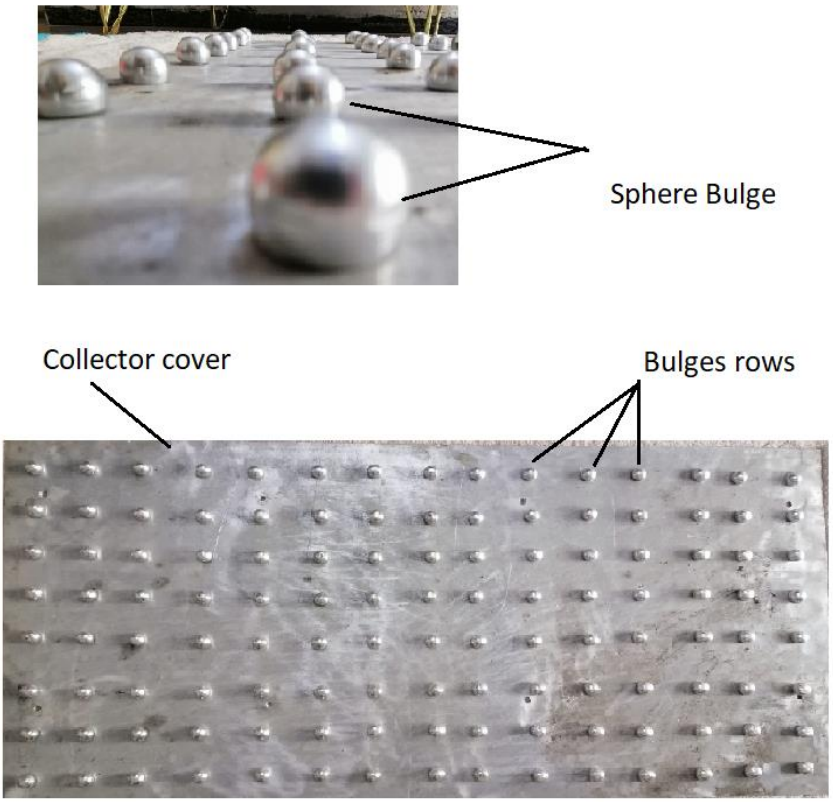

Figure 4.2. Structural pictures of a Model-SS.

4.3.2. Collector Geometry

Figure 4.3 depicts a photograph of the collector section used to investigate the flow of water from the inlet pipe to the outlet pipe. The collector body has dimensions of 600×1100×30 mm, a 13 mm inlet and outlet diameter, it is made of steel. To connect collector cover was used number of screws and rubber band used to prevent water leakage from the edges of the collector.

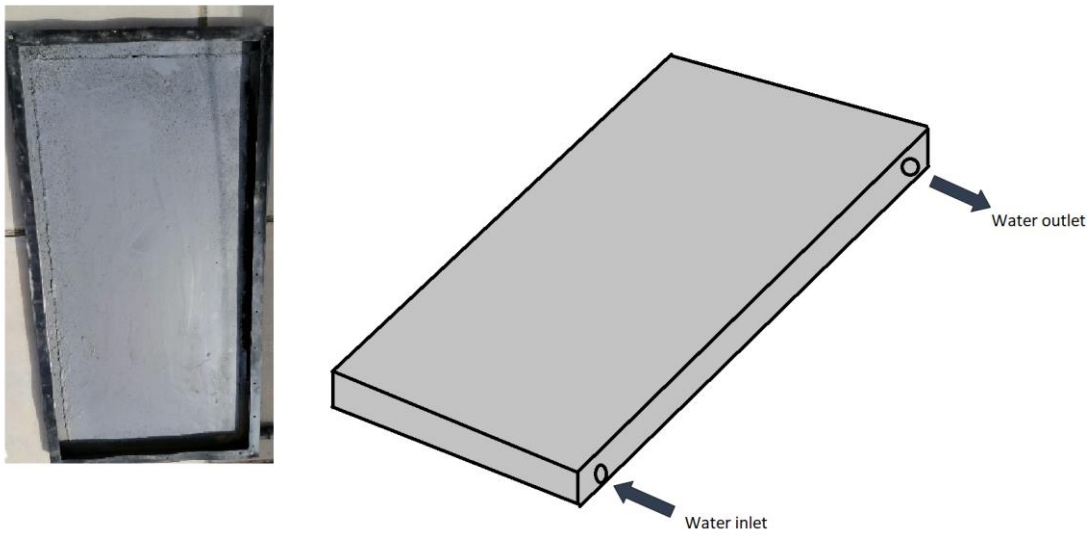

Figure 4.3. Flat plate collector body.

4.4. EXPERIMENTAL SETUP

Experimental investigation of PV panel cooling system design for power generation is an objective of the present study. The subtract heat energy was done using PV/T system by depending on closed circle water flow. The thermal collector (absorber) is attached to the back of a typical PV panel. All experiments were performed in comparison to the PV system to obtain an initial estimate of the PV/T system's characteristics, and a portion of the collected energy was extracted as electricity rather than heat., as shown in Figure 4.4. Both the PV panel and PV/T system inclined with 30^{o} from the horizontal plane. Temperatures for different regions of PV/T system were measured by temperature measurement unit and the Before entering the collector. The flow rate of water was measured using a flow rate device. To precisely control the water flow rate, a one-way valve was used. Calibration curve for these devices shows in Appendix A

Figure 4.4. Experimental setup of the PV and PV/T system.

4.4.1. Photovoltaic PV Panels

Photovoltaic solar cells make up a photovoltaic system. Depending on the material used, a single small PV cell can generate between 1 and 2 Watts of power. PV cells can be linked together to form higher power modules that produce more power. Traditional single-crystalline silicon (Si) solar modules use silicon cells, are typically flat-plate, and are the most efficient solar modules. In this work, two PV panel were used with the module's maximum power capacity is 150 Watt (model MSM150S for MAGNZON company), as shown in Figure 4.5, one of them was used in PV system side while the other used in PV/T system side, and Table 4.1 list the main technical specifications of the PV panel.

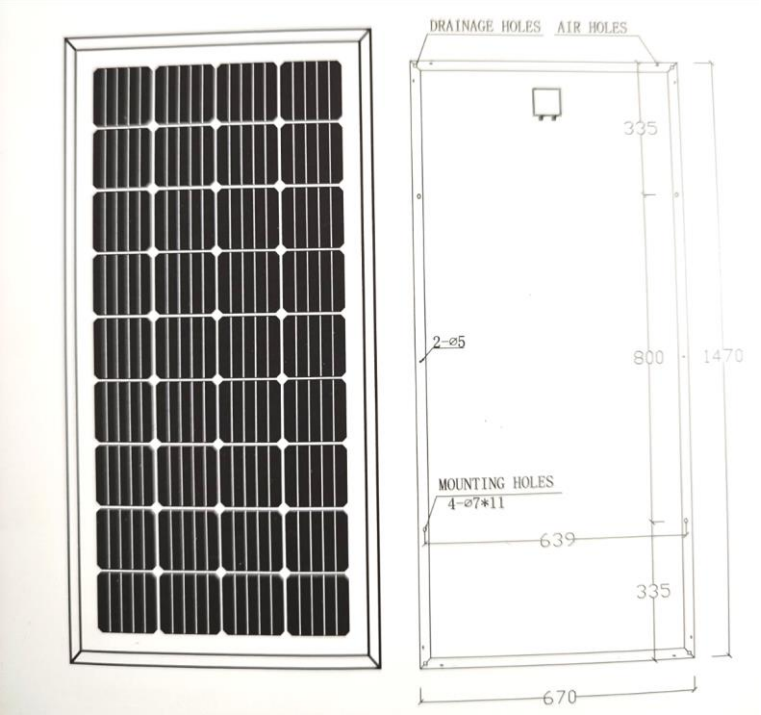

Figure 4.5. Schematic of photovoltaic panel.

Table 4.1. The main technical PV panel specifications.

Model of PV panel	**MSM150S**
Type of cells (mm)	Mono (156×104)
NO. of cells and connections	4×9=36
Dimensions (mm) (L×W×H)	1470×670×30
Weight (kg)	11.0
Glass	3.2mm Tempered glass
Encapsulation	EVA
Rated maximum power (Mp)	150 W
Cell efficiency	17.7%
Open circuit voltage (Voc)	22.4 V
maximum power voltage (Vmp)	17.5 V
Short circuit current (Isc)	9.05 A
maximum power current (Imp)	8.63 A

4.4.2. Measuring Instrumentations

- Various instruments were used to measure tests to carry out an experimental investigation of this study. A measurement investigation was conducted. for the previously described experimental model of the PV/T. Testing positions of

thermocouples type K and roto-meter will be explained to capture variable measurements. The following tools were used to record the experimental measurement variables:

- Temperature measurement unit.
- Water flow rate measurement unit.
- Solar power meter instrument.
- Anemometer instrument.

4.4.2.1. Temperature Measurement Unit

Temperature measurement tests were carried out to conduct an experimental investigation of this study. Experiment procedures were performed on sunny days, with cloudy or cloudy days avoided during testing. All temperature tests on the PV/T model were performed to become acquainted with and confident with the measuring procedure. Experiment measurements were carried out at the solar research facility, where two PV panels one of them it includes the PV/T model installed. Temperature measurement can be divided into several groups; Group-A was used three thermocouples for measuring PV panel surface, Group-B was used two thermocouples for measuring inlet and outlet water temperature, and Group-C was used three thermocouples for measuring collector surface, as shown in Figure (4.6). All thermocouples were used by Type-K with selector switch and digital thermometer, as shown in Figure 4.7. All specific properties for all parts of temperature measurement system shown in table 4.2. Calibration of temperature measurement system is explained as described in Appendix (A).

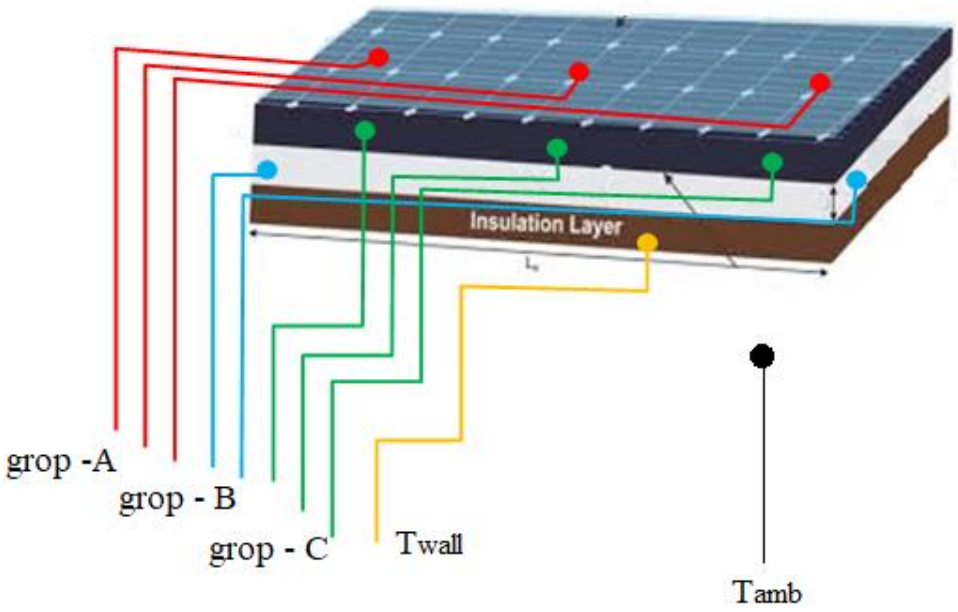

Figure 4.6. Positioning schematic of temperature measurement in the PV/T system.

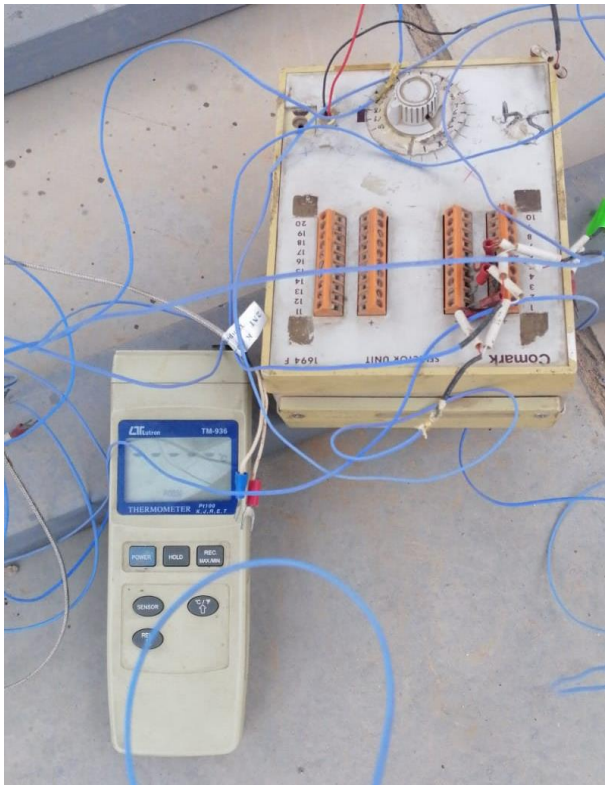

Figure 4.7. Temperature measurement instruments.

Table 4.2. All specific properties for all parts of temperature measurement system.

No.	Type of Thermocouples	position	Accuracy	Reader Thermometer – Tm-936
1	Probe type-K	2 points, inlet and outlet collector	± 0.3	Accuracy ± (0.2 % + 0.5 ℃)
2	Wire type -K	6 points, on PV panel and PV/T system	± 0.2	
3	Wire type-K	3 points, on Collector cover	± 0.2	
4	Wire type-K	4 points, to measuring Ambient temperature, collector body	± 0.2	

4.4.2.2. Water Flow Rate Measurement Unit

Flow meter (Rotameter model M-15 measuring range 1-7 LPM) instrument, shown in Figure 4.8, is connecting with water flow line can measure and volumetric flow rate in LPM (l/min). Specifications of rotameter instrument was described in Table 4.3.

Figure 4.8. Rota-meter instrument.

Table 4.3. Specifications of Rotameter instrument.

Specifications	Quantity
Internal Hole Diameter:	12mm
Overall Size:	21 x 3.2cm (L*D)
Accuracy	± 0.5% of reading
Material:	Plastic Metal

4.4.2.3. Solar Power Meter Instrument

Figure 4.9 depicts a portable solar power meter (model: SPM-1116 SD) that Irradiation can be measured and displayed for spot checks measurements in W/m^2. The amount of energy emitted by solar radiation in a specific location on Earth can be measured. be processed by a solar-meter instrument. The solar-meter instrument was designed to measure the sum of direct and diffuse solar radiation is the total global solar radiation. Table 4.4 describes the specifications of a solar-meter instrument Its sensor is a strained silicon cell that is not particularly sensitive to temperature changes. Through a diffusor and a correction filter, it absorbs solar radiation. The sensor's output voltage is proportional to the amount of radiation received. After a measurement is requested to be stopped, the results are saved.

Figure 4.9. Solar power meter instrument.

Table 4.4. Specifications of solar power meter instrument.

Specifications	Quantity
Solar Irrigation Range	1 W/m^2 to 1200 W/m^2
Calculation Frequency (W/m^2)	1/ min
Accuracy	± 5% of reading
Operating Temperature	from -10°C to +50°C
Frequency of The Measure	2 Hz

4.4.2.4. Wind Speed Instrument (Anemometer)

Instrument for measuring wind speed (Anemometer model: AM-4826), shown in Figure (4.10), is a portable instrument which can measure wind speed or air flows in channel in m/sec (km/hr). Specifications of Anemometer instrument was described in Table 4.5.

Figure 4.10. Anemometer instrument.

Table 4.5. Specifications of anemometer instrument.

Specifications	Quantity
Wind speed Range	0.3–30 m/s,1.4-108 km/hr
Accuracy	± 0.7% of reading+ 2 digit
Operating Temperature	from 10°C to +60°C
Power Supply	4×1.5V Battery

4.5. DATA COLLECTION

This section presents in the study of PV/T systems, an experimental procedure that was used in the outdoor measurement technique. Experiment procedures were conducted on sunny days, with cloudy or cloudy days avoided during testing. To become acquainted with and confident with the measuring procedure, basic tests of water temperature, surface temperatures, wind speed, water flow rate, and solar intensity were performed at various positions of the PV/T system. Also, the period time ranges were chosen from 7:00 am to 7:00 pm provide a range for study effect of PV panel heating due to solar radiation on its performance.

The experimental procedure used in this study is described as follows. The first set of experiments for Model-CC collector was conducted by temperature measurement system and water circling system for recording PV panel surface temperature, water inlet and outlet temperatures, as well as collector surface temperature from collector with varied water flow rates at several days, also solar meter was used to solar intensity measuring through daily time, as mentioned in Table 4.6.

The following experiment sets, the experiments for Model-SS collector were conducted by temperature measurement system and water circling system for recording PV panel surface temperature, collector surface temperature, as well as collector water inlet and outlet temperatures varied water flow rates at several days, also solar meter was used to solar intensity measuring through daily time, as mentioned in Table 4.6.

Table 4.6. Data collected for PV/T system.

Model-CC						
No.	Water flow	T-PV	Tco	G Watt/m^2	Tamb	Twin, Two
1	1.5 l/min	3 points	3 points	24-1112	1	2 points
2	2.0 l/min	3 points	3 points	24-1112	1	2 points
3	2.5 l/min	3 points	3 points	24-1112	1	2 points
4	3.5 l/min	3 points	3 points	24-1112	1	2 points
Model-SS						
6	1.5 l/min	3 points	3 points	24-1112	1	2 points
7	2.0 l/min	3 points	3 points	24-1112	1	2 points
8	2.5 l/min	3 points	3 points	24-1112	1	2 points
9	3.5 l/min	3 points	3 points	24-1112	1	2 points

4.6. UNCERTAINTY ANALYSIS

Uncertainty analysis in the tests is very important to provide a high level of confidence in all results. It is obtained by determining the repeatability and increasing interest the results. All tests were repeated thrice. The variants of the predicted values of water flow rates, temperatures and solar intensity were used to calculate the uncertainty using the percent relative standard error. It is unlikely that the error components. At the same time, they will be at their maximum value and have the same polarity. The square root of the sum of the individual errors is used in the root-sum-of-squares method. is a more realistic approach. as shown in Equations (4.1 and 4.2) [50].

$$\delta_{total} = \sqrt{(\delta_{sensor)}{}^2 + (\delta_{instrument})^2} \tag{4.1}$$

$$Min.\&\,Max.Uncer.\%) = 100 \times \left(\frac{\delta_{total}}{Min\&Max.Reading}\right) \tag{4.2}$$

Overall experimental uncertainty, σ_k was calculated

$$\sigma_{k=}\sqrt{\ (\sigma q_1)^2\ + (\sigma q_2)^2 + . \ . \ . + (\sigma q_n)^2} \tag{4.3}$$

Where σ_k is the total uncertainty and σq_1 , σq_2 and σq_n are uncertainty of individual parameters.

where, δ_{total} is the total degree of uncertainty The following formula was used to calculate the percentage of uncertainty in the maximum and minimum values of recorded data: The percentage uncertainty of the measured experimental yield values is shown in Table 4.7.

Table 4.7. Uncertainties of the measured parameters.

Parameter	Max. value	Min. value	Min. Uncertainty	Max. Uncertainty
Water flow rate	3.5 l/min	1.5 l/min	± 0.62	± 0.56
Temperatures	85°C	25°C	± 1.16	±1.05
Solar intensity	1112 W/m^2	29 W/m^2	± 1.91	±1.7
Wind speed	2.4 m/s	1.2 m/s	± 0.11	±0.08
I (amp)	3.1 amp	0.04 amp	±0.11	± 0.09
V (Volt)	15.5 volt	0.23 volt	±0.63	±0.47
Total Uncertainty			±2.24	±2.01

PART 5

RESULT AND DISCUSSION

5.1. CHAPTER OVERVIEW

This chapter includes a discussion and analysis of our experimental and numerical results, which included two path . The first axis: the impact of the specifications of the new design on the performance of the solar collector, where the results of the SS design, the CC type design, the change in cell surface temperatures, the amount of heat lost and the electrical efficiency of the cell over time, will be presented and these specifications are compared for both designs. Considering and analyzed the effect of water flow rate on the performance of the solar collector and studying the effects of that on temperatures, the energy used, and the electrical efficiency of the cooled cell over time. The second axis discusses theoretical results, such as the effect of water flow rate on the surface temperature of the coulter and its impact on the performance of the solar collector, as well as the comparison of experimental and theoretical results.

5.2. EXPERIMENTAL RESULTS OF PV/T SYSTEM

Figure 5.1 describes the experimental Because solar energy is the primary source of energy, result and the main observations obtained in this work. Because solar energy is the main energy to the PV /T system therefore experimental measurement of the solar intensity, for the period 7-23 April. Solar radiation and ocean temperature are discussed.

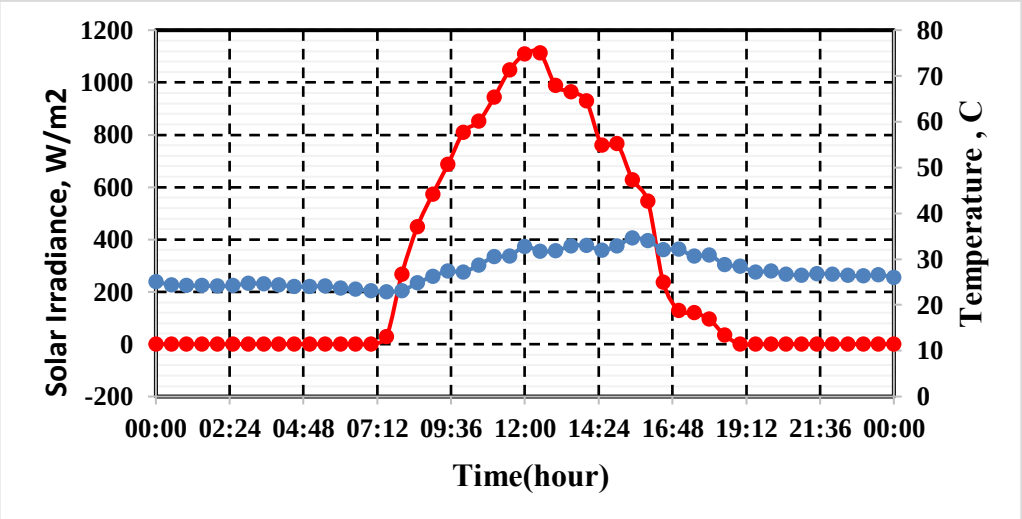

Figure 5.1. Variation of solar irradiation with temperature through daylight hours.

5.2.1. Effect of Collector Design (Bulge Shape) on PV/T System Performance

5.2.1.1. Effect of Collector Design (Bulge Shape) on PV/T System Performance on Cell Temperature Surface

The temperature of the cell surface changes when different designs are used, as shown in Figure 5.2. The uncooled cell temperature is known to be too high due to a lack of cooling, resulting in a decrease in electrical efficiency. We conducted some practical experiments with two designs, bulge SS and bulge CC. At 1:00 PM, the uncooled cell temperature was 71 °C. We observed their effects on the system as the cell temperature decreased using water cooling and a flow rate of 1.5 liters per minute. According to the results, there was a slight improvement in swell CC due to cooling and the use of SS swell. The ratio of uncooled cell to CC and SS bulge was 8.4% and 9.8%, respectively.

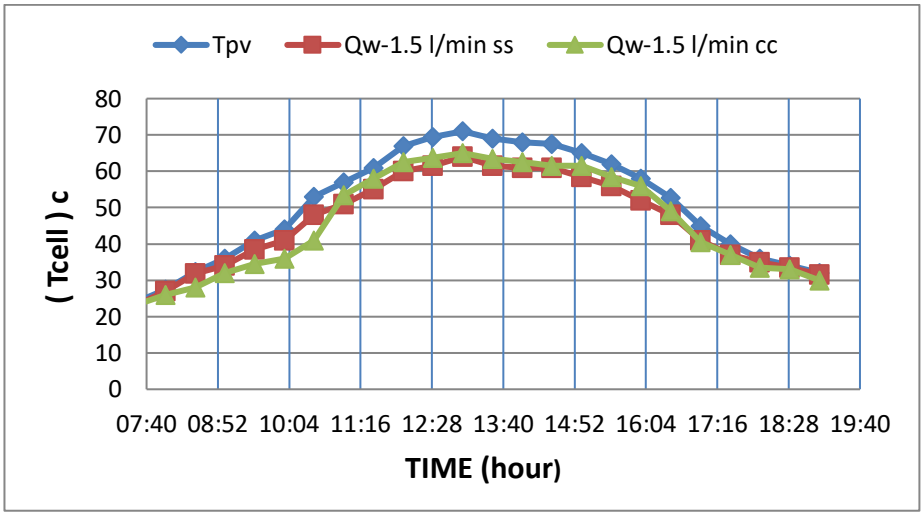

Figure 5.2. Variation of cell surface temperature with time during the day. flow rate =1.5 l/min

5.2.1.2. Effect of Collector Design (Bulge Shape) on PV/T System Performance on Collector Temperature

Figure 5.3 When cooling with water and using different designs for the purpose to reduce cell temperatures and raise electrical efficiency, we get thermal results such as hot water and some other uses. We notice some changes to the system using two different designs such as Bulge SS and Bulge CC where the uncooled cell temperature is very high due to the lack of cooling 71°C at 1:00 PM. While when cooling at the flow rate (1.5 l/min), we notice that there is a clear improvement as the collector temperature decreased, according to Figure (5.3), in the SS bulge, while the improvement in the CC bulge is less, and the reason is that the SS bulge has a streamlined design and the fluid is in contact with it from all sides, which increases the suction process. Where the percentage of the difference in temperature between uncooled cell and the CC model and the SS model is at 1:00, it is the ratio (23.9%) (25.3%). From the results, we note that the higher the radiation, the higher the heat output and thus the higher the heat gain

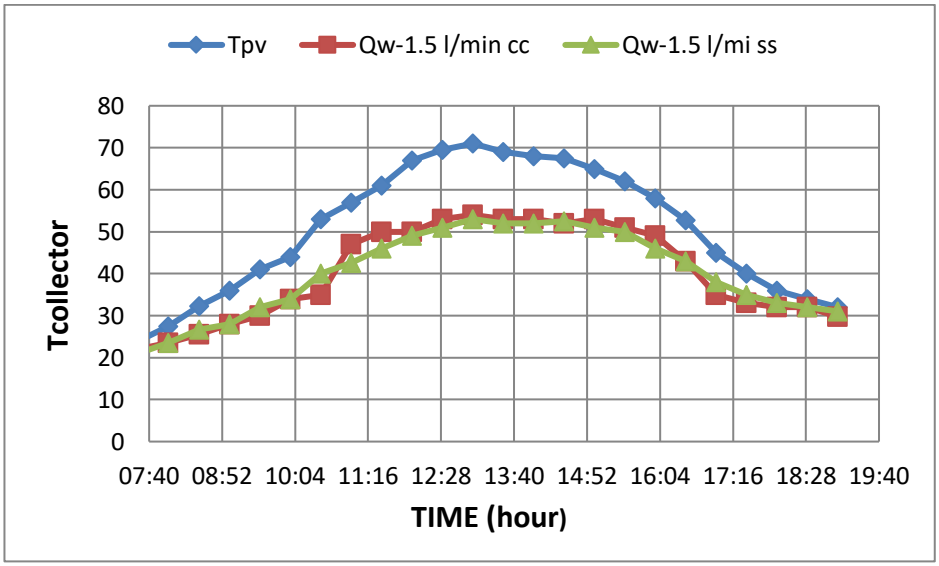

Figure 5.3. Variation temperature surface collector with time during the day. flow rate =1.5 l/min

5.2.1.3. Effect of Collector Design (Bulge Shape) on PV/T System Performance Relation to (ΔT)

Figure 5.4 When performing the practical program and beginning with daily measurements during the day and entering some parameters into the system and using two different designs such as the SS bulge and the CC bulge at a certain flow rate, the heat gain is determined first by the input and output of the water, and in general, the amount of radiation entering the photovoltaic cell plays the most important role. Part of this radiation can be dissipated, and the other part can be reflected, but the largest part enters the cell and then turns into heat, meaning 75% of the heat enters the collector. Thus, when comparing the SS model with the CC model for the same flow rate, when using a flow rate of 3.5 l/min ,we notice that the temperature difference for the SS bulge is better than the CC bulge, and the reason for this is that the SS bulge has a spherical design, which gives more suction capacity Where the percentage of the difference in temperature for the CC model and the SS model is at 12:30, it is the ratio (1.01%). we note that the higher the rate of flow, the difference in temperature decreases.

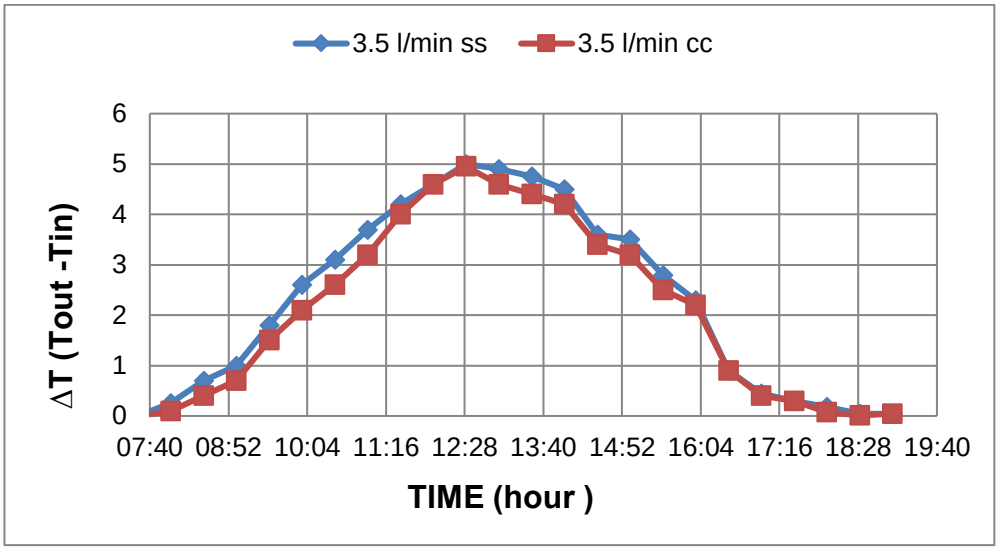

Figure 5.4. Variation different temperature ΔT(Tout –Tin) with time during the day. flow rate=3.5 l/min

5.2.1.4. Effect of Collector Design (Bulge Shape) On PV/T System Performance on Heat Gained

Figure 5.5 When searching for practical results and knowing the extent to which the system has changed and the design effect on it, we have used different designs, such as the SS bulge and the CC bulge, and pushed a certain flow rate through an electric pump. We notice some changes in the system that result in heat gains, such as the acquired energy, which depends on the heat capacity of the water. The heat gain of water is higher than that of air. When comparing the SS bulge and the CC bulge with a flow rate of (1.5 l/min) from the results, we note that the SS bulge gives better energy gain than the CC bulge, and the reason is the same as the previous explanations. Where the percentage of the difference in energies gained for the CC model and the SS model is at 1:00, it is the ratio (6.08%). From the investigation, we find that the heat gains increase with increasing radiation, and the higher the rate of flow, the greater the energy gained.

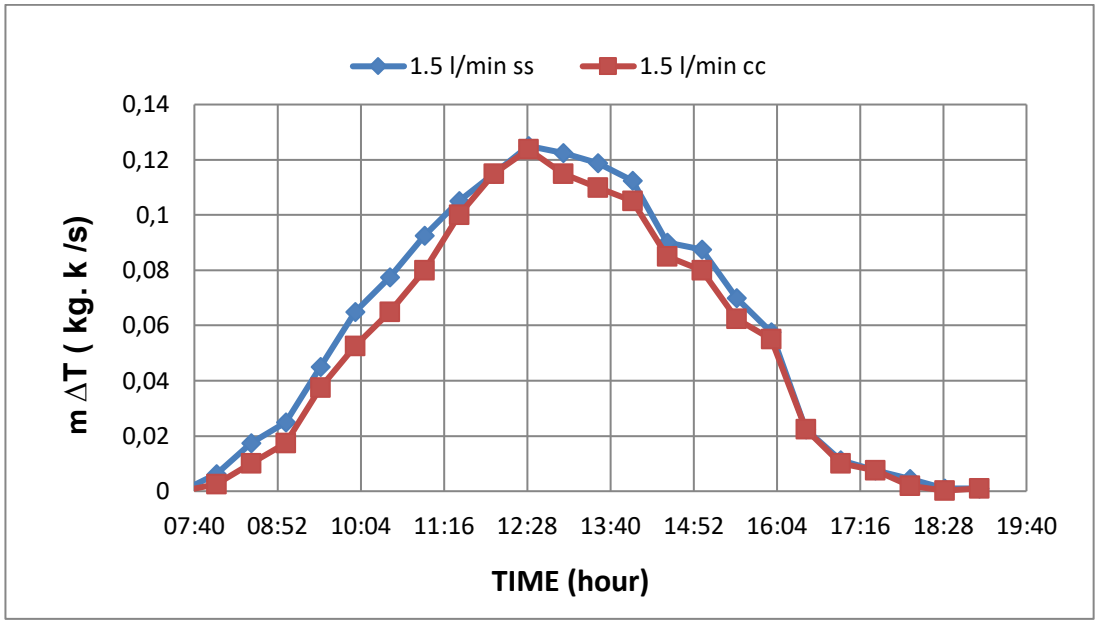

Figure 5.5. Variation heat gained with time during the day. flow rate =1.5 l/min

5.2.1.5. Effect of Collector Design (Bulge Shape) on PV/T System Performance Relation to Thermal Efficiency

Figure 5.6 When entering parameters into the system, such as the change in the rate of flow and the use of some different designs, when entering and leaving the water, we find there are heat gains, and these heat gains depend mainly on the difference in temperature. We note that the more radiation, the direct (th) increases When cooling at a flow rate of 3.5 l/min and the use of two different designs, such as the SS bulge and the CC bulge. We see that there is an improvement in the SS bulge that is better than the CC bulge. The reason for this is that when using the SS bulge design, the thermal suction is higher, which gives a higher thermal efficiency, and from the practical results, the percentage difference between the CC model and the SS model is at 1:00, it is the ratio (6.06%). It is known that the higher the flow rate, the higher the thermal efficiency, while the higher the flow rate, the lower the temperature difference, according to the amount of radiation.

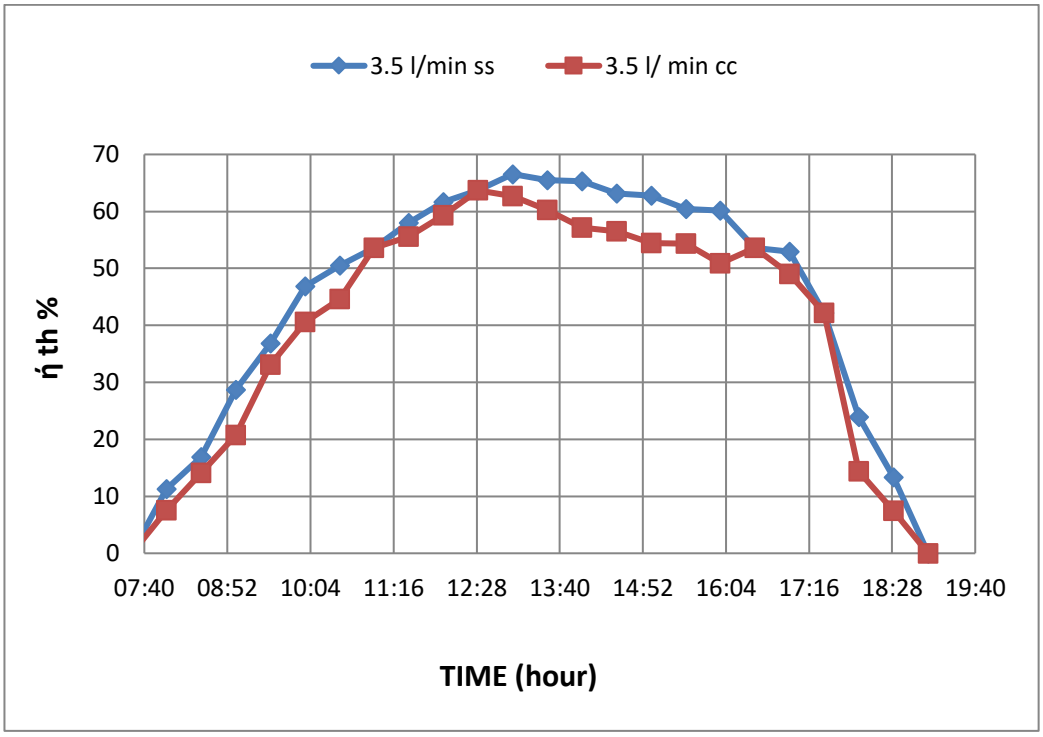

Figure 5.6. Variation thermal efficiency with time during the day. flow rate =3.5 l/min

5.2.1.6. Effect of Collector Design (Bulge Shape) on PV/T System Performance Relation to Electrical Efficiency

Figure5.7 We notice some changes in system parameters, such as electrical efficiency, when we begin the practical experiment and use different designs. Two different designs were used, such as bulge SS and bulge CC, and at a certain flow rate, we notice that there is an improvement in electrical efficiency in bulge SS that is better than in bulge CC. The reason is that the spherical bulge design enables the fluid flowing through it and the fluid touching it from all sides From the results, the electrical efficiency of the uncooled cell is at the highest radiation 13.6% at 12:30 pm, and when cooling at a flow rate of (3.5 l/min) the electrical efficiency increases where the increase is In the ratio between the electrically efficient uncooled cell and the CC model and the SS model at 12:30, which is the ratio (6.6%),(8.08%) respectively and from this we find that the higher the flow rate, the higher the electrical efficiency. The increase depends on the incoming radiation.

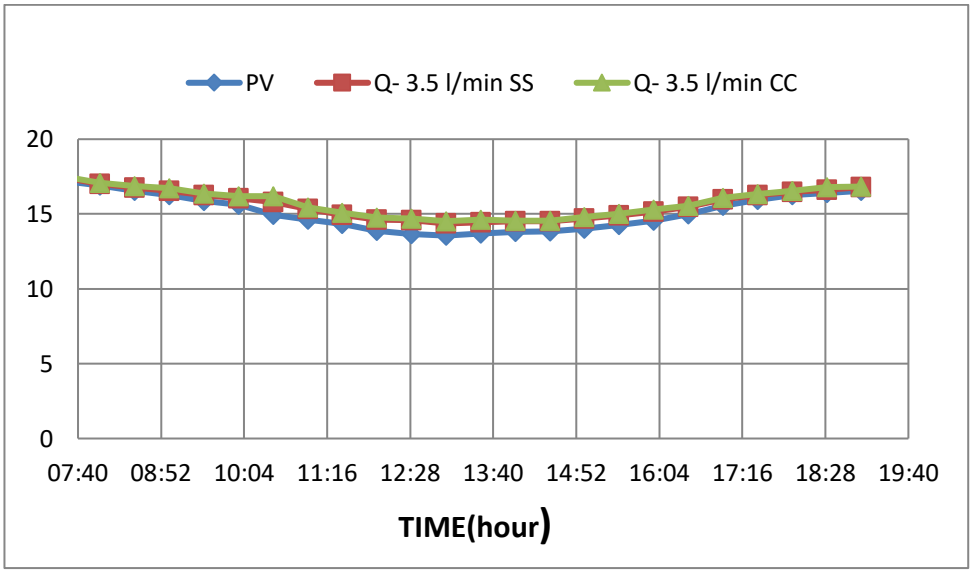

Figure 5.7. Variation of electrical efficiency with time during the day. flow rate =(3.5 l/min)

5.2.2. Effect of Water Flow Rate on PV/T System Performance

5.2.2.1. Effect of Mass Flow Rate (mw) On Solar Cell Surface Temperature (Tcell) For Model CC

Figure 5.8 The efficiency per moment of a photovoltaic cell is a function of its temperature. It shows the changes in temperature (Tcell) under a certain radiation and mass flow rate, and from these differences we note that an increase in intracellular radiation (G) increases Tcell with a certain mass flow rate (mw) and thus (Tamp). From practical results, the highest Tcell values are achieved at the lowest flow rate (1.5 l/min), but the higher the flow rate, the lower the cell surface temperature and the reverse process. The reduction ratio between the uncooled cell and the cooled cell for cell surface temperature and flow rates of (1.5 l/min), (2 l/min), (2.5 l/min), (3.5 l/min), where the ratio is (8.4%), (9.8%), (14.08%), and (15.4%) respectively at 1:00 p.m. This decrease in the cell surface temperature is due to the cooling capacity of the high temperature of the water. This work is close to the work of the researcher Said Abdel-Ganyo as in Al-Biber. [42] where the tube reduction ratio (3C) is between the cooled and uncooled cell at a flow rate of (1.5 l/min).

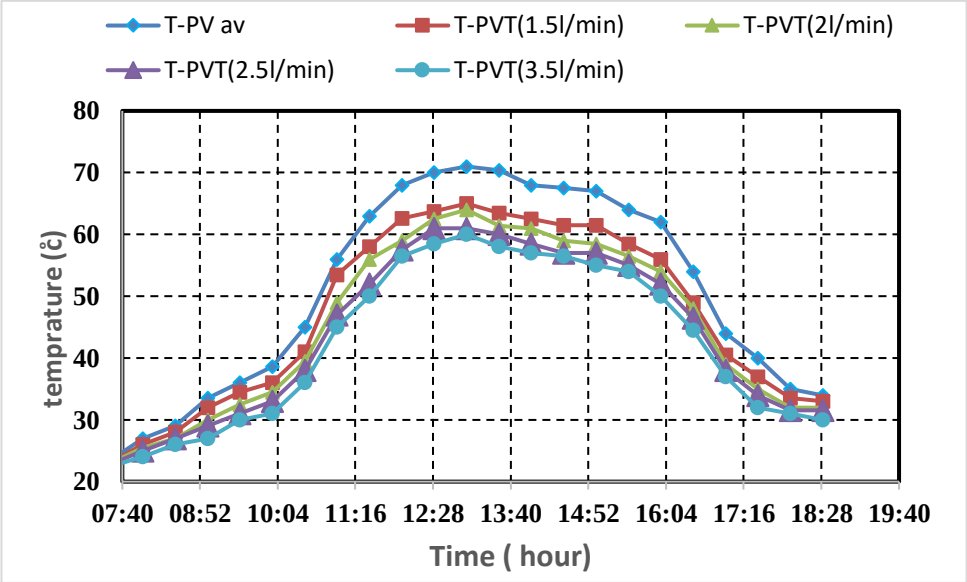

Figure 5.8. Change of temperature Tcell with time during the day. different flow rates.

5.2.2.2. Effect of Mass Flow Rate(mw) On (ΔT) For Model CC

Figure 5.9 The heat energy gain is the change in temperature (ΔT) between the temperatures of the inlet and outlet water (Tout-Tin). Figure (5.9) shows that ΔT is affected by some parameters such as (G) and mw. An increase in radiation leads to an increase in ΔT. Therefore, an increase in flow rates for a given input leads to a decrease in TΔ. From the results, the difference in temperature decreases with the increase in the water flow rates, where the decrease rates were 15.1%, 25.2% and 43.4% when changing the flow rates of 2 l/m, 2.5 l/min, and 3.5 l/min , respectively at 12:30 pm, Tout is the basis for comparison, limitations, which is higher at higher temperatures. This work is like that of the researcher Saeed Abdel-Ganyo, where the ΔT at the flow rate is 3.5 l/min (1.3) and at the flow rate is 1.5 l/min (3.6) as in the bibber [42].

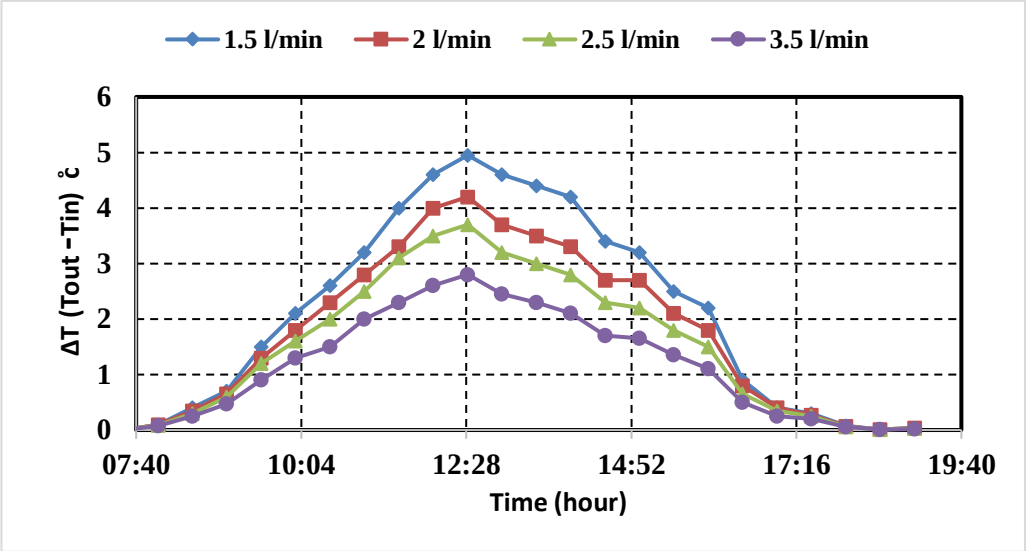

Figure 5.9. Variation ΔT(Tout –Tin) with time during the day. flow rate = (1.5 l/min to 3.5 l/min).

5.2.2.3. Effect of Mass Flow Rate (mw) on Energies Gained for Model CC

Figure 5.10 represents the relationship between the energy gained and time during the day with different flow rates. The increase in radiation leads to an increase in ΔT. The higher the flow rate, the greater the energy gained. The energy gains are the relationship of temperature change. between the incoming and outgoing water, as well as the increase in radiation, lead to an increase in heat gained. On this basis, the higher the flow rate from the temperature parameters (Tout), rthe greater the energy gained, as the energy gained increases at the following flow rates (2 l/min), (2.5 l/min) and (3.5 l/min) where the proportions The increase (12.1%) (26.01%) (36.5%) respectively in relation to the flow rate (1.5 l/ min) at 12:30 pm, Also, an increase in ΔT leads to an increase in heat losses, and the reason is the high temperature of the exiting water. Thus, losses decrease as the rate of flow increases.

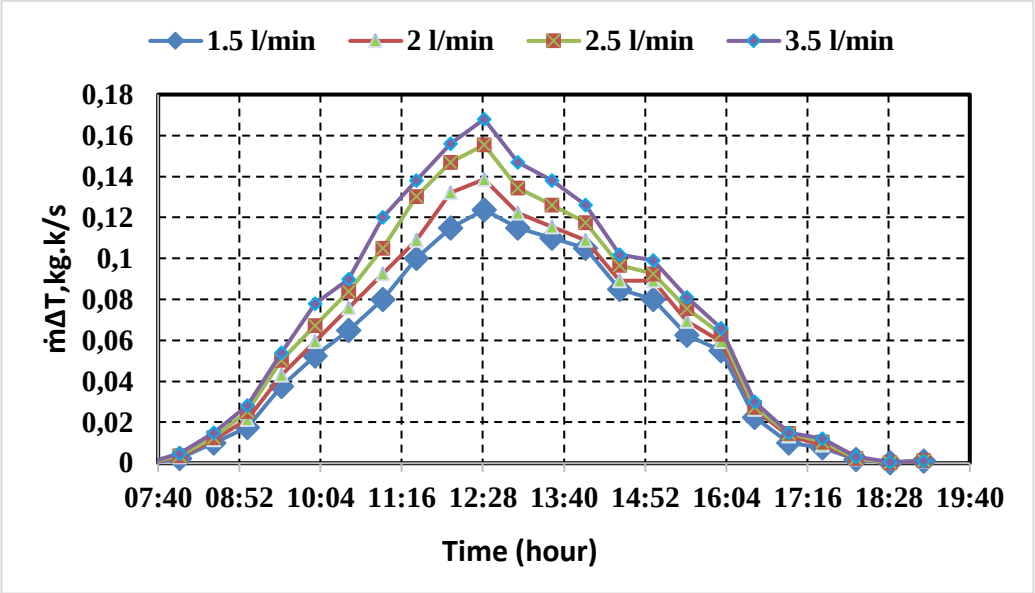

Figure 5.10. Variation of m ΔT(Tout –Tin) with time during the day .flow rate =(1.5 l/min to 3.5 l/min).

5.2.2.4. Effect of Flow Rate (mw) on Thermal Efficiency, ηth for Model CC

Figure 5.11 The thermal efficiency of PV/T can be known by the input of solar energy, and it can be converted into thermal gain. Upon investigation, we found noticeable changes in the thermal efficiency (ήth) of the solar collector (PVT) with radiation (G) at different flow rates. The radiation is directly proportional to the (th). When the flow rate is increased, the thermal efficiency increases, and thus at the highest radiation the highest thermal efficiency is achieved as the thermal efficiency increases at the following flow rates (2 l/min), (2.5 l/min) and (3.5 l/min) where the proportions The increase (11.9%) (25.5%) (35.6%) respectively in relation to the flow rate (1.5 l/min) at 12:30 pm The thermal efficiency can be extracted from the results discussed on the PVT unit. both ηel and ήth increased with the increase of flow rate. This work is like that of researcher Saeed Abdul-Ganiyu, where it is thermal efficiency (ήth) from 42.46% to 45.60% as in Bibber [42].

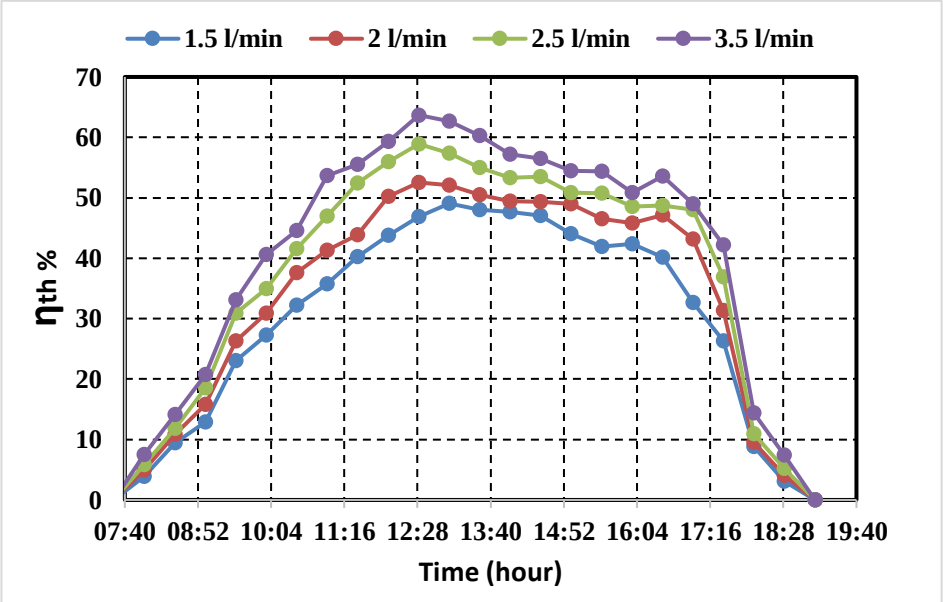

Figure 5.11. Change of thermal efficiency with time during the day .different the flow rates.

5.2.2.5. Effect of Mass Flow Rate (mw) on Electrical Efficiency, ηel

Figure 5.12 represents the relationship between electrical efficiency (ηel) with time during the day at different flow rates. For a certain flow rate that (ηel) decreases with (G) increase the reason is due to the increase of Tcell. When increasing the flow rate through the thermal collector and a constant amount of radiation (G), which increases the cooling of the photovoltaic cell, this in turn leads to a relatively low temperature, resulting in large increases in (ηel). Thus, the highest electrical efficiency (ηel) is at the highest flow rate (MW) at a constant radiation. As can be seen from the curves in Figure (5.12). The electrical efficiency of the uncooled cell was (13.6 %) at 12:30 pm when using flow rates (1.5 l/min), (2 l/ min), (2.5 l/min) and (3.5 l/min). Electrical efficiency increased by the following percentages. (3.6%), (4.4%), (5.1%), (6.6%) respectively. This work is like the work of researcher Said Abdel-Ghani where the electrical efficiency increases from 10.1% to 10.83% with increasing flow rate from 1.5 to 3.6 l/min as in Bibber [42].

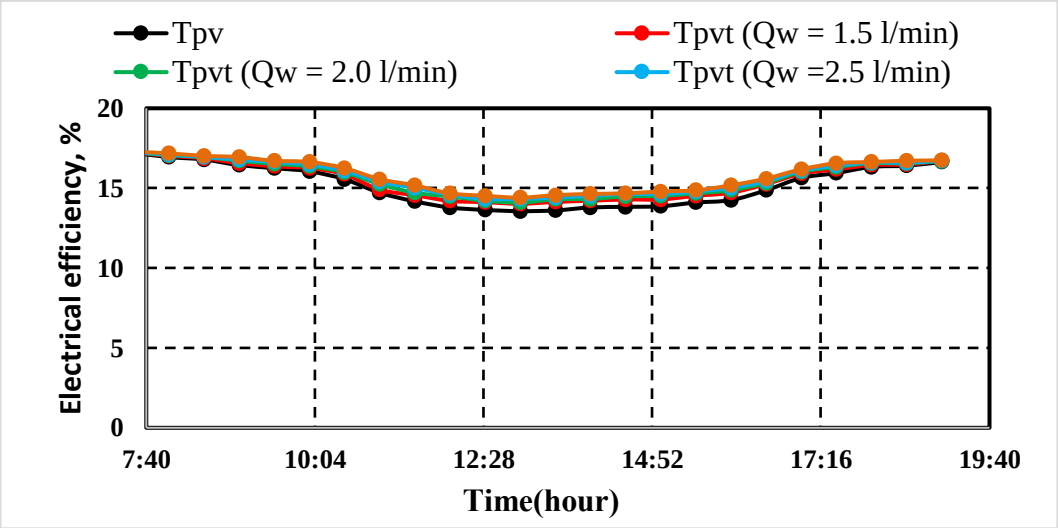

Figure 5.12. Variation of electrical efficiency with time during the day. different the flow rates.

5.2.2.6. Effect of Mass Flow Rate (mw) on Solar Cell Temperature (Tell) for Model SS

Figure 5.13 The efficiency at each moment of the photovoltaic cell is a function that depends on its temperature. It shows the changes in the temperature (Tcell) under a certain radiation and the mass flow rate and from these differences We note that the increase in radiation inside the cells (G) increases the Tcell at a certain mass flow rate (mw) thus (Tamb). From the practical results, the highest Tcell values are achieved at the lowest flow rate (1.5 l/min), but the higher the flow rate, the lower the cell surface temperature and the reverse process. The reduction ratio between the uncooled cell and the cooled cell for cell surface temperature and flow rates (1.5 l/min), (2 l/min), (2.5 l/min), (3.5 l/min), where the ratio is (9.8%), (12.6%), (14.7%), (17.6%) respectively at 1:00 p.m This decrease in the degree of The temperature of the cell surface is due to the cooling capacity, and the high temperature of the water. The work is like that of the researcher Said Abdel-Ganyo, as in the Bibber. [42] where the tube reduction ratio (3C) between the uncooled cell and the cooled at the flow rate is (1.5 l/min).

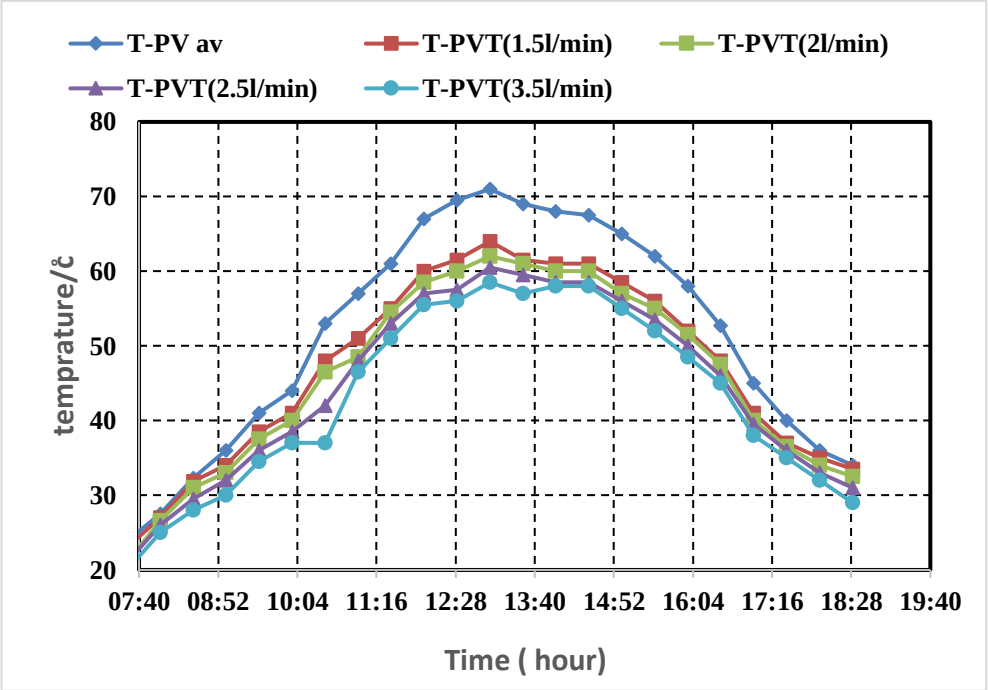

Figure 5.13. Change of temperature with time during the day. different flow rates.

5.2.2.7. Effect of Mass Flow Rate (mw) on ΔT for Model SS

Figure 5.14 shows that the thermal energy gain is the change in temperature (T) between the temperature of the inlet and outlet water (Tout-Tin). Figure 5.14 shows that ΔT is affected by some parameters such as Gp and mw. An increase in radiation leads to an increase in ΔT. Therefore, an increase in flow rates during a given input decreases ΔT by this value. It is lower T with higher flow rate and this leads to increased efficiency, and the highest temperature difference is at the highest radiation at 12:30 pm. From the results, the difference in temperature decreases with the increase in the water flow rates, where the decrease rates were 14 %, 26.2% and 44% when changing the flow rates of 2 l/min, 2.5 l/min, and 3.5 l/min respectively at 12:30 pm, and accordingly the heat loss increases as a result of cooling the water and reaching a higher temperature, and from this the loss decreases when the flow rate increases, and this work is similar to researcher Saeed Abdel Ghanio with a flow rate of (3.5 l/ min) (ΔT) equals (1.3) and at a flow rate (1.5 l/min) equal to (3.7) as in a bibber [42].

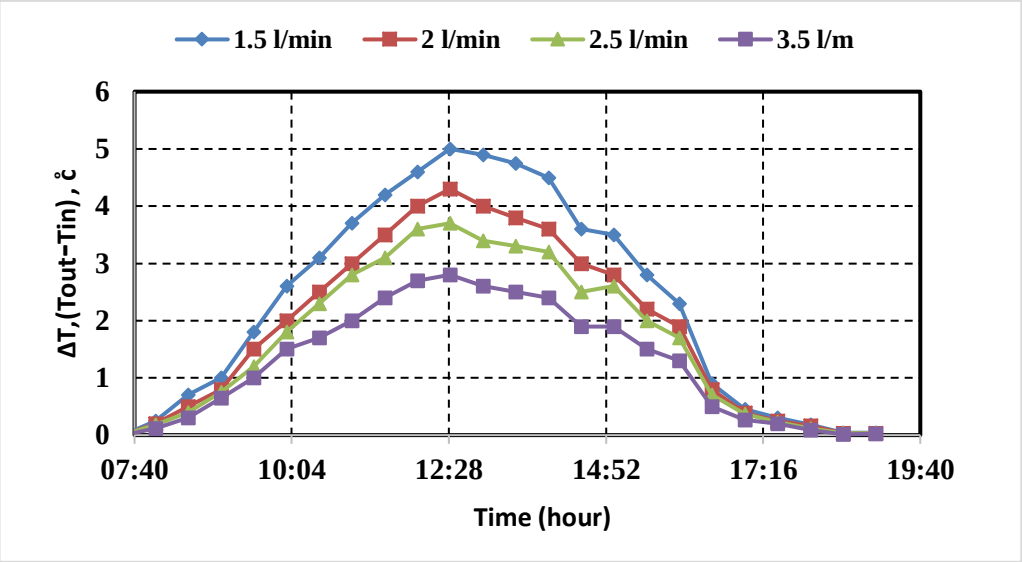

Figure 5.14. Change of ΔT (Tout –Tin) with time during the day. flow rate =(1.5 l/min to 3.5 l/min).

5.2.2.8. Effect of Flow Rate (mw) on Energies Gained for Model SS

Figure 5.15 represents the relationship between the energy gained and time during the day with different flow rates. The increase in radiation leads to an increase in ΔT. The higher the flow rate, the greater the energy gained. The energy gains are the relationship of temperature change. between the incoming and outgoing water, as well as the increase in radiation, lead to an increase in heat gained. On this basis, the higher the flow rate from the temperature parameters (Tout), the greater the energy gained, as the energy gained increases at the following flow rates (2 l/min), (2.5 l/min) and (3.5 l/min) where the proportions The increase (12.8%) (24%) (34.4%) respectively in relation to the flow rate (1.5 l/ min) at 12:30 pm. An increase in ΔT also leads to an increase in heat loss, the reason being the higher temperature of the exiting water. Hence, it decreases with increasing flow rate.

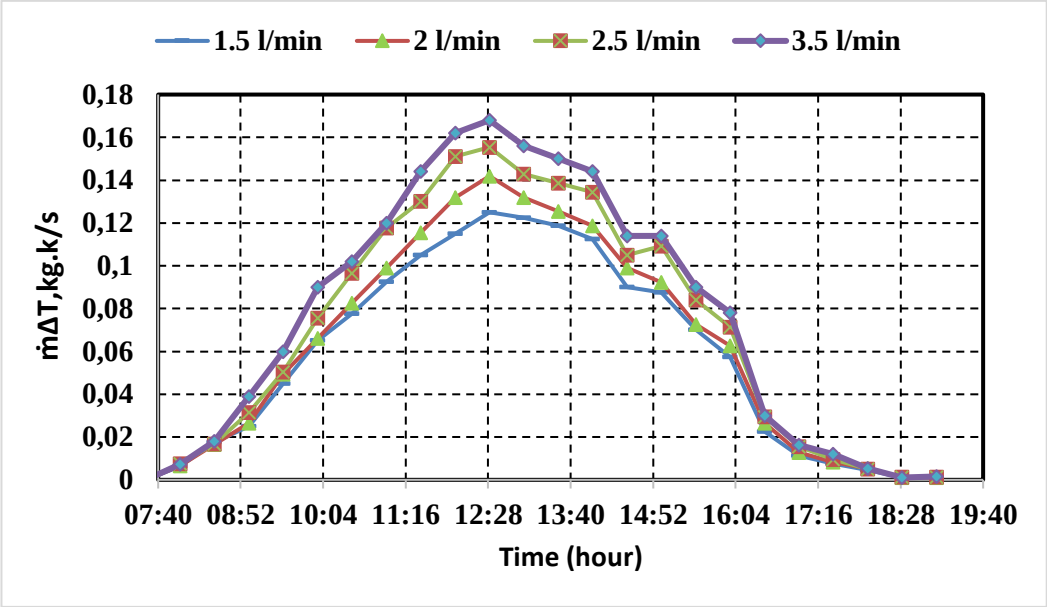

Figure 5.15. Change mΔT (Tout –Tin) with time during the day .flow rate =(1.5 l/min to 3.5 l/min).

5.2.2.9. Effect of Flow Rate (mw) on Thermal Efficiency, ηth for Model SS

Figure 5.16 The thermal efficiency of PV/T can be known by the input of solar energy and it can be converted into thermal gain. Upon investigation, we found noticeable changes in the thermal efficiency (ήth) of the solar collector PV/T with radiation (G) at different flow rates. The radiation is directly proportional to the (th). When the flow rate is increased, the thermal efficiency increases, and thus at the highest radiation the highest thermal efficiency is achieved as the thermal efficiency increases at the following flow rates (2 l/min), (2.5 l/min) and (3.5 l/min) where the proportions The increase (7.8%) (16.6%) (27.3%) respectively in relation to the flow rate (1.5 l/min) at 1:00 pm The thermal efficiency can be extracted from the results discussed on the PVT unit. both ηel and ήth increased with the increase of flow rate. This work is like that of researcher Saeed Abdul-Ganiyu, where it is thermal efficiency (ήth) from 42.46% to 45.60% as in Bibber [42].

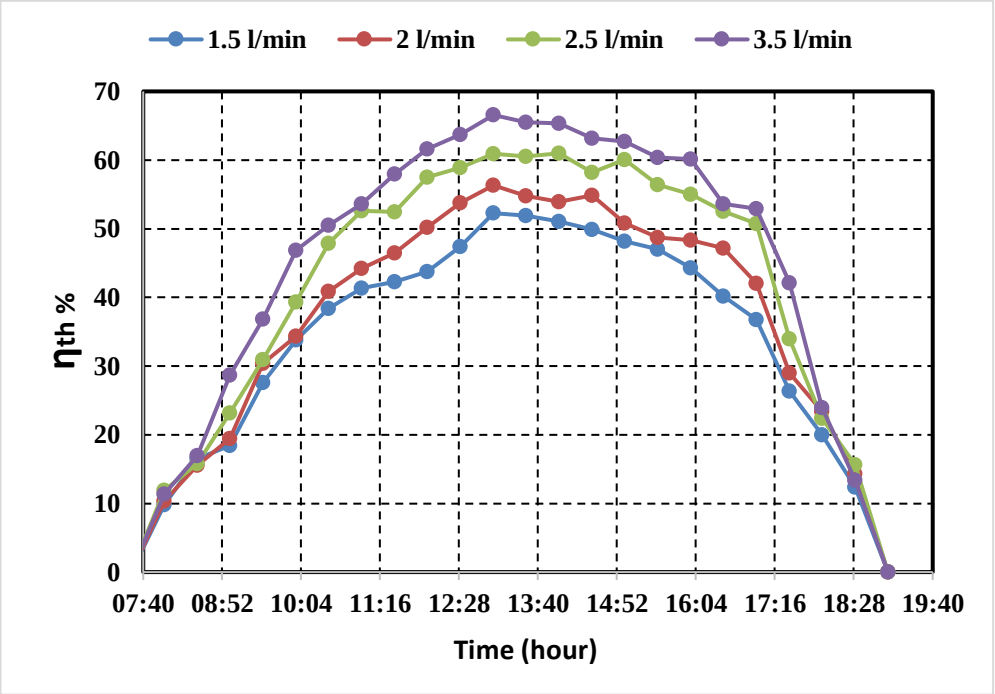

Figure 5.16. Change of thermal efficiency with time during the day. different the flow rates

5.2.2.10. Effect of Mass Flow Rate (mw) on Electrical Efficiency, ηel

Figure 5.17 represents the relationship between electrical efficiency (ηel) with time during the day at different flow rates. For a certain flow rate that (ηel) decreases with (G) increase the reason is due to the increase of Tcell. When increasing the flow rate through the thermal collector and a constant amount of radiation (G), which increases the cooling of the photovoltaic cell, this in turn leads to a relatively low temperature, resulting in large increases in (ηel). Thus, the highest electrical efficiency (ηel) is at the highest flow rate (MW) at a constant radiation. As can be seen from the curves in Figure (5.17), The electrical efficiency of the uncooled cell was (13.5 %) at 1:00 pm when using flow rates (1.5 l/min), (2 l/min), (2.5 l/min) and (3.5 l/min). Electrical efficiency increased by the following percentages. (4.3%), (5.1%), (5.9%), (7.4%) respectively at 1:00 pm. This work is like that of researcher Saeed Abdul-Ganiyu. Electrical efficiency increases from 10.1% to 10.83% with an increase in the flow rate from 1.5 to 3.6 l/min., as in the Bibber [42].

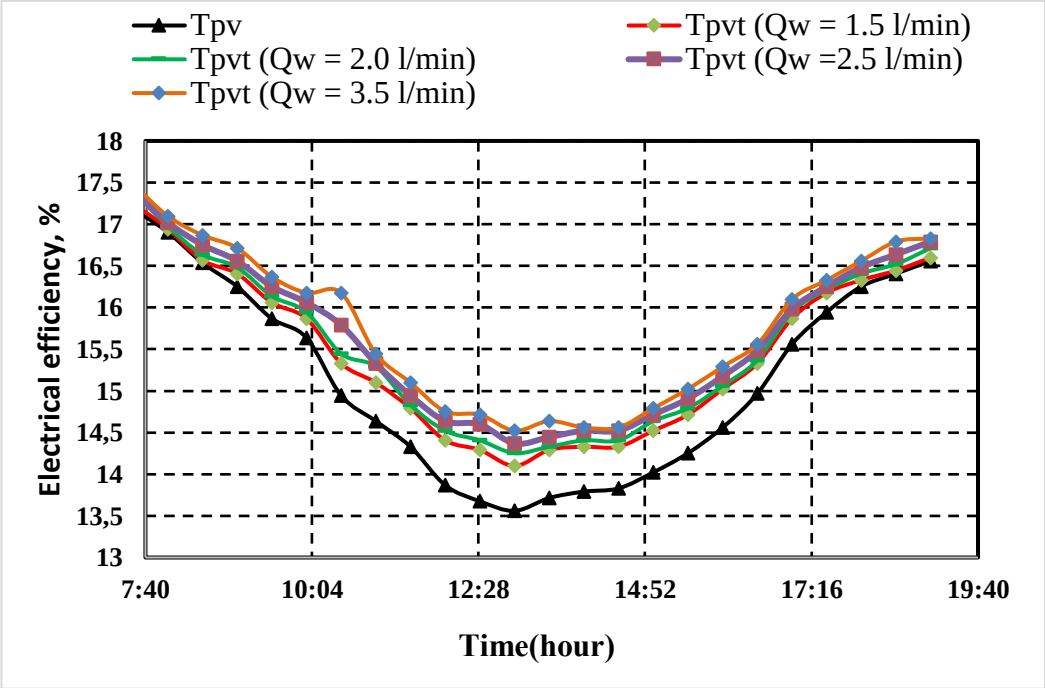

Figure 5.17. Change of electrical efficiency with time during the day. flow rate =(1.5 l/min to 3.5 l/min).

5.3. NUMERICAL SIMULATION RESULTS

5.3.1. Result of PV/T Model CC for (1.5 l/min Flow Rate)

Figure 5.18 contours of temperature distribution the collector for flow rate 1.5 l/min for model- CC (a) at 8 a.m., (b) at 10 a.m., (c) at 1 p.m., (d) at 6 p.m. We note from the theoretical program that when cooling with water and entering the fluid into the collector, there was a decrease in the entry temperatures, but at the exit the temperature of the fluid increased due to the suction process and the fluid absorbing heat when using the CC bulge design from the figure we noticed the rise in the temperature of the contour as we went to the top.

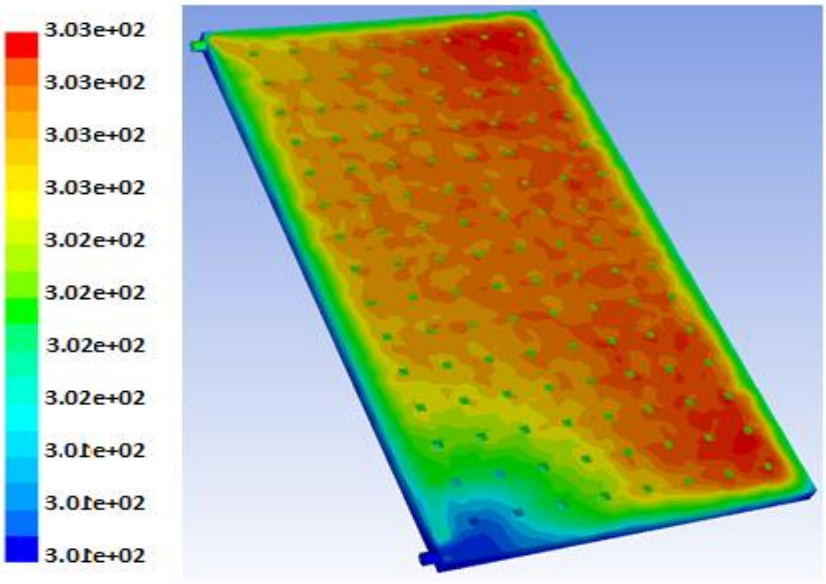

(a) at 8:00 Am

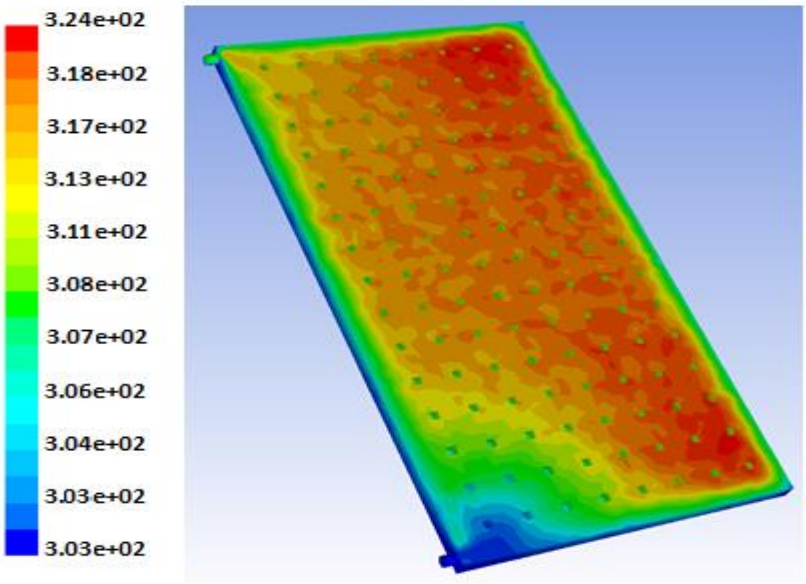

(b) at 10:00 Am

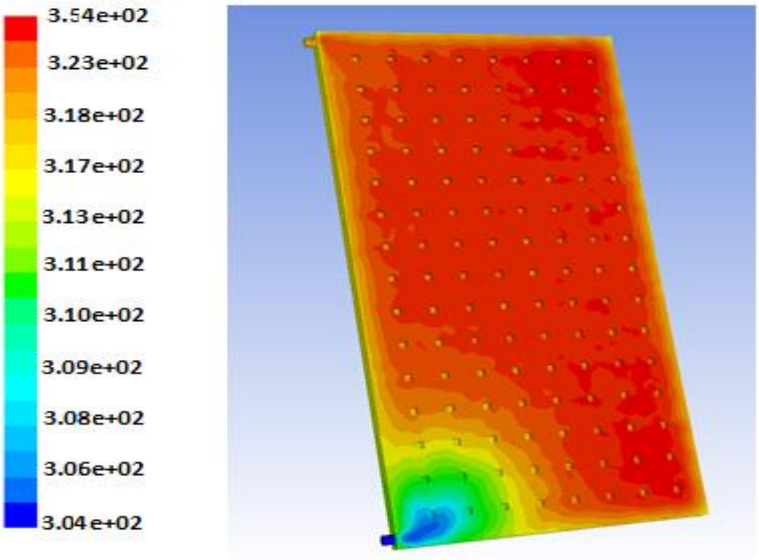

(c) at 1:00 Pm

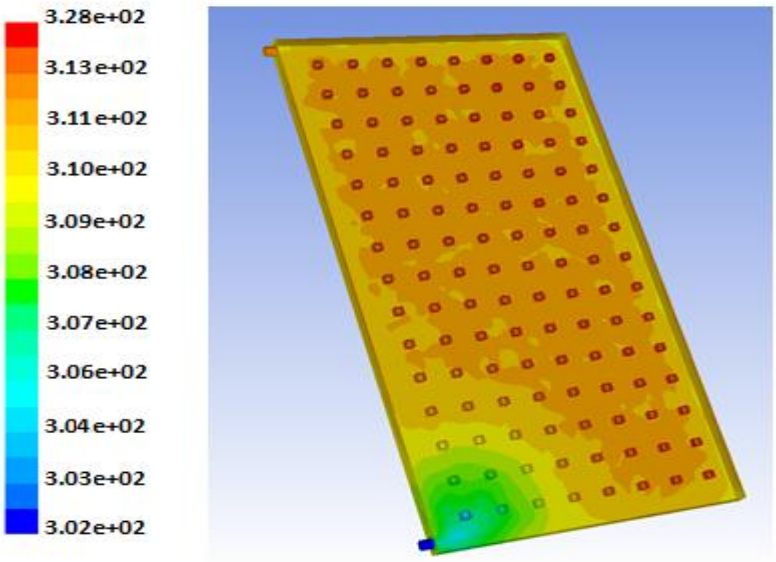

(d) at 6:00 Pm

Figure 5.18. Contours of temperature distribution for Model-CC collector= (1.5 l/min flow rate); (a) at 8 a.m., (b) at 10 a.m., (c) at 1 p.m., (d) at 6 p.m.

5.3.2. Result of PV/T Model CC for (Flow Rate 3.5 l/min)

Figure 5.19 contours of temperature distribution in the collector at 3.5 l/min flow rate for model-CC (a) at 8 a.m., (b) at 10 a.m., (c) at 1 p.m., and (d) at 6 p.m. From the theoretical program, we note that when cooling with water and entering the fluid into the collector, there was a decrease in the entry temperatures, but at the exit the temperature of the fluid increased due to the suction process and the fluid absorbing heat when using the CC bulge design. From the figure, we noticed the rise in the temperature of the contour as we went to the top.

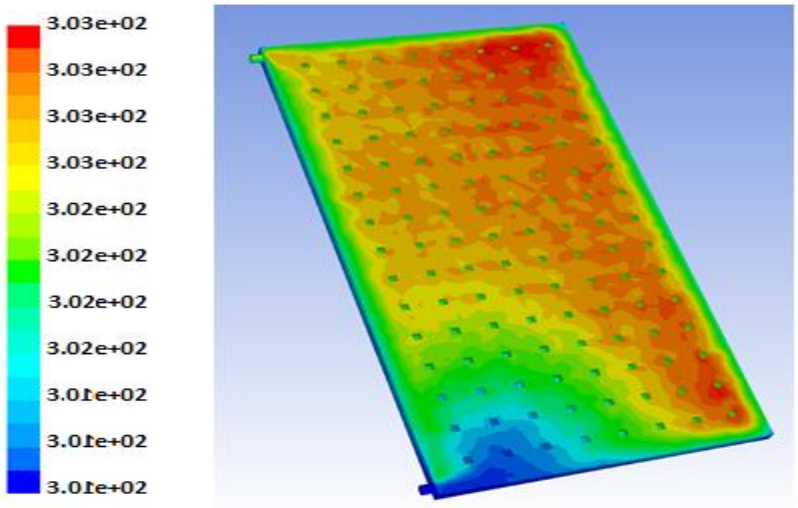

(a) at 8:00 Am

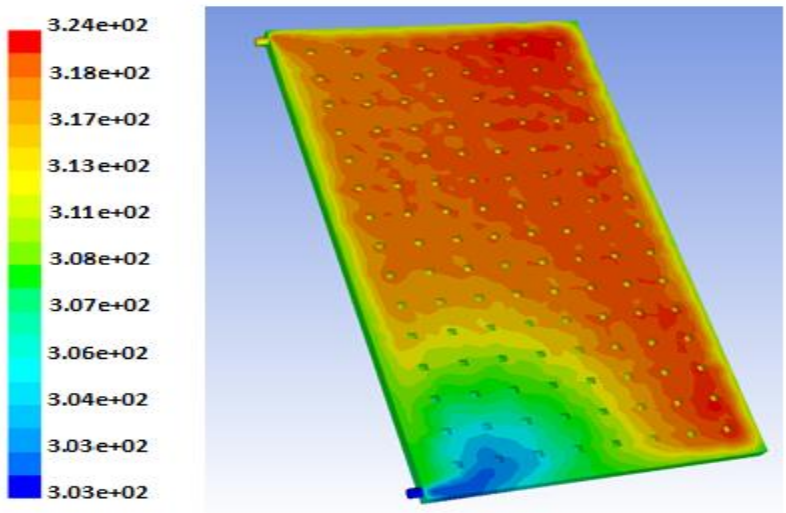

(b) at 10:00 Am

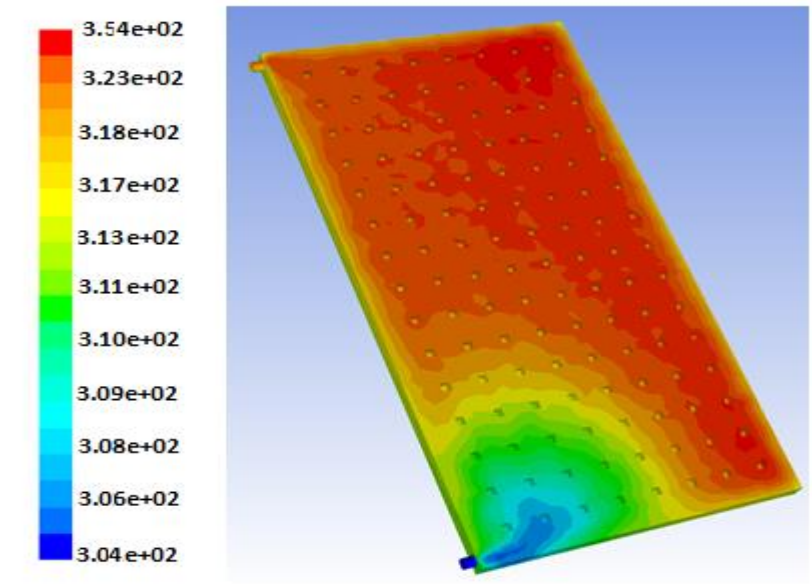

(c) at 1:00 Pm

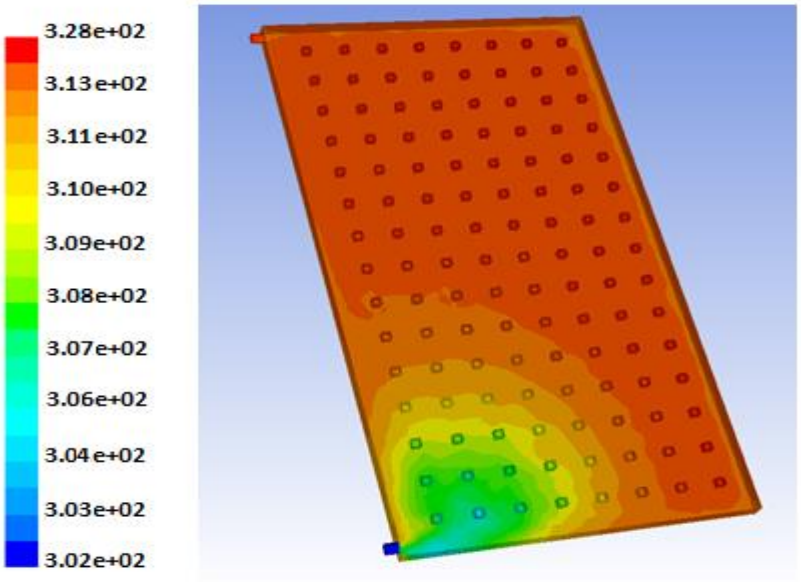

(d) at 6:00 Pm

Figure 5.19. Contours of temperature distribution for Model-CC collector= (3.5 l/min flow rate); (a) at 8 a.m., (b) at 10 a.m., (c) at 1 p.m., (d) at 6 p.m.

5.3.3. Simulated Different Water Temperature

Figure 5.20 Represents the relationship between (ΔT) with time during the day where we notice from the theoretical program when cooling with water and releasing different flow rates that the higher the flow rate, the lower the temperature difference, while the highest difference is at the lowest flow rate. Theoretical results showed that the difference in inlet and outlet temperatures decreases with increasing water flow rates, with the decreasing percentages being 11.8%, 12.7% and 12.9% when changing the flow rates to 2 l/min, 2.5 l /min, 3.5 l /min, respectively.

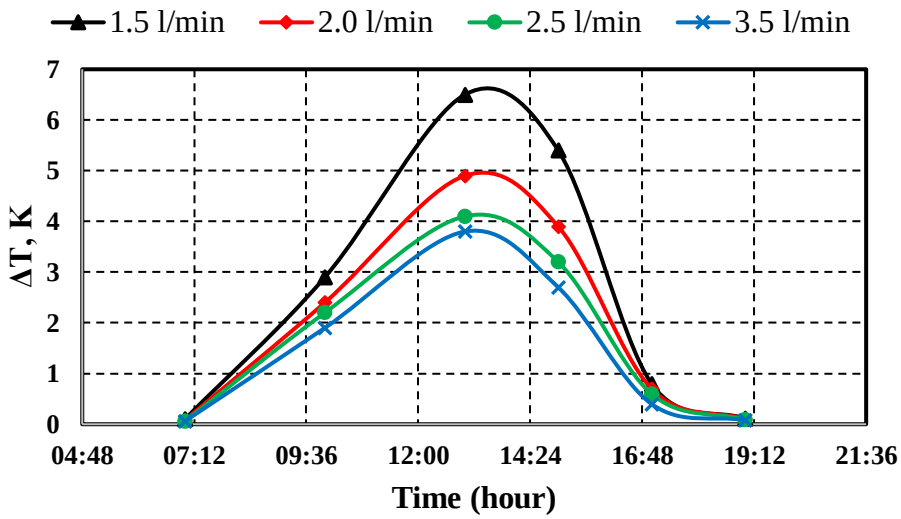

Figure 5.20. Simulated difference water temperature between the inlet and output for Model-CC collector at different flow rates.

5.3.4. Simulated Average Temperature of Collector

Figure 5.21 represents the relationship between the temperature of the collector cap with time during the day, where we notice that the higher the flow rate, the lower the collector temperature due to cooling, and there is an improvement in the system parameters such as efficiency and energy gained where shows that the average temperature of the collected cap decreases with the increase in water rates, where the percentages of variation , were 4.1%,6.3%, and 8.4 % when changing the flow rates to 2 l/min, 2.5 l/min , 3.5 l/min, respectively

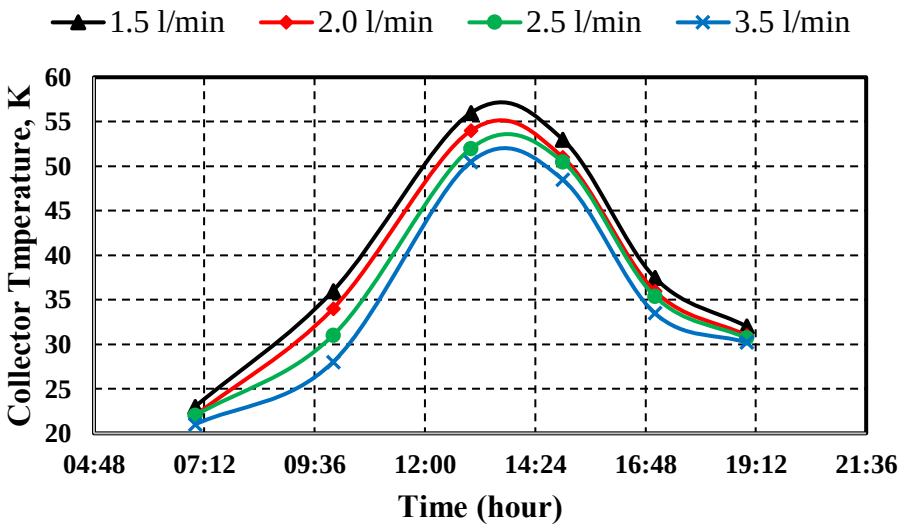

Figure 5.21. Simulated average temperature of collector cover for Model-CC at different flow rates.

5.3.5. Result of PV/T Model SS for (1.5 l/min Flow Rate)

Figure 5.22 temperature distribution contours in the collector for a flow rate of 1.5 l/min for model-SS (a) at 8 a.m., (b) at 10 a.m., (c) at 1 p.m., and (d) at 6 p.m. From the theoretical program, we note that when cooling with water and entering the fluid into the collector, there was a decrease in the entry temperatures, but at the exit the temperature of the fluid increased due to the suction process and the fluid absorbing heat when using the SS bulge design. From the figure, we noticed the rise in the temperature of the contour as we went to the top.

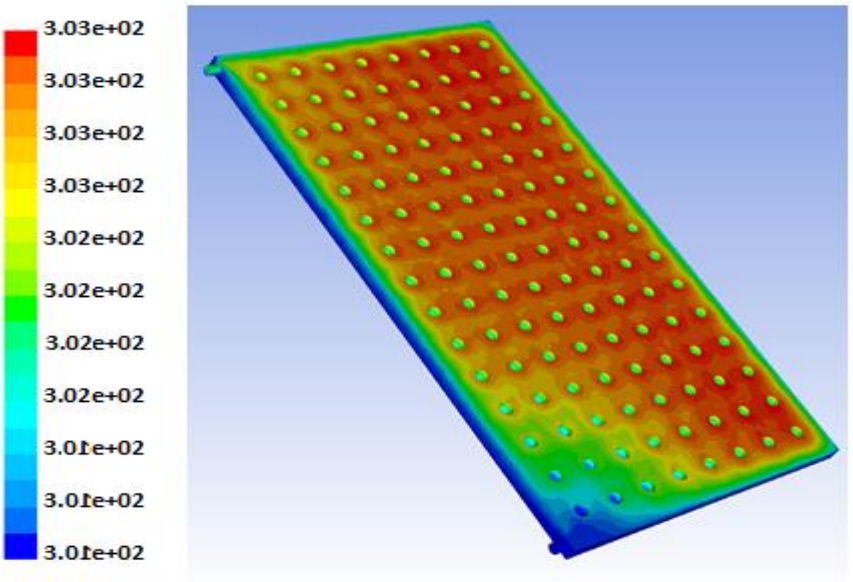

(a) at 8:00 Am

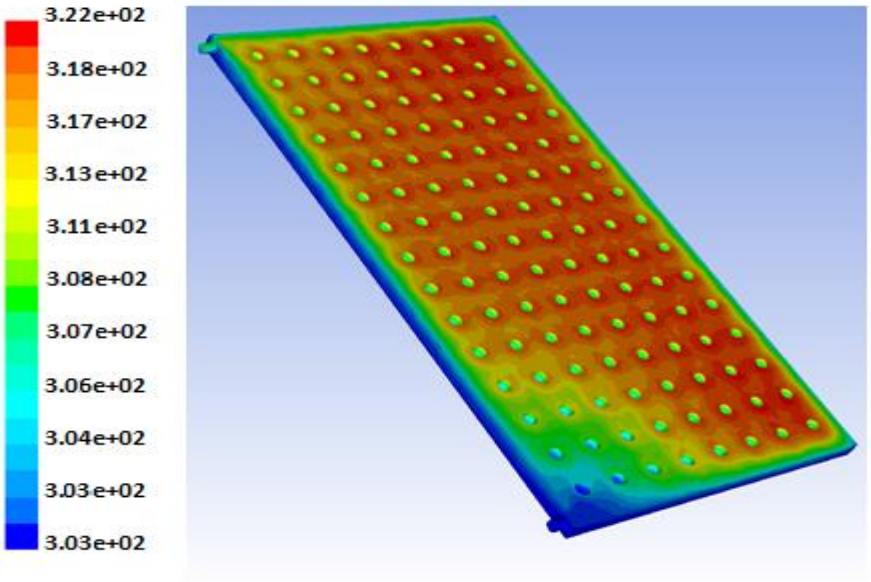

(b) at 10:00 Am

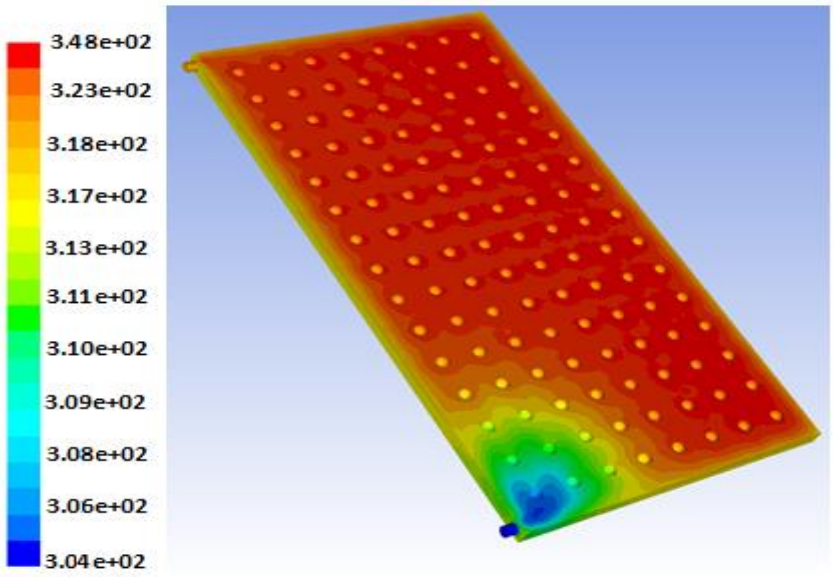

(c) at 1:00 Pm

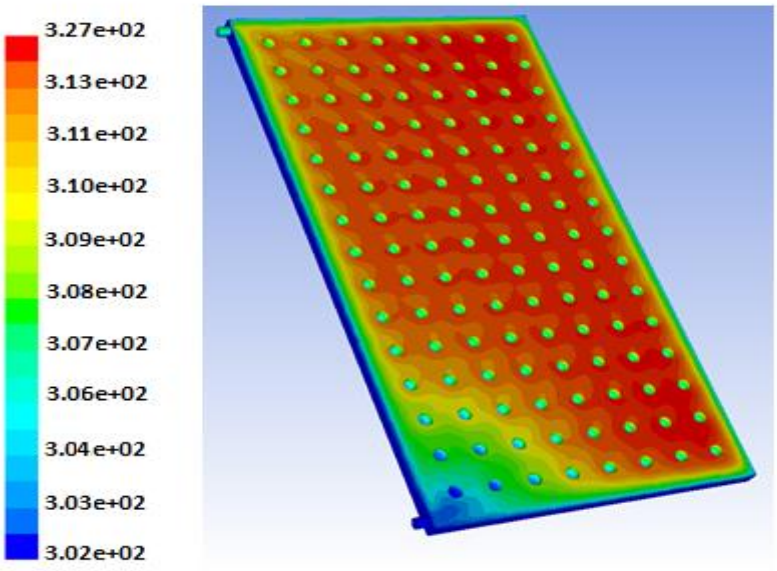

(d) at 6:00 Pm

Figure 5.22. Contours of temperature distribution for Model-SS collector = (1.5 l/min flow rate); (a) at 8 a.m., (b) at 10 a.m., (c) at 1 p.m., (d) at 6 p.m.

5.3.6. Result of PV/T Model SS for (3.5 l/min Flow Rate)

Figure 5.23 contours of temperature distribution the collector for flow rate 3.5 l/min for model- SS (a) at 8 a.m., (b) at 10 a.m., (c) at 1 p.m., (d) at 6 p.m. We note from the theoretical program that when cooling with water and entering the fluid into the collector, there was a decrease in the entry temperatures, but at the exit the temperature of the fluid increased due to the suction process and the fluid absorbing heat when using the SS bulge design, from the figure we noticed the rise in the temperature of the contour as we went to the top.

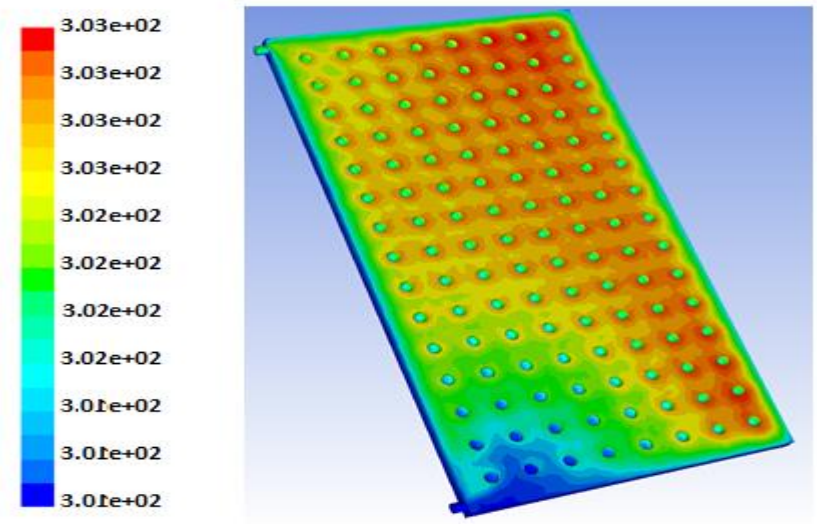

(a) at 8:00 Am

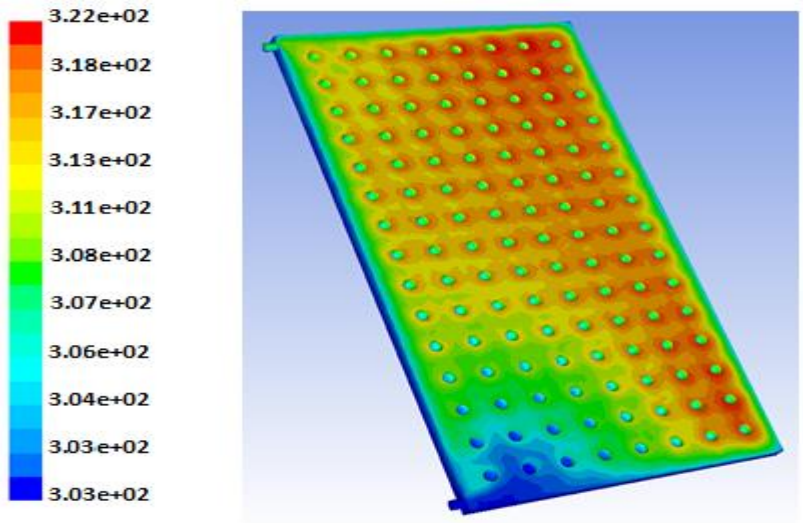

(b) at 10:00 Am

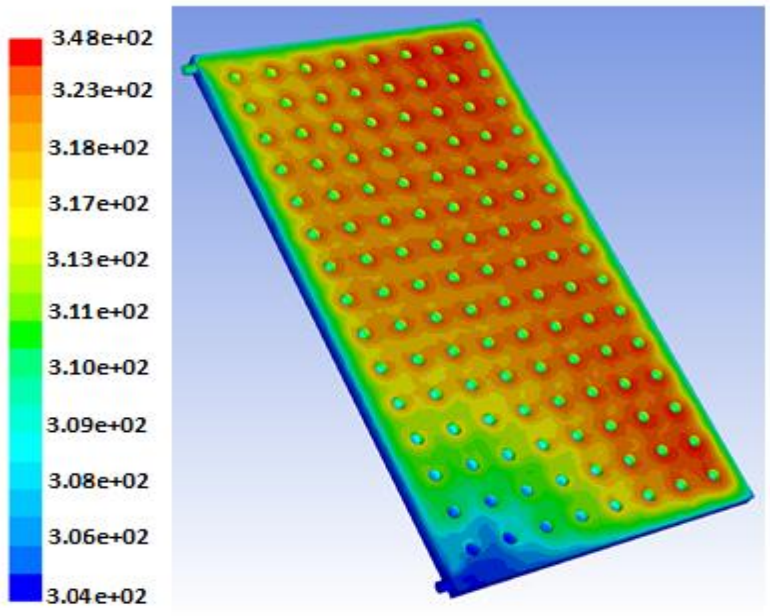

(c) at 1:00 Pm

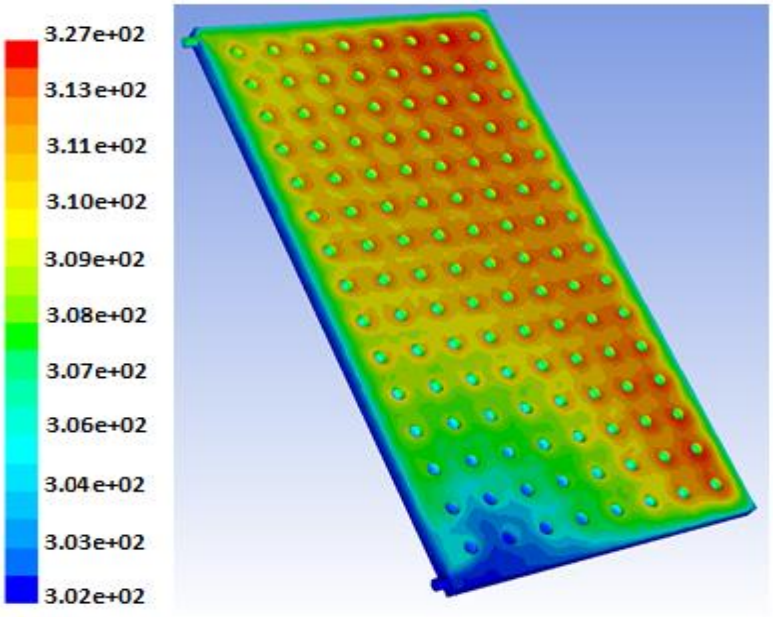

(d) at 6:00 Pm

Figure 5.23. Contours of temperature distribution for Model-SS collector = (3.5 l/min flow rate); (a) at 8 a.m., (b) at 10 a.m., (c) at 1 p.m., (d) at 6 p.m.

5.3.7. Simulated Different Water Temperature Model-SS

Figure 5.24 represents the relationship between (ΔT) with time during the day. We notice from the theoretical program when cooling with water and releasing different flow rates that the higher the flow rate, the lower the temperature difference, while the highest difference is at the lowest flow rate. Theoretical results showed that the difference in inlet and outlet temperatures decreases with increasing water flow rates, with the decreasing percentages being 9.8%, 10.7%, and 11.2% when changing the flow rates to 2 l/min, 2.5 l/min, and 3.5 l/min, respectively.

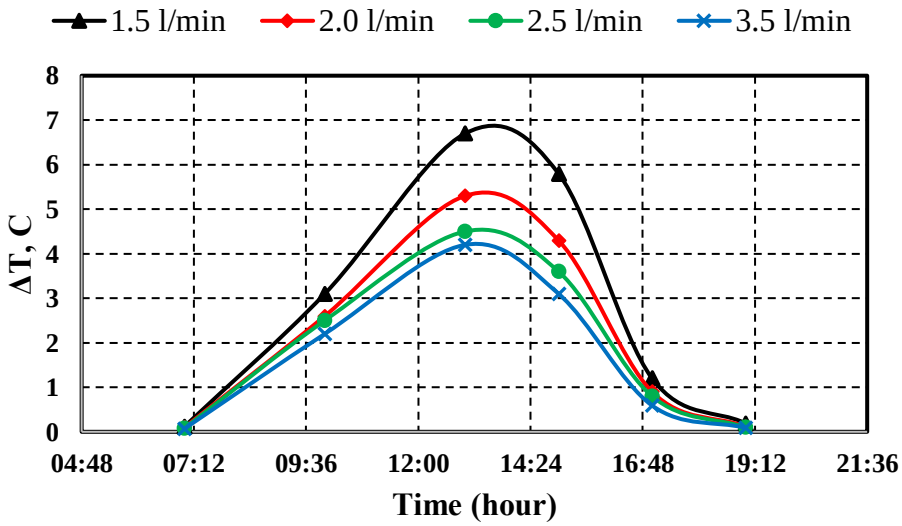

Figure 5.24. Simulated difference water temperature between the inlet and output for Model-SS collector at different flow rates.

5.3.8. Simulated Average Temperature of Collector Model-SS

figure 5.25 this represents the relationship between the temperature of the collector cap with time during the day, where we notice that the higher the flow rate, the lower the collector temperature due to cooling, and there is an improvement in the system parameters such as efficiency and energy gained. The results show that the average temperature of the collected cap decreases with the increase in water rates where the decreasing rates were 3.2%, 4.8%, and 5.9% when changing the flow rates to 2 l/min, 2.5 l/min, and 3.5 l/min, respectively.

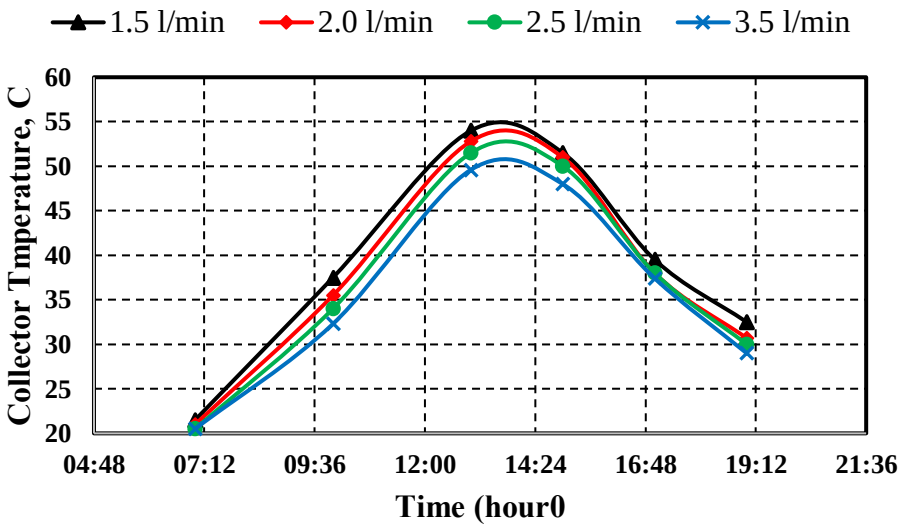

Figure 5.25. Simulated average temperature of collector cover for Model-SS at different flow rates.

5.4. VALIDATION OF NUMERICAL MODELING

5.4.1. Validation of Numerical Result of Different Water Temperature Model - cc and model - SS

Figure 5.26 represents the relationship between (ΔT) with time during the day and a comparison between the theoretical and practical for the flow rates of (1.5 l/min and 3.5 l/min), where it was noticed that when cooling with water and releasing different flow rates, the higher the flow rate, the lower the temperature difference, while the difference was highest at the lowest flow rate. The theoretical and practical results showed that the difference in the entry and exit temperatures decreases with the increase in water flow rates. The total difference (error) percentage between the numerical and experimental was 13.8% for 1.5 l/min and 9.8% for 3.5 l/min for model-CC. and the total difference (error) percentage between the numerical and experimental was 11.6% for 1.5 l/min and 8.7% for 3.5 l/min for model-SS.

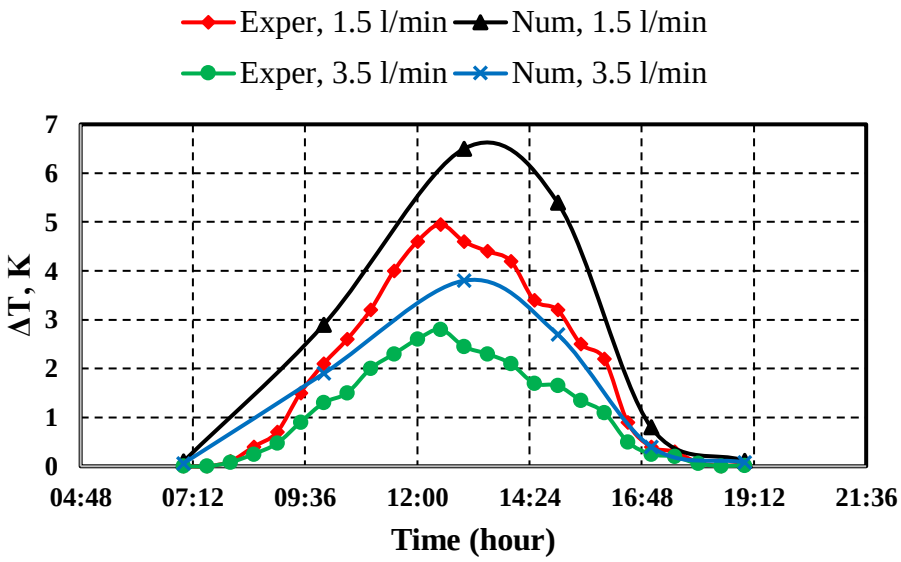

(a) for model-CC.

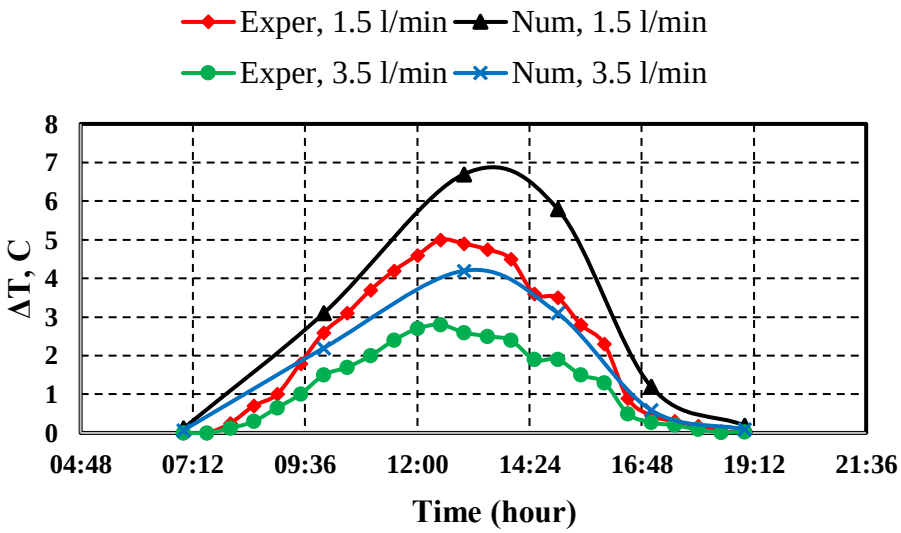

(b) for model-SS

Figure 5.26. Compared results of difference water temperature between the inlet and output =1.5 and 3.5 l/min flow rates; (a) for Model-CC, (b) for Model-SS.

5.4.2. Validation Results of Average Temperature of Collector Cover Model –cc model- SS

Figure 5.27 it represents the relationship between the temperature of the collector cover with time during the day and the comparison between the theoretical and practical, where we note that the higher the flow rate, the lower the temperature of

the collector cover due to cooling, and there is an improvement in system parameters such as efficiency and energy gained. The results showed that as water rates increased, the average temperature of the collected cap decreased. The total difference (error) percentage between the numerical and experimental was 4.6% for 1.5 L/min and 3.2% for 3.5 L/min for the CC model. The total difference (error) percentage between the numerical and experimental was 3.4% for 1.5 l/min and 3.1% for 3.5 l/min for the SS model.

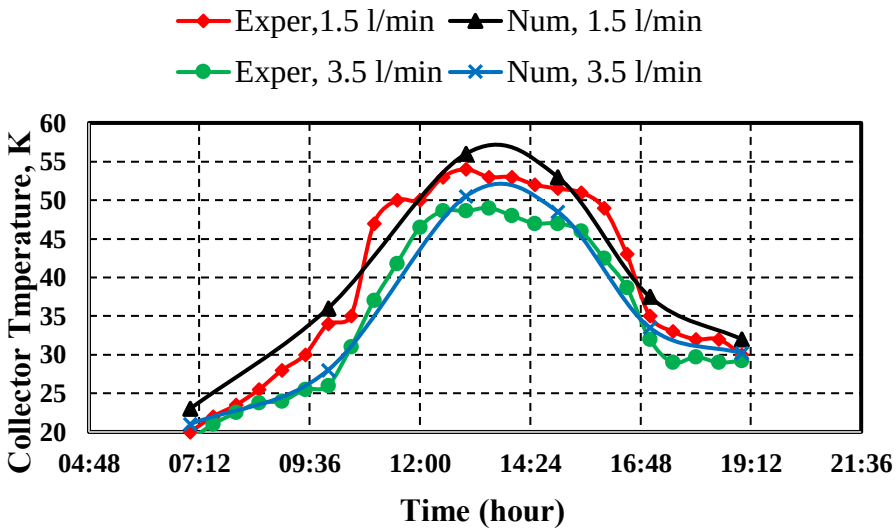

(a)for model-CC.

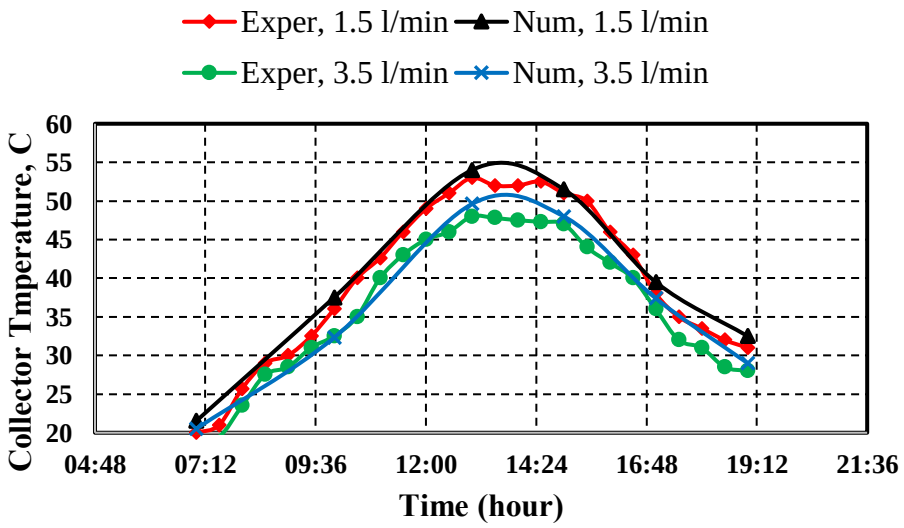

(b)for model-SS

Figure 5.27. Compared results of average temperature of collector cover =1.5 and 3.5 l/min flow rates; (a) for Model-CC, (b) for Model-SS.

5.4.3. Comparation Experimental Results with Literature Work

Figure 5.18 When comparing practically with other researchers in the electrical efficiency, we notice that there is a variable difference according to the type of flow, as the researcher used (Saeed Abdul-Ganiyu 41) a sheet tube, the electrical efficiency was10.7%at 1:00 pm and when as the researcher used (Di Su, Yuting Jia,48) a direct flow rate with two lanes, the electrical efficiency was 10.8%, according to the charts next.

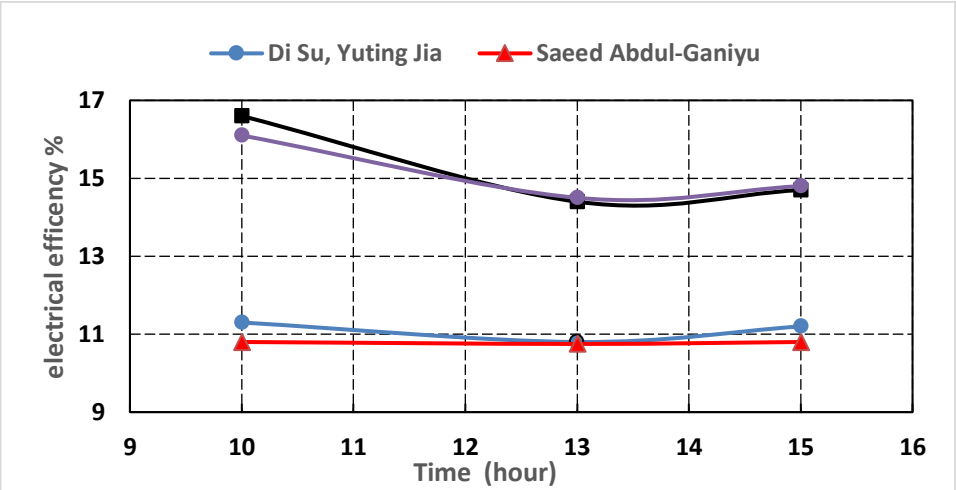

Figure 5.28. Comparison electrical efficiency with other researchers during the day.

5.5. ECONOMIC ANALYSIS

Through the economic feasibility study, we obtained the financial cost, the percentage of improvement in electrical efficiency, and the percentage of decrease in temperature. When using the collector compared to the uncooled cell, we got an increase in the cost by 50%, as shown in Table (5.1), and the second table shows the energy production for each of these mentioned parts, i.e. the financial cost in dollars, as in Table (5.2) it represents the energy produced and its cost in dollars The American, where the total production capacity when using CC compared to the uncooled cell increased by 618.5% and when using the complex S S the production capacity increased by 621%.

Table 5.1. Economic analysis.

No.	part name	prise	electrical effciency	thermal effceincy	T cell
1	PV panal	80$	13.50%		71c
2	PV/T CC type	120$	14.40%	63.60%	60c
3	PV/T SS type	125$	14.50%	66.50%	58.5c

Table 5.2. Economic analysis.

part name	elec.power w	thermal power w	total w	costs
PV	114.4	nill	114.4	3183
PV/T CC	122	700	822	22869
PV/T SS	123	703	825	22952

PART 6

CONCLUSION AND RECOMMENDATIONS

6.1. CONCLUSION

In this research, we used two different designs for collectors and studied the effect of the design on the system, water flow rate and radiation on the PVT system. The first type is CC model, where this design is in the form of measuring cubes (15 * 15 * 15 mm) and the second type is the SS model, which is designed in the form of balls diameter (25 mm), and we obtained the following results

6.1.1. Experimental Result of PV/T System

1. Effect of collector design (bulge shape) on PV/T system performance on cell temperature was and the ratio difference was between uncooled cell and the bulge CC and the bulge SS (8.4%)(9.8%) at 1:00 pm.
2. Effect of collector design (bulge shape) on PV/T system performance on collector temperature Where the percentage of the difference in temperature between uncooled cell and the CC model and the SS model is at 1:00 pm it is the ratio (23.9%) (25.3%).
3. effect of collector design (bulge shape) on PV/T system performance relation to (ΔT) Where the percentage of the difference in e for the CC model and the SS model is at 12:30, it is the ratio (1.01%).
4. Effect of collector design (bulge shape) on PV/T system performance on heat gained Where the percentage of the different for the CC model and the SS model is at 1:00, it is the ratio (6,08%).
5. effect of collector design (bulge shape) on PV/T system performance relation to thermal efficiency Where the percentage of the different between for the CC model and the SS model is at 1:00, it is the ratio (6.06%).

6. Effect of collector design (bulge shape) on PV/T system performance relation to electrical efficiency the ratio between uncooled cell and the CC model and the SS model at 12:30, which is the ratio (6.6%), (8.08%) respectively and from this we find that the higher the flow rate, the higher the electrical efficiency. The increase depends on the incoming radiation.
7. Effect of mass flow rate (mw) on solar cell surface temperature (Tcell) for model CC The reduction ratio between the uncooled cell and the cooled cell for cell surface temperature and flow rates (1.5 l/min), (2 l/min), (2.5 l/min), (3.5 l/min), where the ratio is (8.4%), (9.8%), (14.08%), (15.4%) respectively at 1:00 p.m
8. Effect of mass flow rate(mw) on (ΔT) for model CC, the difference in temperature decreases with the increase in the water flow rates, where the decrease rates were 15.1% , 25.2% and 43.4% when changing the flow rates of ,2 l/min , 2.5 l/min, and 3.5 l/min, respectively at 12:30 pm.
9. Effect of mass flow rate (mw) on energies gained for model CC), as the energy gained increases at the following flow rates (2 l/min), (2.5 l/min) and (3.5 l/min) where the proportions were The increase (12.1%) (26.01%) (36.5%) respectively in relation to the flow rate (1.5 l/min) at 12:30 pm.
10. Effect of flow rate (mw) on thermal efficiency, ηth for model CC as the thermal efficiency increases at the following flow rates (2 l/min), (2.5 l/min) and (3.5 l/min) where the proportions The increase (11.9%) (25.5%) (35.6%) respectively in relation to the flow rate (1.5 l/min) at 12:30 pm.
11. Effect of mass flow (mw) on electrical efficiency for model CC, the electrical efficiency of the uncooled cell was (13.6%) at 12:30 pm when using flow rates (1.5 l/min), (2 l/min), (2.5 l/min) and (3.5 l/min). Electrical efficiency increased by the following percentages. (3.6%), (4.4%), (5.1%), (6.6%) respectively
12. Effect of mass flow rate (mw) on solar cell temperature (Tell) for model SS The reduction ratio between the uncooled cell and the cooled cell for cell surface temperature and flow rates (1.5 l/min), (2 l/min), (2.5 l/min), (3.5 l/min), where the ratio is (9.8%), (12.6%), (14.7%), (17.6%) respectively at 1:00 p.m.

13. Effect of mass flow rate(mw) on ΔT for model SS. From the results, the difference in temperature decreases with the increase in the water flow rates, where the decrease rates were 14 %, 26.2% and 44% when changing the flow rates of 2 l/ min, 2.5 l/min , and 3.5 l/min respectively at 12:30 pm.
14. Effect of mass flow rate (mw) on energies gained for model SS, as the energy gained increases at the following flow rates (2 l/min), (2.5 l/min) and (3.5 l/min) where the proportions The increase (12.8%) (24%) (34.4%) respectively in relation to the flow rate (1.5 l/min) at 12:30 pm.
15. Effect of flow rate (mw) on thermal efficiency, ηth for model SS as the thermal efficiency increases at the following flow rates (2 l/min), (2.5 l/min) and (3.5 l/min) where the proportions The increase (7.8%) (16.6%) (27.3%) respectively in relation to the flow rate (1.5 l/ min) at 1:00 pm.
16. Effect of mass flow rate (mw) on electrical efficiency, ηel for model SS The electrical efficiency of the uncooled cell was (13.5 %) at 1:00 pm when using flow rates (1.5 l/min), (2 l/min), (2.5 l/min) and (3.5 l/min). Electrical efficiency increased by the following percentages. (4.3%), (5.1%), (5.9%), (7.4%) respectively at 1:00 pm.

6.1.2. Theoretical Result of PV/T System

1. Simulated different water temperature with the decreasing percentages being 11.8%, 12.7% and 12.9% when changing the flow rates to 2 l/min, 2.5 l/min, 3.5 l/min, respectively.
2. Simulated average temperature of collector where the percentages of variation, were 4.1%,6.3%, and 8.4 % when changing the flow rates to 2 l/min, 2.5 l/min, 3.5 l/min, respectively
3. Simulated different water temperatures were the decreasing percentages being 9.8%, 10.7%, and 11.2% when changing the flow rates to 2 l/min, 2.5 l/min, 3.5 l/min, respectively.
4. Simulated average temperature of collector where the decreasing rates were 3.2%, 4.8%, and 5.9% when changing the flow rates to 2 l/min, 2.5 l/min, and 3.5 l/min, respectively.
5. Validation of numerical result of different water temperature model - cc and

model - SS The total difference (error) percentage between numerical and experimental were 13.8% for 1.5 l/min and 9.8% for 3.5 l/min for model- CC and the total difference (error) percentage between numerical and experimental were 11.6% for 1.5 l/min and 8.7% for 3.5 l/min for model- SS.

6. Validation results of average temperature of collector cover model –cc model- SS The total difference (error) percentage between numerical and experimental was 4.6% for 1.5 l/min and 3.2% for 3.5 l/min for the CC model. The total difference (error) percentage between numerical and experimental was 3.4% for 1.5 l/min and 3.1% for 3.5 l/min for the SS model.

6.2. RECOMMENDATIONS FOR FUTURE WORK

New researchers in the future should use bromide, as well as nano materials as a coolant, and from practical experience, they should use shapes with designs that help thermal suction in larger quantities than used in this research.

REFERENCES

1. Kazem, H. A., Chaichan, M. T., & Yousif, J. H., "Evaluation of oscillatory flow Photovoltaic/Thermal system in Oman", ***International Journal of Computation and Applied Sciences,*** 10 (1): 429-436 (2019).

2. Hernández-Moro, J., & Martinez-Duart, J. M., "Analytical model for solar PV and CSP electricity costs: Present LCOE values and their future evolution", ***Renewable and Sustainable Energy Reviews,*** 2(10): 119-132 (2013).

3. Mughal, S. S., Yog R., Jarial, R. K., "A review on solar photovoltaic technology and future trends", ***International Journal of Scientific Research in Computer Science, Engineering and Information Technology,*** 4(1): 227-235 (2015).

4. Abd Alrahman, C., "Evaluation of a PVT Air Collector", ***Master Level Thesis European Solar Engineering School,*** Belgium, 23-56 (2015).

5. Kaya, M., "Thermal and electrical performance evaluation of PV/T collectors in UAE", ***Master of Science Thesis KTH School of Industrial Engineering and Management,*** Stockholm, 34-67 (2013).

6. Zondag, H. A., "Flat-plate PV-Thermal collectors and systems: A review", ***Renewable and Sustainable Energy Reviews,*** *12*(4): 891-959 (2008).

7. Othman, M. Y., Yatim, B., Sopian, K., & Bakar, M. N. A., "Performance studies on a finned double-pass photovoltaic-thermal (PV/T) solar collector", ***Desalination,*** 209(3): 43-49 (2007).

8. Joshi, A. S., Tiwari, A., Tiwari, G. N., Dincer, I., & Reddy, B. V., "Performance evaluation of a hybrid photovoltaic thermal (PV/T) (glass-to-glass) system", ***International Journal of Thermal Sciences,*** *48*(1): 154-164 (2009).

9. Jin, G. L., Ibrahim, A., Chean, Y. K., Daghigh, R., Ruslan, H., Mat, S., & Sopian, K., "Evaluation of single-pass photovoltaic-thermal air collector with rectangle tunnel absorber", ***American Journal of Applied Sciences,*** *7*(2): 277 (2010).

10. Sarhaddi, F., Farahat, S., Ajam, H., Behzadmehr, A. M. I. N., & Adeli, M. M., "An improved thermal and electrical model for a solar photovoltaic thermal (PV/T) air collector", ***Applied Energy,*** 87(7): 2328-2339 (2010).

11. Teo, H. G., Lee, P. S., & Hawlader, M. N. A., "An active cooling system for photovoltaic modules", ***Applied Energy***, 90(1): 309-315 (2012).

12. Yeh, H. M., & Ho, C. D., "Collector efficiency in downward-type double-pass solar air heaters with attached fins and operated by external recycle", ***Energies,*** *5*(8): 2692-2707 (2012).

13. Amori, K. E., & Al-Najjar, H. M. T., "Analysis of thermal and electrical performance of a hybrid (PV/T) air based solar collector for Iraq", ***Applied Energy,*** 9(8): 384-395 (2012).

14. Bakari, R., Minja, R. J., & Njau, K. N., "Effect of glass thickness on performance of flat plate solar collectors for fruits drying", ***Journal of Energy,*** *20(14): 341-366* (2014).

15. Amori, K. E., & Abd-AlRaheem, M. A., "Field study of various air based photovoltaic/thermal hybrid solar collectors", ***Renewable Energy,*** 6(3): 402-414 (2014).

16. Leow, W. Z., Irwan, Y. M., Asri, M., Irwanto, M., Amelia, A. R., Syafiqah, Z., & Safwati, I., "Investigation of solar panel performance based on different wind velocity using ANSYS", ***Indonesian Journal of Electrical Engineering and Computer Science,*** *1*(3): 456-463 (2016).

17. Boulfaf, N., Chaoufi, J., Ghafiri, A., & Elorf, A., "Thermal study of hybrid photovoltaic thermal (PV-T) solar air collector using finite element method", ***International Journal of Renewable Energy Research,*** 6(1): 171-182 (2016).

18. Ahmed, O. K., & Mohammed, Z. A., "Dust effect on the performance of the hybrid PV/Thermal collector", ***Thermal Science and Engineering Progress,*** 3(4): 114-122 (2017).

19. Slimani, M. E. A., Amirat, M., Kurucz, I., Bahria, S., Hamidat, A., & Chaouch, W. B., "A detailed thermal-electrical model of three photovoltaic/thermal (PV/T) hybrid air collectors and photovoltaic (PV) module: Comparative study under Algiers climatic conditions", ***Energy Conversion and Management,*** 13(3): 458-476 (2017).

20. Ahmed, O. K., & Mohammed, Z. A., "Influence of porous media on the performance of hybrid PV/Thermal collector", ***Renewable Energy,*** 11(2): 378-387 (2017).

21. Kasaeian, A., Khanjari, Y., Golzari, S., Mahian, O., & Wongwises, S., "Effects of forced convection on the performance of a photovoltaic thermal system: An experimental study", ***Experimental Thermal and Fluid Science,*** *8(5):* 13-21 (2017).

22. Omer, K. A., & Zala, A. M., "Experimental investigation of PV/thermal collector with theoretical analysis", ***Renewable Energy Focus,*** 2(7): 67-77 (2018).

23. Lenin, N., Sivamurugan, P., Srimanickam, B., Ramanan, P., & Siva Kumar, M., "Thermal and electrical performance evaluation of PV/T collectors in Southern India", ***International Journal of Ambient Energy,*** *42*(7): 751-757 (2021).

24. Kim, S. M., Kim, J. H., & Kim, J. T., "Experimental study on the thermal and electrical characteristics of an air-based photovoltaic thermal collector", ***Energies,*** 12(14): 26-61 (2019).

25. Choi, H. U., & Choi, K. H., "Performance evaluation of PV/T air collector having a single-pass double-flow air channel and non-uniform cross-section transverse rib", ***Energies,*** 13(9): 2203 (2020).

26. Ahn, J. G., Yu, J. S., Boafo, F. E., Kim, J. H., & Kim, J. T., "Simulation and Performance Analysis of Air-Type PVT Collector with Interspaced Baffle-PV Cell Design", ***Energies,*** 14(17): 53-72 (2021).

27. He, W., Chow, T. T., Ji, J., Lu, J., Pei, G., & Chan, L. S., "Hybrid photovoltaic and thermal solar-collector designed for natural circulation of water", ***Applied Energy,*** 83(3): 199-210 (2006).

28. Ibrahim, A., Othman, M. Y., Ruslan, M. H., Alghoul, M., Yahya, M., Zaharim, A., & Sopian, K., "Performance of photovoltaic thermal collector (PVT) with different absorbers design", ***WSEAS Transactions on Environment and Development,*** 5(3): 321-330 (2009).

29. Dubey, S., & Tay, A. A., "Testing of two different types of photovoltaic–thermal (PVT) modules with heat flow pattern under tropical climatic conditions", ***Energy for Sustainable Development,*** *17*(1): 1-12 (2013).

30. Rahou, et al. "Performance study of a photovoltaic thermal system with an oscillatory flow design", ***Journal of Solar Energy Engineering,*** 20(14): 135-178 (2014).

31. Michael, J. J., & Selvarasan, I., "Experimental investigation of a copper sheet-laminated solar photovoltaic thermal water collector", ***Energy Efficiency,*** *10*(1): 117-128 (2017).

32. Al-Shamani, A. N., Sopian, K., Mat, S., Hasan, H. A., Abed, A. M., & Ruslan, M. H., "Experimental studies of rectangular tube absorber photovoltaic thermal collector with various types of nanofluids under the tropical climate conditions", ***Energy Conversion and Management,*** 12(4): 528-542 (2016).

33. Hussein, H. A., Numan, A. H., & Abdulrahman, R. A., "Improving the hybrid photovoltaic/thermal system performance using water-cooling technique and Zn-H2O nanofluid", ***International Journal of Photoenergy,*** 2(1): 143-157 (2017).

34. Sachit, F. A., Tamaldin, N., Rosli, M. A. M., Misha, S., & Abdullah, A. L., "Current progress on flat-plate water collector design in photovoltaic thermal (PV/T) systems: A Review", ***Journal of Advanced Research in Dynamical and Control Systems,*** 10(4): 680-89 (2018).

35. Hasan, H. A., Sopian, K., & Fudholi, A., "Photovoltaic thermal solar water collector designed with a jet collision system", ***Energy,*** 16(1): 412-424 (2018).

36. Yuan, W., Ji, J., Li, Z., Zhou, F., Ren, X., Zhao, X., & Liu, S., "Comparison study of the performance of two kinds of photovoltaic/thermal (PV/T) systems and a PV module at high ambient temperature", ***Energy,*** 14(8): 1153-1161 (2018).

37. Fudholi, A., Razali, N. F. M., Ridwan, A., Yendra, R., Hartono, H., Desvina, A. P., & Sopian, K., "Overview of photovoltaic thermal (PVT) water collector", ***International Journal of Power Electronics and Drive Systems,*** *9*(4): 18-91 (2018).

38. Razali, N. F. M., Fudholi, A., Ruslan, M. H., & Sopian, K., "Experiment study of water based photovoltaic-thermal (PV/T) collector", ***International Journal of Electrical and Computer Engineering,*** 9(1): 118 (2019).

39. Kazem, H. A., "Evaluation and analysis of water-based photovoltaic/thermal (PV/T) system", ***Case Studies in Thermal Engineering,*** 1(3): 100-401 (2019).

40. Abdullah, A. L., Misha, S., Tamaldin, N., Rosli, M. A. M., & Sachit, F. A., "Technology Progress on Photovoltaic Thermal (PVT) Systems with Flat-Plate Water Collector Designs: A Review", ***Journal of Advanced Research in Fluid Mechanics and Thermal Sciences,*** 59(1): 107-141 (2019).

41. Yu, Q., Hu, M., Li, J., Wang, Y., & Pei, G., "Development of a 2D temperature-irradiance coupling model for performance characterizations of the flat-plate photovoltaic/thermal (PV/T) collector", ***Renewable Energy***, 15(3): 404-419 (2020).

42. Abdul-Ganiyu, S., Quansah, D. A., Ramde, E. W., Seidu, R., & Adaramola, M. S., "Study effect of flow rate on flat-plate water-based photovoltaic-thermal (PVT) system performance by analytical technique", ***Journal of Cleaner Production,*** 3(21): 128-985 (2021).

43. Al-Zurfi, H. A., Balla, H. H., Al-Shamani, A. N., & Hayder, A. M., "Numerical Study to Enhance the Electrical and Thermal Efficiency of PV/T System", ***In IOP Conference Series: Materials Science and Engineering***, 928(2): 22-136 (2020).

44. Zhang, Y., Shen, C., Zhang, C., Pu, J., Yang, Q., & Sun, C., "A novel porous channel to optimize the cooling performance of PV modules", ***Energy and Built Environment,*** *3*(2): 210-225 (2022).

45. Abdin, Z. U., & Rachid, A., “Bond graph modeling of a water-based photovoltaic thermal (PV/T) collector”, ***Solar Energy,*** *2(20):* 571-577 (2021).

46. Guo, C., Ji, J., Sun, W., Ma, J., He, W., & Wang, Y., “Numerical simulation and experimental validation of tri-functional photovoltaic/ thermal solar collector”, ***Energy,*** 8(7): 470-480 (2015).

47. Mojumder, J. C., Chong, W. T., Ong, H. C., & Leong, K. Y., “An experimental investigation on performance analysis of air type photovoltaic thermal collector system integrated with cooling fins design”, ***Energy and Buildings,*** 13(10): 272-285 (2016).

48. Su, D., Jia, Y., Huang, X., Alva, G., Tang, Y., & Fang, G., “Dynamic performance analysis of photovoltaic–thermal solar collector with dual channels for different fluids”, ***Energy Conversion and Management,*** *12(10):* 13-24 (2016).

49. Hussain, M., “Performance Evaluation of Photovoltaic/Thermal (PV/T) System Using Different Design Configurations”, ***Sustainability,*** 12(22): 95-120 (2005).

50. Coventry, J. S., "Performance of a concentrating photovoltaic/thermal solar collector", ***Solar energy,*** *78*(2): 211-222 (2005).

51. Brogren, M., & Karlsson, B., "Low-concentrating water-cooled PV-thermal hybrid systems for high latitudes", ***In Conference Record of the Twenty-Ninth IEEE Photovoltaic Specialists Conference***, New Orleans, USA, 1733-1736 (2002).

52. Bahaidarah, H., Subhan, A., Gandhidasan, P., & Rehman, S., "Performance evaluation of a PV (photovoltaic) module by back surface water cooling for hot climatic conditions", ***Energy,*** 5(9): 445-453 (2013).

53. Zondag, H. A., De Vries, D. W., Van Helden, W. G. J., Van Zolingen, R. J. C., & Van Steenhoven, A. A., "The yield of different combined PV-thermal collector designs", ***Solar Energy,*** 74(3): 253-269 (2003).

54. Hosseini, R., Hosseini, N., & Khorasanizadeh, H., "An experimental study of combining a photovoltaic system with a heating system", ***In World Renewable Energy Congress-Sweden,*** Sweden 2993-3000 (2011).

55. Agbo, S. N., & Okoroigwe, E. G., "Analysis of Thermal Losses in the Flat-Plate Collector of a Thermosiphon Solar Water Heater", ***Research Journal of Physics,*** *1*(1): 35-41 (2007).

56. Klein, S. A., Duffie, J. A., & Beckman, W. A., "Transient considerations of flat-plate solar collectors", ***Journal of Engineering for Power,*** 96(2): 432-489 (1974).

57. Kroiß, A., Präbst, A., Hamberger, S., Spinnler, M., Tripanagnostopoulos, Y., & Sattelmayer, T., "Development of a seawater-proof hybrid photovoltaic/thermal (PV/T) solar collector", ***Energy Procedia,*** 5(2): 93-103 (2014).

58. Kordzadeh, A., "The effects of nominal power of array and system head on the operation of photovoltaic water pumping set with array surface covered by a film of water", ***Renewable Energy,*** *35*(5): 1098-1102 (2010).

59. Jakhar, S., Soni, M. S., & Gakkhar, N., "Performance analysis of photovoltaic panels with earth water heat exchanger cooling", ***In MATEC Web of Conferences***, 5(5): 20-30 (2016).

60. Handbook, A. F., "American society of heating, refrigerating and air-conditioning engineers", ***Inc.:*** Atlanta, USA, 45-77 (2009).

61. Probst, D. M., Senecal, P. K., Qian, P. Z., Xu, M. X., & Leyde, B. P., "Optimization and uncertainty analysis of a diesel engine operating point using CFD", ***In Internal Combustion Engine Division Fall Technical Conference,*** South Carolina, USA, 87-99 (2016).

APPENDIX A.

INSTRUMENTATION CALIBRATION

A.1. CALIBRATION OF THERMOCOUPLE

Thermocouples type (K) has been used with data logger for temperature measuring at fixed positions of experimental model of the SVE. A thermocouple is a sensor consisting of two wire legs made from different metals, for type K are (positive leg is composed of 90% nickel, 10%chromium and a negative leg is composed of 95% nickel, 2% aluminum, 2% manganese and 1% silicon). The wires legs are welded together at one end, generating a junction. This junction is where the temperature is measured. When the junction experiences a change in temperature, a voltage is generated. The voltage can then be interpreted using a data logger to record the temperature. Thermocouples type K have a smaller temperature range and a shorter lifespan at higher temperatures. Thermocouples type K are well suited to oxidizing atmospheres as a bare consideration. Temperature range for thermocouples type K is -270˚C to 1260˚C.

Before commencing the measurements, a calibration of thermocouples type K was carried out with the digital thermometer. Thermocouples calibration curve, shown in figure A.1, has been analyzed and a linear expression was represented the calibration relationship as shown below:

$$y = 0.7939x + 6.1547 \quad \text{(A.1)}$$

Where *y* represents thermocouples reading and *x* represents the digital thermometer reading, all readings in centigrade scale. That's mean any corrected testing temperature used in analyzing collected results can be calculated as below:

$$x = (y - 6.1547)/0.7939 \quad \text{(A.2)}$$

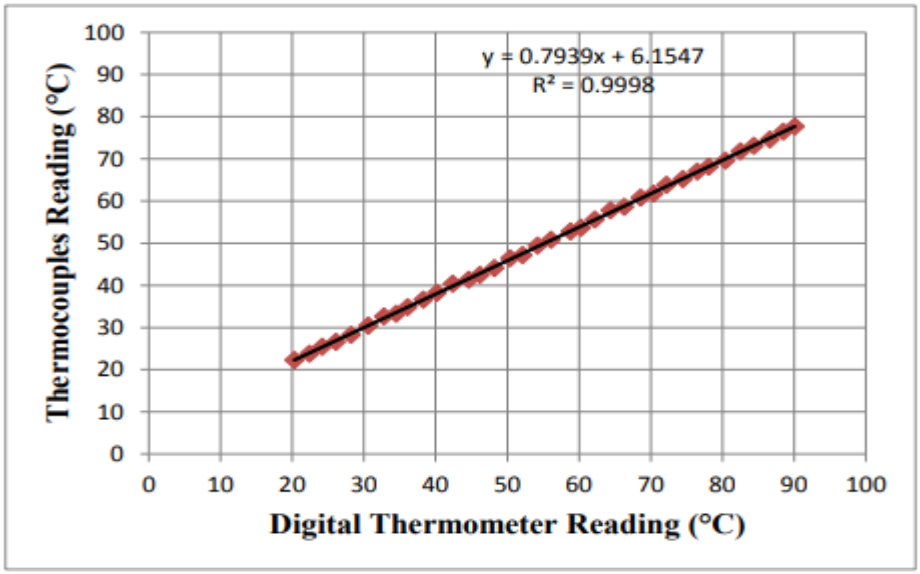

Figure Appendix A.1. Calibration curve of K-type thermocouples.

A.2. CALIBRATION OF FLOW METER

Before commencing the measurement, a calibration of Roto-meter was carried out by the volume of the calibrated tank was pre-calibrated by the volume and its height. The time taken to get 2 litter of water into the tank was recorded, calibration curve shown in Figure B.2.

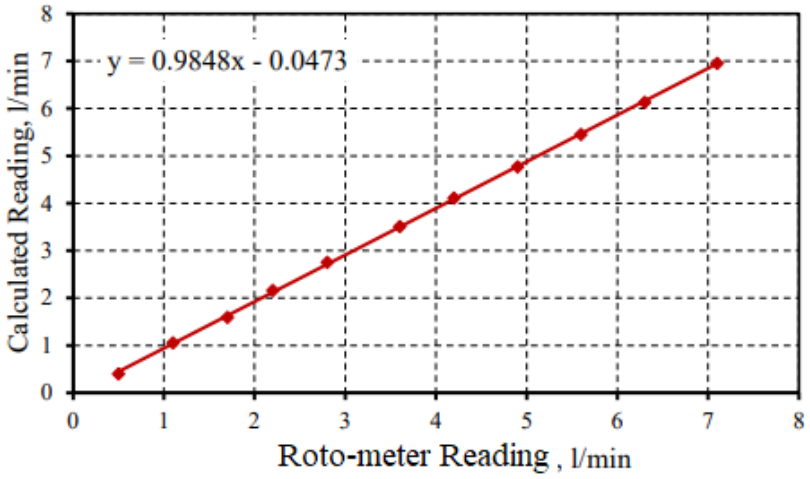

Figure Appendix A.2. Calibration curve of Roto-meter.

APPENDIX B.

DATA

1.5 l/m , modell cc							
Time	**Tpv**	**T pvt**	**To-Ti**	**T col**	**G W/m2**	**T amb**	**ws m/s**
07:00	21	21	0	20	3	20	0.9
07:30	23.4	23.2	0	22	35	21	1
08:00	26.3	26	0.1	23.5	230	21	1
08:30	28.2	28	0.4	25.5	406	21	1.7
09:00	33	32	0.7	28	500	23	1.6
09:30	35.5	34.5	1.5	30	634	24	2
10:00	37	36	2.1	34	796	25.1	2.1
10:30	44	41	2.6	35	830	26.2	1.8
11:00	54	53.5	3.2	47	905	31	1.7
11:30	61	58	4	50	955	34	1.7
12:00	67	62.6	4.6	50	983	35.4	1.9
12:30	68.2	63.7	4.95	53	1047	38.7	2.3
13:00	68.7	65	4.6	54	970	40	2.5
13:30	68	63.5	4.4	53	972	40	2.3
14:00	67	62.5	4.2	53	900	38	2.1
14:30	67	61.5	3.4	52	760	37	2.3
15:00	66.5	61.5	3.2	53	747	33	2.2
15:30	64	58.5	2.5	51	600	32	2.3
16:00	60	56	2.2	49	500	30	1.7
16:30	52.5	49	0.9	43	213	27	1.8
17:00	42	40.5	0.4	35	110	25	1.6
17:30	39.5	37	0.3	33	100	23.3	1.9
18:00	34	33.5	0.08	32	71	23	1.5
18:30	33.7	33	0.01	32	18	22	1.5
19:00	30.6	30	0.04	29.7	0	21	1.5

3.5 l/m / , modell cc							
time	**tpv**	T_pvt_	**To-Ti**	T col	ws m/s	**G W/m2**	**T amb**
07:00	21	21	0	19.5	0.6	4	20
07:30	23.2	22.5	0	21.5	0.8	39	20
08:00	26.8	24	0.08	22.5	0.9	244	20.5
08:30	28.6	26	0.25	24	1.1	417	22
09:00	33.2	27	0.47	24	1.7	518	24
09:30	35.7	30	0.9	25.5	2	645	25.3
10:00	37.4	31	1.3	26	2	803	25.7
10:30	44.2	36	1.5	31	2.1	846	26
11:00	55.7	45	2	37	2	917	32
11:30	61.3	50	2.3	41.8	1.9	962	35
12:00	67.7	56.5	2.6	46.5	1.7	991	38.8
12:30	68.9	58.5	2.8	48.6	2.1	1071	39.7
13:00	69	60	2.45	48.6	2.2	979	40.3
13:30	69.4	58	2.3	49	2.3	990	40
14:00	67.2	57	2.1	47	2.1	916	39.1
14:30	67.1	56.5	1.7	48	2.3	780	38.2
15:00	67	55	1.65	47	2.4	759	33
15:30	64	54	1.35	46	2.3	611	33
16:00	61	50	1.1	42.5	1.9	519	29
16:30	53	44.5	0.5	38.7	1.8	231	28
17:00	42.8	37	0.25	32	1.6	128	26
17:30	40	32	0.2	29	1.4	118	25
18:00	34	31	0.054	29.7	1.7	82	25
18:30	34	30	0.01	29	1.3	27	21
19:00	30	29.7	0.02	29.2	1.1	0	20

wate flow rate =1.5 l/m(modell ss)							
Time	T Pv(C°)	Tpvt (C °)	To-Ti (C °)	T col (C °)	Gw/m2	T amb (C°)	windS m/s
07:00	21.2	21	0	20	9	20	1.1
07:30	23.5	23	0	21	24	20.3	1.1
08:00	27.3	27	0.25	25.7	204	20.8	1.1
08:30	32	31.9	0.7	29	406	22.7	2.1
09:00	35	34	1	30	572	23.6	2.2
09:30	40	38.5	1.8	32.5	617	24.8	1.7
10:00	42.8	41	2.6	36	793	25.7	1.7
10:30	51	48	3.1	40	862	26.3	1.7
11:00	55.7	51	3.7	42.6	921	34	1.7
11:30	60	55	4.2	46	944	36.7	1.7
12:00	65.4	60	4.6	49	972	39.5	1.7
12:30	68.5	61.5	5	51	1089	40	2.3
13:00	70	64	4.9	53	999	40.8	2.3
13:30	69	61.5	4.75	52	989	40	2.3
14:00	66.7	61	4.5	52	909	39.1	2.3
14:30	67.5	61	3.6	52.5	773	38	2.3
15:00	64.5	58.5	3.5	51	768	37	2.3
15:30	61	56	2.8	50	620	34.4	2.3
16:00	58	52	2.3	46	522	30	1.8
16:30	52.5	48	0.9	43	217	27	1.8
17:00	44	41	0.45	38	146	26.5	1.8
17:30	41	37	0.3	35	132	25	1.9
18:00	36	35	0.18	33.5	87	24	1.9
18:30	34	33.5	0.04	32	17	21	1.9
19:00	32	31.5	0.04	31	0	20	1.6

water flow rate =3.5 l/m(modell ss)							
Time	**T Pv(C°)**	**Tpvt (C °)**	**To-Ti (C °)**	**T col (C °)**	**G w/m2**	**windS m/s**	**T amb (C°)**
07:00	21.5	20.8	0	19.5	1	1	20
07:30	23.9	20	0	19.5	29	1.1	20.5
08:00	27.5	25	0.12	23.5	268	1.3	21
08:30	32.3	28	0.3	27.5	448	1.7	23
09:00	36	30	0.65	28.5	573	2.1	24
09:30	41	34.5	1	31	687	1.7	25
10:00	44	37	1.5	32.5	810	1.8	26
10:30	53	37	1.7	35	851	1.7	27
11:00	57	46.5	2	40	943	1.6	34
11:30	61	51	2.4	43	1047	1.7	37
12:00	67	55.5	2.7	45	1108	2	40
12:30	69.5	56	2.8	46	1112	2.1	40
13:00	71	58.5	2.6	48	988	2.3	41
13:30	69	58.2	2.5	47.8	965	2.2	40
14:00	68	58	2.4	47.5	929	2.3	39.5
14:30	67.5	58	1.9	47.3	761	2.1	38
15:00	65	55	1.9	47	766	2.2	34
15:30	62	52	1.5	44	628	2.3	33
16:00	58	48.5	1.3	42	547	1.7	30
16:30	52.7	45	0.5	40	236	1.8	28
17:00	45	38	0.27	36	129	1.8	26.5
17:30	40	35	0.2	32	120	1.9	26
18:00	36	32	0.09	31	95	2	25
18:30	34	29	0.018	28.5	34	2	22
19:00	32	28.5	0.027	28	0	2	20

RESUME

Mohammed Gumar AJEL was born in Iraq Anbar and he graduated primary, elementary, and high school in this city, after that, he started Studying Mechanical Engineering In The Anbar University / Engineering College / Mechanical Engineering Department In 1995. Then, in 2020, he started at Karabuk University Mechanical Engineering to complete his M. Sc. education.